

---

**INTERAFACIAL TENSION AND SURFACTANT  
STABILISATION DURING MEMBRANE EMULSIFICATION**

Doctoral Thesis

Submitted by

Pedro Tiago Santos Silva

Supervised by

Professor Richard G. Holdich

Professor Victor M. Starov

Submitted in partial fulfilment of the requirements for the award of  
Doctor of Philosophy of Loughborough University

9<sup>th</sup> July 2018

© by Pedro Tiago Santos Silva 2018

---

---

*“A person who never made a mistake never tried anything new”*

## **ACKNOWLEDGEMENTS**

I would like to express my sincere appreciation and gratitude to my supervisor, Professor Richard Holdich, for presenting me with the fantastic opportunity to be a part-time PhD student in Chemical Engineering and gain professional experience in his company, Micropore Technologies Ltd. I feel truly privileged to have worked with him within an outstanding European framework as CoWet with great scientists and minds. I really appreciate all his guidance, encouragement and positive attitude which facilitated to complete this degree.

A special acknowledgment to my second supervisor, Professor Victor Starov, who has always shown awareness and enthusiasm with my research providing solutions and suggestions when they were most needed.

A kind thanks to Dr. Marijana Dragosavac who has always shown an interest in my work and provided excellent advice and encouragement.

I would like to thank Micropore Technologies team for their support and help throughout these years. Their experience and flexibility were important for me and for my research. A special “thank you” goes to Dr. Michael Stillwell and Dr. Sergey Zhdanov, who were always there for me. I feel that my learning curve and my adaptation to the UK had great input from them and this I will never forget. I also want to thank other Micropore members, Bruce Williams, Dai Hayward, Dave Palmer, Martin Lott and Sam Trotter. Their assistance and management were very valuable.

My journey has also been shaped by a large number of people at various times along the way to its completion. I would like to express my gratitude to my colleagues and friends, Ana B., Ana C., Ana R., Anna, Abdul, Carlos, Gulraiz, Isabel, João, José, Keith, Konstantin, Leandro, Luís, Maria J., Monica, Nina, Omid, Sean and Serena, who contributed in various manners to my research and overall experience at Loughborough University.

A “Dankuwel” to the most special person that I ever met, Stephanie, for her whole-hearted support, patience and unwavering love. Of the six years we’ve met, I’ve been away three but, nevertheless, our relationship grew and strengthen as never before.

Finally, a “Obrigado” to my family: my mother Araci, my father Avelino, my sisters, Camila, Cátia and Zaida and my brothers in law, André e Pedro. Despite the distance you were always present.

This work was supported by Micropore Technologies Ltd and prepared in the framework of the Marie Curie Initial Training Network “Complex Wetting Phenomena” (CoWet). Grant no. 607861.

**ABSTRACT**

A new insight on the interaction between complex fluids and solid surfaces is given in this study. It is demonstrated how these liquid-solid interactions can greatly influence the droplet generation during membrane emulsification and, therefore, resultant emulsion size and uniformity. These aspects of the process are often “underestimated” and poorly comprehended by, specially, industrial colleagues. Thus, that unawareness can lead to poor results and to a disbelief in this upcoming technology.

A novel membrane emulsification system is reported consisting of a tubular metal membrane, periodically azimuthally (tangentially) oscillated with frequencies up to 50 Hz and 7 mm displacement in a gently cross flowing continuous phase. Using an azimuthally oscillating membrane, oil-in-water (o/w) emulsions were experimentally produced with a diameter of 20–120  $\mu\text{m}$ , and a coefficient of variation (CV) of droplet size of 8%. The drop size was correlated with shear stress at the membrane surface using a force balance. In a single pass of continuous phase, it was possible to achieve high dispersed phase concentrations up to 38% v/v.

A vertical oscillation membrane emulsification was used to study the influence of dynamic interfacial tension in membrane emulsification: drop size can be tuned between 35 and 85  $\mu\text{m}$  by changing the surfactant concentration in the continuous phase. In addition, a method to determine the percentage of active pores during membrane emulsification is demonstrated. This method links knowledge acquired in the surfactant adsorption dynamics and drop expansion rate. This study reinforces the importance of dynamic interfacial tension which must be considered in process design, and modelling purposes, particularly in two liquid phase systems using membranes such as membrane emulsification at high injection rates.

Hydrophobization of metal surfaces is reported based on silanization reactions to broaden the use of metal porous membranes to water-in-oil (w/o) emulsion production. The developed

procedure is shown to be a straightforward hydrophobization method, with minimal cost to apply, reproducible, stable and the possibility of reuse of the membrane after losing hydrophobicity by simply reapplying the hydrophobization method.

On the other hand, formation of water-based droplets can be achieved using a hydrophilic porous metal membrane. To investigate this, water-based droplets were produced using a hydrophilic membrane and wetting experiments were also carried out: sessile droplets were used to determine static contact angles and a rotating drum system was used to determine contact angles under dynamic conditions. In the latter case the three-phase contact line was observed between the rotating drum and two immiscible liquids. It was observed that the oil phase can preferably wet a hydrophilic surface in case when a surfactant is present in the oil phase, and above a certain concentration, even in the presence of the water phase.

Apart from membrane emulsification, spontaneous formation of water droplets in kerosene was observed, facilitated by the presence of an oil soluble surfactant: Span<sup>®</sup> 80. This process was characterized and the influence of chemical potential between both phases was evaluated. Nano-sizing analyses were performed for a set of experiments, where the influence of the surfactant concentration in the organic phase, as well as the influence of NaCl concentration in the aqueous phase, was studied. Water droplets between 100 and 400 nm were measured in kerosene. Interfacial tension between both phases, was not lower than 4 mN/m. Therefore, ultra-low interfacial tension was not required for this process to occur spontaneously.

Continuous production of spherical polymeric particles, via membrane emulsification, was demonstrated. An o/w emulsion was used as precursor and, by solvent removal, solid particles were obtained. In addition, production of polycaprolactone (PCL) particles containing encapsulated (entrapped) protein model was also demonstrated via a double emulsion method.

## **TABLE OF CONTENT**

ACKNOWLEDGEMENTS .....	i
ABSTRACT.....	iii
LIST OF FIGURES .....	viii
LIST OF TABLES .....	xiii
LIST OF SYMOBLS .....	xiv
LIST OF ABBREVIATIONS.....	xvii
Chapter 1 INTRODUCTION.....	1
1.1. Motivation for research .....	1
1.2. Aim and objectives.....	2
1.3. Thesis structure .....	3
Chapter 2 LITERATURE REVIEW.....	5
2.1 Membrane emulsification .....	10
2.1.1 Membranes.....	11
2.1.2 Pores & Patterning .....	14
2.1.3 Interfacial tension, surface chemistry and wetting .....	15
2.1.4 Viscosity effects.....	19
2.1.5 Dispersed phase flow and membrane active pores .....	21
2.1.6 Shear stress control .....	22
2.1.7 Modelling.....	23
2.1.7.1 Dispersed drop size modelling.....	23
2.1.7.2 Membrane oscillation.....	26
2.2.8 Outlook for industrial implementation.....	27
2.2. Spontaneous Emulsification.....	29
2.2.1 Microemulsions.....	29

---

Chapter 3 EXPERIMENTAL .....	32
3.1 Emulsification devices .....	32
3.1.1 Dispersion Cell.....	32
3.1.2 Vertical oscillating membrane system .....	36
3.1.3 Azimuthally oscillating membrane system (Micropore Technologies Ltd) .....	38
3.2 Determination of mean droplet size and droplet size distribution .....	43
3.3 Surface modification .....	44
3.3.1 Developed procedure .....	44
3.3.2 Durability and stability tests .....	45
3.4 Contact angle, surface and interfacial tension measurements .....	46
3.4.1 Sessile droplet experiments.....	46
3.4.1.1 Home built setup .....	46
3.4.1.2 Droplet shape analyser .....	48
3.4.2 Rotating drum experiments.....	49
3.4.3 Surface and interfacial tension measurements .....	50
3.5 Spontaneous emulsification experiments.....	51
Chapter 4 MEMBRANE PROPERTIES AND COMPLEX FLUIDS BEHAVIOUR .....	52
4.1 Membranes characterization .....	52
4.1.1 Pore size distribution.....	55
4.1.2 Surface modification .....	57
4.2 Surface and Interfacial tension measurements.....	63
4.3 Static contact angles.....	67
4.4 Dynamic contact angles .....	70
4.5 Spontaneous emulsification of water in oil at appreciable interfacial tensions .....	79
4.5.1 Characterization of the water droplets present in the organic phases .....	79
4.5.2 Sessile droplets experiments .....	81



Chapter 5 CONTROLLED DROPLET FORMATION: DISTINCT FORMULATIONS AND APPLICATIONS .....	85
5.1 Different uniform emulsions using a hydrophilic membrane .....	85
5.1.1 Drop formation experiments with the Dispersion Cell (w/o emulsion).....	85
5.1.2 Drop formation experiments with the Dispersion Cell (o/w emulsion).....	87
5.2 Influence of dynamic interfacial tension in membrane emulsification.....	90
5.2.1 Drop formation experiments with vertical oscillating membrane system .....	90
5.2.2 Surfactant dynamics adsorption (method to determine % active pores).....	93
5.3 Investigation of membrane emulsification in a continuous mode suitable for industrial use .....	98
5.3.1 Drop formation experiments with azimuthally oscillating membrane system .....	98
5.3.2 Production of polycaprolactone particles using azimuthally oscillating membrane system .....	106
5.4 Overview of system scalability .....	112
Chapter 6 OUTLOOK AND CONCLUSIONS .....	118
6.1 Recommendations and Future Work .....	123
References.....	125
List of Publications in Peer Reviewed Journals.....	140
Patent.....	140
Conference participation.....	141
Training: “Marie Curie” scientific schools .....	142
Outreach activities .....	142

## LIST OF FIGURES

Figure 1.1 Flow chart of the thesis structure.....	3
Figure 2.1 Power requirement of emulsifying machinery. ....	7
Figure 2.2. Representation of the ideal chemical structure of the fluoroalkylsilane/metallic interphase region $R=CH_2CH_2(CF_2)_7CF_3$ (adapted from [65]). ....	14
Figure 2.3. Contact angle and the different interfacial tensions involved during drop formation at a membrane pore, adapted from [10]. ....	16
Figure 2.4. Schematic side view of the rotating drum and the resultant advancing and receding contact angle in a half-filled chamber by one (or two, immiscible) liquid(s).....	18
Figure 2.5 Influence of the contact angle on the final drop size.....	24
Figure 3.1 3D illustration of all the components from the Dispersion Cell.....	32
Figure 3.2 Schematic diagrams showing (a) the stirred cell, (b) the shear profile under the stirrer, and (c) the annular radial ring membrane for dispersion. Adapted from [47]. ....	34
Figure 3.3 Representation of the vertical oscillating membrane emulsification device used with an inset showing the regular pore pattern of the membrane (triangular array) and the shape of the tubular membrane used. Adapted from [48]. ....	36
Figure 3.4 a) Schematic illustration of the Micropore Technologies Ltd Oscillating Membrane Emulsification system; b) Overhead view of the shaft that contains the membrane, illustrating the oscillatory movement of the membrane; c) Side view of the shaft with membrane covering lower parallel sided section (55 mm high and 40 mm diameter).....	38
Figure 3.5 Chemical structure of 1H, 1H, 2H, 2H-Perfluorodecyltriethoxysilane (FAS) .....	44
Figure 3.6 Diagram of the experimental set up for sessile droplet experiments: 1 - aqueous droplet with (or without) added salt; 2 - organic phase with (or without) Span <sup>®</sup> 80 surfactant, 3 - hydrophobic support. ....	47
Figure 3.7 Rotating drum system (a) setup 3D view; (b) stainless steel drum; (c) cameras view .....	49
Figure 4.1 Top view of the entry and exit side of a stainless steel membrane with pores of 5 $\mu\text{m}$ (a) entry side – square pore pattern (b) single pore on the entry side (c) exit side – square pore pattern (d) – single pore of the exit side. These pictures were obtained using a SEM – JEOL JSM 7100F.....	52
Figure 4.2 Top view of the entry and exit side of a stainless steel membrane with pores of 10 $\mu\text{m}$ (a) entry side – square pore pattern (b) single pore on the entry side (c) exit side – square	

pore pattern (d) – single pore on the exit side. These pictures were obtained using a SEM – JEOL JSM 7100F.....	53
Figure 4.3 Top view of the entry and exit side of a nickel membrane with pores of 10 $\mu\text{m}$ (a) entry side – triangular pore pattern (b, c) single pore on the entry side (d) exit side – triangular pore pattern (e, f) – single pore on the exit side.....	54
Figure 4.4 Pore size distribution of a 5, 10 and a 20 $\mu\text{m}$ stainless steel membrane determined by optical microscopy and Image J analysis.....	56
Figure 4.5 $\Theta_{\text{app}}$ monitoring water drop contact angle on metal sheets that were exposed to 4M NaOH (“alkali”), 2% wt. citric acid or 10% wt. HCl over a variable drying period. ....	57
Figure 4.6. Apparent contact angle ( $\Theta_{\text{app}}$ ) measurements of sessile water drops on stainless steel sheets that were “FAS treated” using different concentrations of 1H,1H,2H,2H-Perfluorododecyltriethosylsilane (0.0001M, 0.001M, 0.01M and 0.1M) in undecane for various periods of time (1-7 days) at room temperature. As control, the presence of FAS chemical was avoided, exposing the surface only to undecane. The stainless steel used in the set named “0.01M No HCL” was not cleaned using HCl, all the others were. ....	58
Figure 4.7. Apparent contact angle ( $\Theta_{\text{app}}$ ) measurements of sessile water drops on stainless steel sheets that were “FAS treated” using a concentration of 0.01M of 1H,1H,2H,2H-Perfluorododecyltriethosylsilane in undecane for 4 hours and 24 hours at 45°C. ....	59
Figure 4.8. Image of a sessile water drop on a hydrophobic stainless steel (FAS treated) surface: (a) in vapour and (b) in kerosene, illustrating the interfacial tensions involved.....	60
Figure 4.9 Contact angle measurements before and after of 5 stainless steel sheets being exposed for 24 hours to different aqueous solutions: water, 4M NaOH and 2% wt. citric acid. ....	61
Figure 4.10. w/o emulsions produced using (a-PTFE) a new PTFE coated membrane, (b-PTFE) PTFE coated membrane after 4 uses, (c- FAS) a new FAS treated membrane and (d- FAS) a FAS treated membranes after 4 uses.....	62
Figure 4.11 The structures of surfactants: a) Tween <sup>®</sup> 20 and b) Span <sup>®</sup> 80. ....	63
Figure 4.12 a) CMC determination of Tween 20 by measuring equilibrium surface tension using the pendant drop method. b) Equilibrium interfacial tension measurements between (commercial) sunflower oil and water with different Tween <sup>®</sup> 20 concentrations. ....	64
Figure 4.13 Interfacial tension between drop phases: ● pure water; ○ saline water (10% (w/w) NaCl) and ▲ 13.5% (w/w) PVA in water) and surrounding phase that contained different surfactant (Span <sup>®</sup> 80) concentrations present in kerosene using pendant drop technique.....	64

Figure 4.14 Dynamic interfacial tension determined by pendant drop method between distilled water (a) or 13.5% wt. PVA in water (b) and kerosene that contained different concentrations of Span <sup>®</sup> 80 dissolved: 0.1, 0.25, 0.5, 0.75, 1, 5, 10 and 30 mM plotted as a function of aging drop time. ....	65
Figure 4.15 Contact angles of three different drop phases (● pure water; ○ salty water (10% (w/w) NaCl) and ▲ 13.5% (w/w) PVA in water) surrounded by different surfactant concentrations present in kerosene on a non-treated (hydrophilic) stainless steel sheet. These measurements were performed using the DSA 100.....	68
Figure 4.16 Liquid drop on a solid surface showing the interfacial tensions at the three phase contact line. ....	68
Figure 4.17 Dynamic advancing and receding contact angles against rotation speed for different surfactant concentrations (three phase contact: hydrophobic drum, vapour and water in the presence of Tween <sup>®</sup> 20). ....	70
Figure 4.18 Dynamic advancing and receding contact angles against rotation speed for different surfactant concentrations (three phase contact: hydrophobic drum, vapour and water in the presence of Pluronic <sup>®</sup> L-35).....	71
Figure 4.19 Schematic representation of the region around the three-phase contact line [82]. ....	72
Figure 4.20 Dynamic advancing and receding contact angles against rotation speed using two different drums (hydrophilic, no modification, and hydrophobic treated) half immersed in water and kerosene without presence of surfactants.....	74
Figure 4.21 Dynamic advancing and receding contact angles against rotation speed for different surfactant concentrations (three phase contact: hydrophobic drum, kerosene and water in the presence of Tween <sup>®</sup> 20).....	75
Figure 4.22 Dynamic advancing and receding contact angles against rotation speed for different surfactant concentrations (three phase contact: hydrophilic drum, kerosene in the presence of Span <sup>®</sup> 80 and water).....	76
Figure 4.23 Pictures of advancing and receding contact angle between the organic phase (OP) and the aqueous phase (AP) before and after film formation for concentrations above 12.5% of the CMC in the OP using a hydrophilic drum. ....	77
Figure 4.24 Example of the surfactant concentration influence on the self-emulsification process: each vial contains 10 mL of water (lower liquid layer) and 10 mL of kerosene (top liquid layer) with different concentration of Span <sup>®</sup> 80: samples BW, BX, BY and BZ contain	

pure water, 1.14, 11.4 and 114 times the CMC, respectively. There is no visible detection of microemulsion formation in vials BW and BX, but they are present in vials BY and BZ.....	80
Figure 4.25 Formation of a cloud of nano-sized droplets and a film at the droplet base assisted by swollen micelles present in the organic phase (kerosene). .....	82
Figure 4.26 Influence of surfactant concentration on the water sessile droplet solubilisation in to the surrounding phase .....	83
Figure 4.27 Schematic representation of spontaneous emulsification being driven by the swollen micelles.....	83
Figure 4.28 Influence of salt in the aqueous phase on the drop volume evolution.....	84
Figure 5.1 Influence of two different injection rate used on the droplet size ( $d_{50}$ ) and on droplet size distribution (CV) as a function of surfactant concentration. ....	86
Figure 5.2 Droplets formed during injection of 13.5% PVA solution at $0.2 \text{ mL min}^{-1}$ in to kerosene with 50 mM Span <sup>®</sup> 80 concentration using a surface shear of 5.8 Pa using a (non-treated) hydrophilic membrane, i.e., relying on the surfactant present in the organic phase to wet membrane and avoid its dewetting by the (aqueous) dispersed phase.....	87
Figure 5.3 SEM pictures of freeze dried PLGA particles.....	89
Figure 5.4. Median droplet diameters ( $\circ$ ) and coefficient variation (CV) values ( $\bullet$ ) of PVA droplets in kerosene as a function of concentration of Span <sup>®</sup> 80 for a (constant) flow of $1 \text{ mL min}^{-1}$ during membrane emulsification of a FAS treated metal (nickel) membrane. Error bars are reported showing the standard deviation of the measurements. Note the CMC of Span <sup>®</sup> 80 in kerosene is less than 1 mM (see section 4.5.2). .....	91
Figure 5.5. Droplets formed during injection of 13.5% wt. PVA solution at $1 \text{ mL min}^{-1}$ in to kerosene with 40 mM Span <sup>®</sup> 80 surfactant concentration using a surface shear of 7.3 Pa.....	92
Figure 5.6. Estimated interfacial tension values for 13.5% wt. PVA solution injected in to kerosene for experiments performed at an injection rate of $1 \text{ mL min}^{-1}$ . .....	93
Figure 5.7. (a) Dynamic interfacial tension determined by pendant drop method of distilled water in kerosene that contained different concentrations of surfactant (Span <sup>®</sup> 80) dissolved: 0.1, 0.25, 0.5, 0.75, 1, 5, 10 plotted according to eq. 5.2; with (b) inset showing surfactant adsorption coefficient for the different surfactant concentrations tested. ....	94
Figure 5.8. (a) Dynamic interfacial tension determined by pendant drop method of 13.5% PVA in kerosene that contained different concentrations of surfactant (Span <sup>®</sup> 80) dissolved: 0.1, 0.25, 0.5, 0.75, 1, 5, 10 and 30 mM plotted according to eq. 5.2; with (b) inset showing surfactant adsorption coefficient for the different surfactant concentrations tested. ....	95

Figure 5.9. Drop frequency against fraction of active pores for a PVA drop size of 35.8  $\mu\text{m}$ .  
 .....96

Figure 5.10 Oscillation wave form profiles used in the experiments .....99

Figure 5.11 Photographs of emulsions produced using different operational parameters: (a) and (b) use compound cosine wave form (c) and (d) use a sinusoidal wave form. ....99

Figure 5.12 (a) Droplet size and (b) Coefficient of variation (CV) as a function of shear stress at different injection rates. Two different wave forms were testes: compound modified cosine wave form (“cos wave”) and sinusoidal wave form (“sine wave”). ..... 101

Figure 5.13 (a) Droplet size and (b) Coefficient of variation (CV) as a function of shear stress obtained with same shear stress using different combinations of displacement and frequency: Sine waves I and II use data obtained under conditions reported in Table 5.3 and Table 5.4, respectively. .... 102

Figure 5.14 Droplet size and CV variation as a function of oil phase in emulsion concentration using a sinusoidal wave form..... 104

Figure 5.15 Drop size and drop size distribution evaluation as a function of injection time. 105

Figure 5.16 Median particle diameters and coefficient variation (CV) values of PCL/DCM droplets in water/PVA as a function of maximum shear stress for a (constant) superficial velocity of  $57.7 \text{ L m}^{-2} \text{ h}^{-1}$  during membrane emulsification using a  $15 \mu\text{m}$  pore size stainless steel membrane. .... 108

Figure 5.17 Drop size and drop size distribution evaluation over a 45 min injection and microscope pictures of the w/o emulsions produced. .... 109

Figure 5.18 Drop size and drop size distribution evaluation over a 45 min injection and microscope pictures of the multiple (w/o/w) emulsions produced. .... 110

Figure 5.19 Pressure readings for different interstitial velocities tested using sunflower oil as dispersed phase and comparison with the estimated pressure based on Dagan method and capillary pressure. .... 112

## LIST OF TABLES

Table 4.1 Pore size characterization of a 5, 10 and 20 $\mu\text{m}$ membrane determined by optical microscopy and Image J analysis.....	55
Table 4.2: Static contact angles obtained from sessile drop experiments using the DSA 100. The error value reported is the standard deviation from at least three measurements performed. ....	67
Table 4.3 Droplet concentration with salt and surfactant concentration during the spontaneous formation of aqueous droplets in kerosene determined by Nanosight size analyser. ....	80
Table 4.4 Aqueous droplet size with salt concentration in the aqueous phase and surfactant concentration in the organic phase determined by Nanosight size analyser.....	81
Table 5.1 Test parameters used to produce o/w emulsions with the Dispersion Cell .....	88
Table 5.2 Particle sizing analysis of the tests performed using conditions showed in Table 5.1 .....	88
Table 5.3 Operational conditions tested in the comparison of two wave forms.....	98
Table 5.4 Operational conditions tested in the shear stress evaluation.....	101
Table 5.5 Operational conditions tested in the oil loading test.....	103
Table 5.6 Operational parameters and representative pictures of the o/w emulsions obtained for each condition tested.....	107
Table 5.7 Membrane proprieties which determines its porosity and influences the maximum flow rate achievable for a certain interstitial velocity ( $30 \text{ L s}^{-1}\text{m}^{-2}$ ). ....	114
Table 5.8 Dispersed phase Capillary number, Reynolds number, Weber number are determined for a dispersed velocity of $30 \text{ L s}^{-1} \text{ m}^{-2}$ , a resultant drop size of $30 \mu\text{m}$ from $5 \mu\text{m}$ pore diameter. Ohnesorge number, Bond number and ratio between dispersed phase weber number and critical weber number are also determined for the same system. Sunflower oil was the liquid considered to be the dispersed phase in this exercise.....	116

## LIST OF SYMOBLS

$\Delta A$	Interface	m
$a$	Amplitude	m
$A_p$	Area of a single pore	m <sup>2</sup>
$A_s$	Surface (active) area	m <sup>2</sup>
$A_\Delta$	Area of the triangular array	m <sup>2</sup>
$b$	Blade height	m
$Bo$	Bond number	-
$c$	Surfactant concentration	mol m <sup>-3</sup>
$Ca_d$	Capillary number of the dispersed phase	-
$C_s$	Subsurface concentration of surfactant	mol m <sup>-2</sup>
$D$	Diffusion coefficient	m <sup>2</sup> s <sup>-1</sup>
$D_l$	Adsorption coefficient	s <sup>-1</sup>
$d_f$	Drop frequency	s <sup>-1</sup>
$f$	Frequency	Hz
$g$	Gravitational acceleration constant	m s <sup>-2</sup>
$h$	Height	m
$J$	Diffusion flux	m <sup>2</sup> s <sup>-1</sup>
$K_b$	Boltzmann's constant	m <sup>2</sup> Kg s <sup>-2</sup> K <sup>-1</sup>
$L$	Thickness of the pore	m
$M$	Molecular weight of the entire molecule	g mol <sup>-1</sup>
$M_h$	Molecular weight of the hydrophilic portion of the molecule	g mol <sup>-1</sup>
$n$	Number of pores	
$n_b$	Number of blades	-
$Oh$	Ohnesorge number	-
$P_c$	Capillary pressure	Pa
$Q$	Volumetric flow	L h <sup>-1</sup>
$r$	Radius	m
$Re$	Reynolds Number	-
$Re_d$	Reynolds number of the dispersed phase	-
$r_p$	Pore radius	m



$r_{trans}$	Transitional radius	m
$S$	Stirrer width	m
$T$	Tank width	m
$t$	Time	s
$v_o$	Peak velocity	$\text{m s}^{-1}$
$We$	Weber number	-
$We_c$	Critical Weber number	-
$We_d$	Weber number of the dispersed phase	-
$x$	Droplet diameter	m
$\Delta G$	Gibbs free energy	J
$\Delta P$	Drop pressure	Pa
$\Delta S$	Entropy	$\text{J K}^{-1}$
$\tau_{max}$	Maximum shear stress	Pa
$v_d$	Interstitial velocity	$\text{L s}^{-1} \text{m}^{-2}$

## Greek symbols

$\Gamma$	Surface excess concentration	$\text{mol m}^{-2}$
$\gamma$	Interfacial tension	$\text{N m}^{-1}$
$\omega_f$	Angular frequency	$\text{rad s}^{-1}$
$\mu_c$	Continuous phase viscosity	$\text{Pa s}$
$\mu_d$	Dispersed phase viscosity	$\text{Pa s}$
$\gamma_{\text{eq}}$	Equilibrium interfacial tension	$\text{N m}^{-1}$
$\gamma_{\text{lv}}$	Liquid-vapour	$\text{N m}^{-1}$
$\gamma_{\text{mo}}$	Interfacial tensions of the membrane / oil	$\text{N m}^{-1}$
$\gamma_{\text{mw}}$	Interfacial tensions of the membrane / water	$\text{N m}^{-1}$
$\gamma_{\text{sl}}$	Solid liquid interfacial energy	$\text{N m}^{-1}$
$\gamma_{\text{sv}}$	Solid-vapour	$\text{N m}^{-1}$
$\gamma_{\text{wo}}$	Interfacial tension between water / oil	$\text{N m}^{-1}$
$\delta$	Boundary layer thickness	$\text{m}$
$\Theta$	Contact angle	$^{\circ}$
$\mu$	Viscosity	$\text{Pa s}$
$\rho$	Density	$\text{g m}^{-3}$
$\sigma$	Standard deviation	-
$\tau$	Shear stress	$\text{Pa}$
$\Phi$	Porosity of the membrane	-
$\varphi_c$	Surfactant molecule concentration	$\text{mol m}^{-3}$
$\omega$	Angular velocity	$\text{rad s}^{-1}$

## **LIST OF ABBREVIATIONS**

API	Active pharmaceutical ingredient
BSA	Bovine Serum Albumin
CMC	Critical micelle concentration
CV	Coefficient of variation
D50	Median size
DCM	Dichloromethane
DSA	Drop shape analyser
FAS	Fluoroalkylsilanes
FDA	Food and Drug Administration
HLB	Hydrophilic-Lipophilic Balance
o/w	Oil-in-water
o/w/o	Oil-in-water-in-oil
PCL	Polycaprolactone
PEEK	Poly Ether Ether Ketone
PLA	Poly(lactic acid)
PLGA	Poly(lactic-co-glycolic acid)
PTFE	Polytetrafluoroethylene
PVA	Poly(vinyl alcohol)
R&D	Research and development
Span <sup>®</sup> 80	Sorbitan monooleate
SPG	Shirasu Porous Glass
Tween <sup>®</sup> 20	Polyoxyethylene (20) sorbitan monolaurate
w/o	Water-in-oil
w/o/w	Water-in-oil-in-water

## Chapter 1 INTRODUCTION

### 1.1. Motivation for research

Static and dynamic wetting of solid surfaces by complex fluids, is a key aspect of the process of membrane emulsification. This process produces uniformly sized droplets at a specified target size within the micron range and above. Microfluidics is another process capable of producing uniform emulsions, however it does not have the same potential to achieve high productivities to be adopted in an industrial process (e.g. manufacturing). Therefore, membrane emulsification holds great potential and interest for industrial use by replacing conventional emulsification techniques. However, in practice, this adoption by industry has been slow mostly due to a lack of understanding and poor use. Besides this, reliability and reproducible operation also negatively impacts its reputation. Despite the clear advantages of membrane emulsification, formulation is still key in the emulsification process. Thus, this research project was focused to facilitate the optimization of membrane emulsification for various possible systems:

- oil-in-water (o/w) where the dispersed phase can have a lower or higher density than the continuous phase which brings different engineering aspects to the process;
- water-in-oil (w/o) emulsion where it has been conventionally accepted that a membrane with a hydrophobic surface is needed to produce water droplets, which are more difficult to stabilise and have a greater tendency to wet the membrane surface;
- multiple water-in-oil-in-water (w/o/w) emulsion which increase drastically the viscosity of the dispersed phase and needs to be very stable in order to guarantee the control of the process during the injection (and good encapsulation performance).

Another aspect that is slowing down interest from industry in membrane emulsification is wide use of materials that are not commonly used in industry due to fragility and resistance such as ceramics and glass. In this research project, only metal membranes will be used which are acceptable for the clear majority of processes that involve emulsification at industrial scale. Formulations used in this research project were chosen due to possible applications in encapsulated particles for drug, or other ingredient, that needs to be protected and/or controlled delivery, or PVA beads used for medical diagnostic kits and cosmetic formulations.

## 1.2. Aim and objectives

The aim of this research project is to contribute to the understanding of the interaction of complex liquid systems with the porous membrane used to generate emulsions, and the interfacial tension variation due to the different operational conditions used. As part of this, an optical rig was constructed to study the dynamic interaction between solid surfaces and complex fluids, with and without the presence of surfactant.

The research objectives were defined as:

- To determine the mechanisms of interaction of complex liquid system with porous membranes used for membrane emulsification
- To develop an alternative hydrophobic coating/treatment on the metal porous membrane that would allow the generation of uniform w/o emulsions, have a minimal cost to apply, provide adequate stability/durability and determine if metal porous membranes can be recoated/retreated after losing its hydrophobicity
- To investigate whether hydrophilic surfaces can preferably be wetted by the organic phase, assisted by the surfactant, even when an aqueous phase is present and, vice versa, hydrophobic surfaces can preferably be wetted by the aqueous phase, assisted by the surfactant, even when an organic phase is present.
- To develop a method capable of estimating the number of active pores during membrane emulsification process.
- To test with different formulations the capability of a novel azimuthally membrane oscillation system to produce uniform size emulsions over long periods of time continuously, taking in to account the above objectives.

## 1.3. Thesis structure

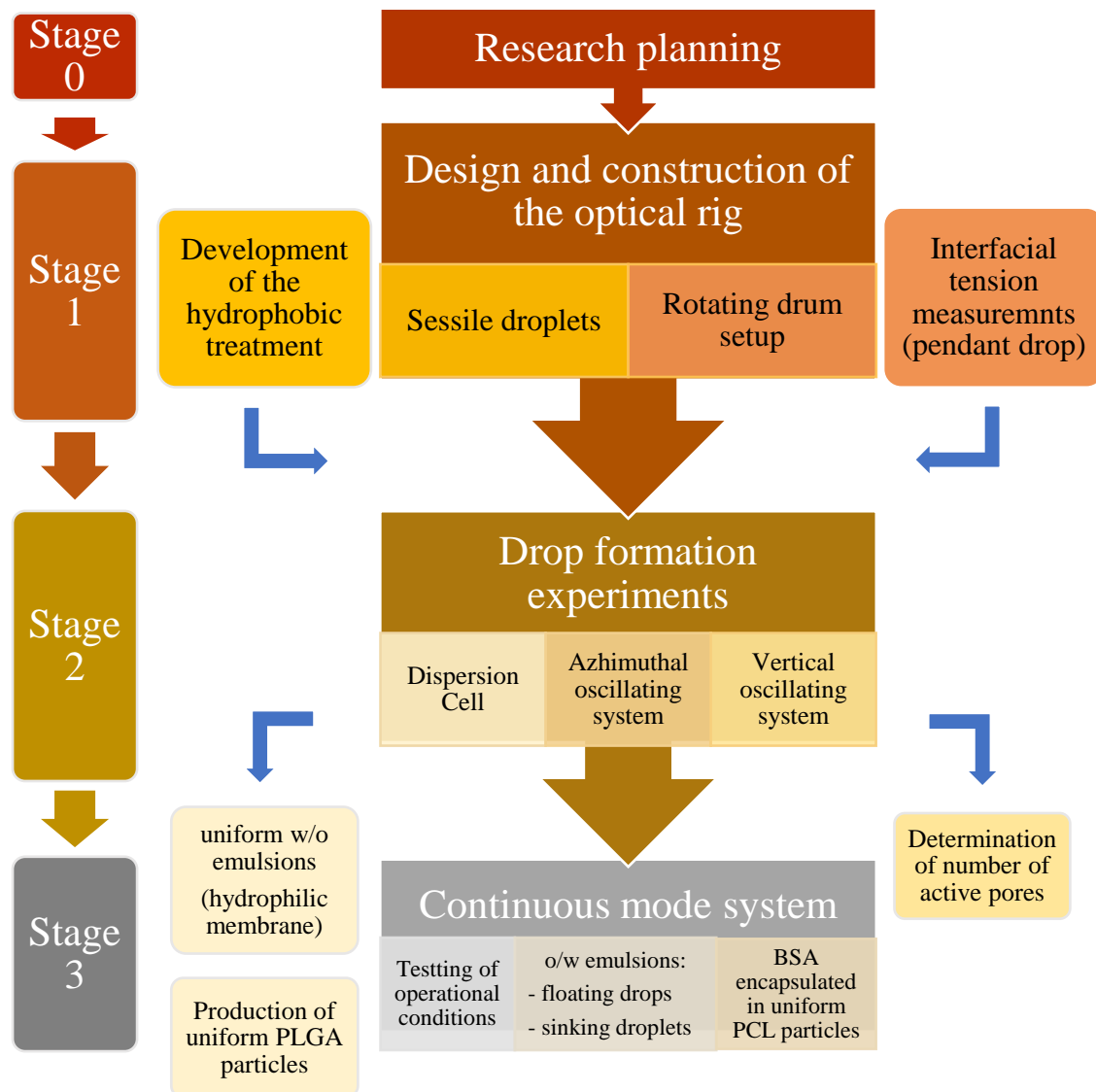


Figure 1.1 Flow chart of the thesis structure

The chart shown in Figure 1.1 represents this research project in four different stages. Stage 0 consisted of finding gaps in literature and understanding how they can be filled with understanding of the mechanisms involved between complex liquid systems and porous metal membranes during the process of membrane emulsification. Stage 1 was an exercise in determining the instruments available to measure interfacial tension, designing and constructing new rigs to perform static and dynamic contact angle measurements and develop an alternative to the current method to hydrophobize the metal porous membranes. In Stage 2 drop formation experiments were designed and performed to complement and verify the results

achieved during stage 1 using the suitable membrane emulsification devices available. Last but not least, in Stage 3, the azimuthally oscillating membrane emulsification system was fully tested varying the operational conditions as well as formulations used and assess its reliability and reproducibility in a continuous mode for droplet production under demanding operational conditions; e.g. high dispersed phase content and multiple emulsions (w/o/w).

## Chapter 2 LITERATURE REVIEW

Emulsion technology is relevant to a wide range of industries and commercial emulsions are formulated to suit a scope of physical, chemical and biological requirements. Many investigations have been reported and knowledge has been acquired and is available on the process of emulsion formation. However, the basic knowledge and industrial challenges does not quite match, i.e., basic knowledge refers to rather idealized and simple systems while an emulsion industrial expert works with complex materials, answering complex requirements, perhaps conflicting, to arrive at the final formulation and equipment specification.

Emulsions are constituted by a dispersed phase (droplets) and a continuous phase (liquid surrounding the droplets). Energy input is required, generally mechanical, to “emulsify” the dispersed phase in the continuous phase and to create the additional interfacial area. Stabilisation of the produced droplets is then required, to avoid coalescence to the thermodynamically more stable condition of minimal interfacial surface area.

The Gibbs free energy increase of the system ( $\Delta G$ ), at constant composition and pressure, after mixing is as follows:

$$\Delta G = \gamma \Delta A - T \cdot \Delta S , \quad \text{eq. 2.1}$$

where  $\Delta S$  is the entropy increase,  $\Delta A$  is the increase of the interface,  $T$  is temperature in Kelvin and  $\gamma$  is the interfacial tension. With increase of the interfacial area, the interface free energy increases, and the system tends to become thermodynamically unstable leading to the recombination of droplets, back to the bulk liquids, ending in phase separation to a two-phase liquid. Emulsification is therefore treated as two independent problems, (a) the formation of new droplets and (b) the stabilization of the droplets once they are produced. The interest of this work lies in forming uniform droplets which on its own will contribute to a more stable system, avoiding ‘ripening’ effects. In short, the destabilization of an emulsion goes through several consecutive and parallel steps before reaching phase separation, starting with flocculation which can lead to coalescence. In parallel, creaming or sedimentation phenomena



can occur which can enhance coalescence. Emulsion stability is described in great depth by Johan Sjöblom [1].

In the clear majority of cases, emulsions are formed by surfactants (surface active agents) which are located at the interface between droplets and continuous phase, lowering the interfacial tension and, therefore, decreasing the free energy for formation as well as stabilizing the two-phase system. In emulsification processes, surfactants are often called emulsifying agents and they consist in amphiphilic molecules, i.e., with hydrophilic head, oriented to the aqueous phase, and hydrophobic tail, oriented to the organic phase. Besides interfacial tension, surfactants affect (increase) surface elasticity [2]. Surfactants can be divided in two main categories: ionic or non-ionic. Ionic (anionic or cationic) surfactants enhance emulsion stability by electric double layer repulsions (electrostatic stabilization) while non-ionic surfactants (e.g. polymeric surfactants) enhance emulsion stability by steric repulsions. Electrosteric stabilization is another mechanism of stabilization which combine electrostatic and steric repulsions and are especially effective in aqueous dispersions and inks [3].

Surfactants can be classified according to the Hydrophilic-Lipophilic Balance (HLB), first introduced by Griffin (1949). This classification is used to identify the surfactants suitable to produce water in oil (w/o) emulsion (oil soluble surfactants,  $3 < \text{HLB} < 6$ ) or oil in water (o/w) emulsion (water soluble surfactants,  $8 < \text{HLB} < 16$ ). Griffin's method for non-ionic surfactants as described in his 1954 work as follows:

$$\text{HLB} = 20 \left( \frac{M_h}{M} \right), \quad \text{eq. 2.2}$$

Where  $M_h$  is the molecular weight of the hydrophilic portion of the molecule and  $M$  is the molecular weight of the entire molecule, giving a result between 0 and 20 [4]. In this work, only non-ionic surfactants were used: Tween<sup>®</sup> 20 (polyoxyethylene (20) sorbitan monolaurate, water soluble), Span<sup>®</sup> 80 (sorbitan monooleate, oil soluble) and poly(vinyl alcohol) (PVA, water soluble, polymeric surfactant).

Currently, several industries rely on conventional emulsification techniques. Mixers, colloid mills or homogenizers are some common apparatus to produce emulsions on a large scale. Sonic and ultrasonic methods can also be found in industry, but to a lesser extent [5, 6]. These

devices require energy not only to create new interfaces, but also to move the liquid against viscous resistance in the emulsifying apparatus. Naturally, the energy required for a certain device will depend upon several factors, like the amounts, nature and viscosity of the liquids, their interfacial tension, the surfactant used, drop size aimed for and final concentration of the emulsion, apart from the design of the machine. In general, it is widely accepted that simple mixers use substantially less power than colloid mills, or homogenizers, but often the minimum droplet size that can be achieved is too large [7].

During the early 1990's, the production of an emulsion using a microporous membrane developed in popularity as a laboratory study, after a publication by Nakashima et al. [8]. This process became known as membrane emulsification, in which a liquid dispersed phase is injected through the pores of a membrane, into a continuous liquid phase. This technique is discussed in section 2.1 and used throughout, the experimental work. Later, in 2004, Nisisako et al. [9] used a new approach to produce emulsions, based on a microfluidic system. Briefly, two immiscible fluids are injected into separate micro-channels ending in a junction where one liquid is forced into the other one, forming droplets, individually. Membrane emulsification and microfluidics systems are often considered “drop by drop” emulsification methods, providing control over the emulsion size produced. Overall, these “drop-by-drop” techniques require less energy input compared to the conventional emulsification methods (Figure 2.1). For instance, in membrane emulsification, the energy input per unit volume is in the range of  $0.05\text{-}5\text{ kJ dm}^{-3}$ , which is 1-2 order of magnitude smaller than in high-pressure valve homogenizers ( $3\text{-}20\text{ kJ dm}^{-3}$ ) [10] being considered a “low energy” process [11, 12].

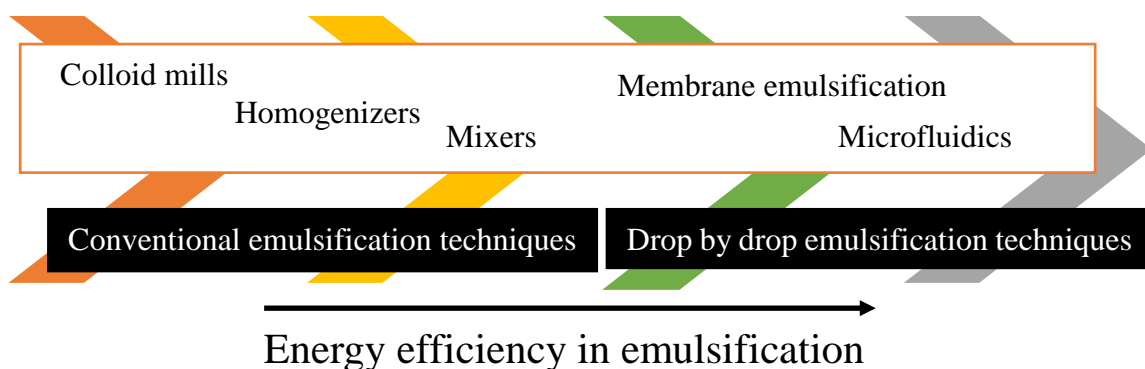


Figure 2.1 Power requirement of emulsifying machinery.

A third technique can be inserted in the “drop-by-drop” emulsification methods category: ultrasonic breakage. Berkland, Kim, Varde and Pack [13, 14] present the production of monosize polymer particles by the ultrasonic breaking of a stream. The dispersed phase flows through a vibrating nozzle which disrupts the jet into droplets using an ultrasonic (piezoelectric) transducer at a desired frequency. The droplets flowed into a beaker that will contain the continuous phase with surfactant. A wide range of drop sizes has been reported, from 10 to 500  $\mu\text{m}$ . Using this approach, double walled particles can be produced by adding an annular flow around the main stream nozzle [15, 16].

Regarding low shear handling products, “drop by drop” emulsification techniques stand out. They offer control over the droplet formation and operate under mild shear stress conditions. Formulation and process parameters are still key factors i.e., combination of parameters such as (dynamic) interfacial tension, type of surfactant, wetting characteristics of material used and viscosity of both liquids can be very important. Therefore, an erroneous choice of these parameters might make the difference between highly uniform, or very polydisperse, emulsions. Comparing the two most common “drop by drop” techniques, microfluidics systems are able to provide higher uniformity drops while higher throughputs are achieved with membrane emulsification.

Emulsions have applications in food, cosmetic, medical, pharmaceutical and chemical industries. The size and size distribution as well as formulation of the droplets play an important role in many applications. Therefore, the possibility to control the size and achieve high throughputs required in industry is of great importance [17]. Based on that fact, membrane emulsification will be thoroughly studied in this thesis, using distinct formulations with different membrane emulsification devices resulting in different process challenges, or offering different solutions, to investigate the engineering of scaling solutions from laboratory to practical throughputs. Thus, membrane emulsification will be evaluated to see if it is a viable alternative emulsification technique for the numerous industries that are interested in improving product quality, performance and, possibly, reducing manufacturing costs.

Emulsification is a common approach to manufacture different types of particles where the (liquid) drops form an early-stage of the process and, downstream, certain post-processing techniques are used to solidify the particles. Therefore, emulsions are used as precursors to prepare polymeric particles, polysaccharide particles, oil-filled microcapsules and inorganic particles in a wide range of sizes. In general, the post-processing techniques required to

fabricate the particles are well known. Therefore, they can be applied or adjusted to any emulsion regardless the chosen emulsification technique. Thus, uniform sized particles are expected to be obtained after producing uniform emulsions.

Emulsion-solvent evaporation is one of the most common methods for production of polymeric particles. Biocompatible polymeric materials such as non-biodegradable hydrophobic polymers [18], and synthetic biodegradable polymers have been widely used as carriers for drug delivery [19]. Biodegradable polymers have been mainly used in the form of spherical particles, since they offer high surface area for adhesion and drug release and a low drag force during mobility in fluids. The most common biodegradable synthetic polymers are poly(lactic acid) (PLA), poly(lactic-co-glycolic acid) (PLGA)[20], and polycaprolactone (PCL) [19, 21], due to their approval by FDA (Food and Drug Administration)[22] and environmental friendly nature. One of the parameters that can be tuned to achieve a desirable drug release rate and meet different dosage requirements is the particle size.

Polysaccharides (carbohydrate polymers) are found in the nature, synthesized by plants, animals or humans and stored for structural support or metabolized for energy. Due to their structure and/or chemical properties can be used to replace other non-environmental friendly products in a microsphere form. Examples of polysaccharide nature particles:

- Alginate gel beads have been developed as encapsulating systems for drugs and (mammalian) cell therapy because of the alginate biocompatibility, biodegradability, mechanical properties and good mass transfer diffusivity [23]. Alginate is a polysaccharide obtained from brown algae.
- Chitosan microspheres can be used in delivery systems and be pH triggered [24]. Chitosan is a biocompatible natural polysaccharide, derivative of chitin produced from crustacean shells, fungi and insects with mucoadhesive properties [25]. It was used for oral gene delivery, oral vaccination and delivery of proteins and drugs [24, 25].
- Cellulose microbeads are being developed to become a sustainable alternative to various non-biodegradable plastic microparticles, currently used in a wide range of consumer products from toothpaste to paints [11]. Cellulose is the most abundant polysaccharide on Earth, present in the cell wall of green plants as cotton fibre, wood and dried hemp [26].
- Agarose beads are widely used in chromatography columns for protein purification [27]. Various grades of agarose beads are already found in the market produced via conventional emulsification techniques. Agarose is often extracted from certain red seaweed.

Inorganic particles can also be produced by an emulsification route. Silica is an example of an inorganic compound that has been comprehensively investigated [28-30] and considered for a wide range of applications where microspheres of silica offer great potential. Silica has a very well-known surface and its surface modification is well understood. Therefore, after silica particles have been produced in a controlled manner they can be modified and functionalised according to the application requirements and specifications [30].

Many applications require oil-based ingredients to be delivered in such a manner that a barrier to keep their required properties, or triggered release, is desirable. A common approach to tackle such challenge is to perform microencapsulation by applying the complex coacervation technique. “Coacervation” is a unique type of electrostatically driven liquid-liquid phase separation, resulting from the association of oppositely charged macro-ions, or polymers. After emulsifying the oil-based component in a water phase that contains simultaneously (at least) two dissolved charged polyelectrolytes. These polyelectrolytes are identically charged during emulsification but when complex coacervation is initiated, polyelectrolytes are oppositely charged, due to a pH shift, precipitating and surrounding the oil droplets forming a capsule. The wall materials for fabrication of microcapsules can be chosen from a wide range. Gelatine and gum Arabic are the most common used wall materials for complex coacervation [31]. Agrochemicals, animal feed, flavours, fragrances and cosmetics are some businesses that use this approach to develop their products answering their customer needs.

## 2.1 Membrane emulsification

Membrane emulsification is, relatively, a recent technique for producing multiple types of single and multiple emulsions. In this process, the dispersed phase is pushed through a microporous membrane directly into the continuous phase. Droplets formed at the pore outlet are detached at the end of the pores by a drop by drop mechanism. Regardless of the use of oscillating, or stationary, membranes the formation and detachment of the droplets are controlled by the shear force created in the continuous phase on the membrane surface (section 2.1.6). This technology is efficient, with much lower consumption of emulsifier and energy to produce the drops. The shear stress used is much lower when compared to conventional emulsification techniques and, therefore, shear-sensitive ingredients may be used in the formulation, such as drugs and proteins [32].

Membrane emulsification is a technique appropriate for scale-up process development, especially when “made to measure” drop size, low shear use and reasonable throughputs are required. However, some requirements need to be considered before implementing this technique at industrial scale, such as chemical compatibility and use of safe approved materials. Over the years, users of this technique tend to use a hydrophilic porous membrane for production of oil in water (o/w) emulsions, or a hydrophobic porous membrane for production of water in oil (w/o) emulsions [33]. The vast majority of materials used to manufacture these porous membranes have a hydrophilic behaviour [10, 34]. Therefore, hydrophobic treatment of these membranes, or coating, is often used when the aim is to produce w/o emulsions.

Frequently, these treatments/coatings applied have problems with longevity and stability. These are crucial aspects, especially at production scale, which normally require long periods of time. The materials used for surface modification also need to be subject of regulatory approval when the production of food, pharma or medical grade products is aimed for, and this possibly becomes an obstacle for adoption of membrane emulsification.

### 2.1.1 Membranes

One of the key aspects within membrane emulsification processing is the membrane itself. Diverse materials can be selected to manufacture the membranes with various pore size geometries influencing the membrane emulsification process in different ways. The membrane parameters that greatly influence the final drop diameter as well as play a role in the resultant flux are: (i) membrane surface properties (wettability), (ii) (average) pore size, (iii) pore size distribution, (iv) inter-pore distance, (v) shape of pore outlet, (vi) porosity and (vii) thickness [6]. As previously mentioned, membrane surface properties will determine whether it is more suitable to produce o/w emulsions (hydrophilic membrane) or w/o emulsions (hydrophobic membrane) and influence the mechanical and chemical resistance of the membrane. Most academic studies use membranes made from ceramics (e.g. alumina oxides) [35-38], silicon [39, 40] or glass (e.g. Shirasu Porous Glass, SPG) [41, 42], surfaces that are naturally hydrophilic, but can be rendered hydrophobic by various treatments. However, there are no reported appreciable manufacturing processes using these techniques, due in part to their low mechanical resistance and pore channel structure that tends to foul with deposited material during use in production. As an alternative, metal microsieves, originally used in filtration

processes [43] are being successfully adopted as metal membranes in membrane emulsification. Nickel and stainless steel membrane types are commonly reported in the literature [44-50]. However, utilizing nickel membranes is not favoured because nickel ions are considered undesirable in food, or pharmaceutical processes at some concentration. In addition, the material selection will determine the membrane fabrication process. Regarding the type of material, a suitable technique must be used to fabricate the pores in order to obtain a good pore shape, e.g. circular or low aspect ratio slotted pores, and a distance between the pores large enough to avoid the contact of droplets whilst they are growing in order to avoid coalescence [51]. Thus, a wide pore size distribution will provide a wider droplet size distribution, and a larger pore size will result in the production of larger droplets [12, 52].

In literature can be found a linear relation between the membrane pore diameter and the average droplet diameter in membrane emulsification:

$$D_d = cD_p \quad \text{eq. 2.3}$$

Where  $D_d$  is the average droplet diameter,  $D_p$  is the average pore diameter, and  $c$  a constant related to the membrane structure and material. Using SPG membranes,  $c$  values range between 2 and 10 while using other types of membrane with a less regular pore structure can range between 2 and 50 [34, 53].

Generally, at industrial scale, metal membranes are more appropriate, mostly because they are less fragile than ones made from ceramics, silicon or glass and present good mechanical and chemical resistance. Furthermore, stainless steel membranes can be submitted to long sterilisation cycles without being deformed which is often required to produce pharma grade products. Besides that, certain characteristics of these microsieve type membranes can be easily tuned such as thickness, porosity and pore size. Due to the production methods of SPG and  $\alpha$ - $\text{Al}_2\text{O}_3$  membranes, it is not possible to choose the porosity independently of the thickness [6].

### 2.1.1.1 Hydrophobization of metal membrane surface

As mentioned before, the vast majority of materials used to manufacture membranes for membrane emulsification technology are hydrophilic and, therefore, they are often rendered hydrophobic, when it is required to produce w/o emulsions (or, oil-in-water-in-oil (o/w/o) emulsions). Different techniques have been used to perform the surface modification. SPG membranes can be hydrophobized by chemical reaction using organosilane compounds [54] while silicon nitride membranes surface can be modified via chemical vapour deposition [55]. Ceramic and nickel membranes can also be made hydrophobic by applying a polytetrafluoroethylene (PTFE) layer, because PTFE has a low surface free energy [56, 57]. This has the disadvantage of being a physical coating and therefore susceptible to “wearing” and, typically, short use which is far from ideal in a multiple use and/or long run applications. Rough micro/nano structures on a hydrophobic surface provide another means to increase the dispersed phase contact angle and consequently increase its hydrophobicity. The link between surface roughness and the measured contact angle is given by the Wenzel equation:

$$\cos(\theta_{app}) = r \cos(\theta) \quad eq. 2.4$$

with the average roughness ratio  $r$ , given as the factor with which the solid-liquid interface is increased due to roughness [58-60].  $\theta$  is the contact angle as defined for ideal smooth surfaces in the Young equation (section 2.1.3) and  $\theta_{app}$  is the apparent contact angle which corresponds to the stable equilibrium state. When dealing with a heterogenous surface, the Wenzel model is not sufficient and a more complex model is needed. This heterogenous surface is considered using the Cassie-Baxter equation [61, 62]. Wenzel and Cassie-Baxter are the two main models that attempt to describe wetting of textured surfaces. However, these equations can only apply when the drop size is sufficiently large compared with the surface roughness scale [62].

Roughness will increase the surface area, and air, or oil continuous phase, will be trapped between the irregularities of the surface, suspending the water drop from the hydrophobic surface such that droplet cannot adhere, but rolls off [28]. However, manufacturing such a



surface adds complexity. Clearly, for commercial operation, coatings must be easy to manufacture, mechanically and chemically resistant, low cost, and long-term stable.

Surfaces that contain available hydroxyl groups can be silanized forming a chemisorbed covalent -Si-O-Si- bond, where the hydroxyl groups attacks and replaces the alkoxy group of the silane [63]. This is a typical approach to render glass membranes hydrophobically [55] but metals should also be able to be hydrophobized by silanization reactions as long as they present an oxide layer. When oxidized, nickel membranes present a nickel oxide layer while stainless steel membranes present a chromium oxide layer. This approach is explored in this work (section 4.1.2). Figure 2.2 demonstrates the process, where an alkoxy group attaches to the surface hydroxyl group and, after a suitable period of time, a network of silanol groups can be chemisorbed onto the metal membrane surface, via the natural oxide coating surface on the membrane. Low surface free energy materials can be achieved using such a treatment employing FluoroAlkylSilane (FAS), which has given rise to what is now known as super-hydrophobic surfaces [64].

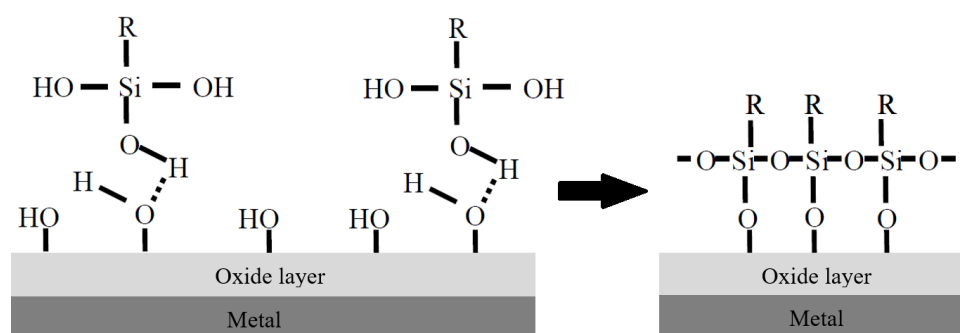


Figure 2.2. Representation of the ideal chemical structure of the fluoroalkylsilane/metallic interphase region  $R = \text{CH}_2\text{CH}_2(\text{CF}_2)_7\text{CF}_3$  (adapted from [65]).

### 2.1.2 Pores & Patterning

Early studies, using different modelling approaches, consider that pore size is directly proportional to final drop size [6, 35, 48, 66]. Besides the pore size diameter, pore distance, pore size distribution, pore array and outlet pore shape are often acknowledged to play an important role, but very difficult to quantify. Initially, in 1998, Williams et al. [12] emphasised

that pore uniformity was crucial to achieve a uniform emulsion. Later, Abrahamse et al. [67] and Zhu and Barrow [68] observed that pores can behave differently even if they are well defined. However, it is a fact that even a membrane with a very uniform pore size distribution will have bigger and smaller pores. In principle, the larger pores will be the first activated and, as long the transmembrane pressure is increased, smaller pores may be gradually activated as well.

In the membrane manufacturing process, porosity of the membranes can be controlled and increases with bigger pore sizes and lower distances between pores. To limit coalescence of neighbouring droplets emerging from the pores, the distance between pores should be significantly greater than the target droplet size. However, in some cases, droplet size larger than the distance between the pores has been shown to provide an additional detachment force for the drops, termed “push-off force”, which encourages drop detachment from adjacent pores [49, 69, 70], but the risk of coalescence makes this an unlikely technique to be adopted commercially. For flat membranes with circular pores, porosity is determined by the ratio of the area occupied by pores to the membrane surface area. However, a significant and highly practical unknown factor whenever modelling, or designing, membrane emulsification processes is the number of “active” pores. It is often reported that the number of pores present that participate in a membrane emulsification is very significantly less than the total number of pores present on the membrane [45, 66]. There is no accepted way to be able to predict the number of active pores and limited methods to estimate the value from operating data [37, 55, 66, 71].

The metal membranes (microsieves) used are acknowledged to be easy to clean [30, 72] and no measurable fouling occurred during testing, which is important for a continuous membrane emulsification process. This “sieve type” membrane design is less likely to foul than conventional “matrix” type of membrane due to the lack of internal tortuous pore channels, such as those made from: glass, ceramic and sintered metal membranes [72].

### *2.1.3 Interfacial tension, surface chemistry and wetting*

Interfacial tension plays an important role in the emulsification process and membrane emulsification is no exception. Normally, a greater interfacial tension between the liquids will provide larger droplets [37, 44] because the interfacial tension will provide some level of

resistance, holding the droplet at the pore. Drops emerging from the membrane will not necessarily experience the equilibrium interfacial tension of the dispersed phase-continuous phase (with surfactant) mixture as the rate of drop growth can be greater than the rate of surfactant adsorption at the emerging interface. This has led to the term dynamic interfacial tension.

From the Young equation, it follows that the wall contact angle is a function of the properties of the solid (metal membrane) and the two immiscible liquids:

$$\cos \theta = \frac{\gamma_{mw} - \gamma_{mo}}{\gamma_{wo}}, \quad \text{eq. 2.5}$$

where  $\gamma_{mo}$  and  $\gamma_{mw}$  are the interfacial tensions of the boundary solid (e.g.: membrane)/dispersed phase (e.g.: oil) and the boundary solid (e.g.: membrane)/continuous phase (e.g.: water), respectively;  $\gamma_{wo}$  is the interfacial tension between the two immiscible liquids (e.g.; water/oil) (Figure 2.3). A lower interfacial tension between the two fluids will, therefore, lead to a smaller wall contact angle.

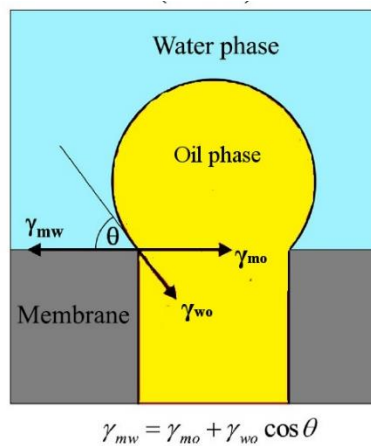


Figure 2.3. Contact angle and the different interfacial tensions involved during drop formation at a membrane pore, adapted from [10].

Surface chemistry is a crucial parameter in membrane emulsification. Knowledge of membrane surface characteristics is required in order to avoid wetting of the membrane surface by the dispersed phase. Once the membrane is wetted by the dispersed phase, the control over the

droplet formation and detachment by the membrane is lost. Some authors [55, 73] have noticed this wetting phenomena, by investigating hydrophilic/hydrophobic surfaces when making o/w emulsions, or w/o emulsions. As a rule, to prevent wetting of the membrane, a hydrophilic membrane surface should be used to produce o/w emulsions whilst a hydrophobic membrane should be used to produce w/o emulsions. Various strategies can be used to change the hydrophobicity/hydrophilicity of a membrane. The chemistry of the system strongly influences the droplet size distribution, especially when there is interaction between the dissolved chemical species and the surface of the membrane, or the forming drops and, therefore, chemical formulation is also a key consideration.

Wetting properties of a system is often characterized by determining the *contact angle* between three phases. There are various methods to characterize the contact angle of a certain system which are selected according to the system aimed to be characterized. The sessile drop method is frequently used for measuring static contact angles between three different phases, e.g., solid, liquid and vapour, but the principle is equally applicable to the interface of two (immiscible) liquids and solid [74, 75]. Experimental observation of the influence of contact angle from drops in a membrane emulsification device is not very straightforward and elaborate approaches must be adopted [76, 77]. The presence of amphiphilic molecules in a solution adds complexity to the problem which affects the wettability of a surface in contact with the solution [78].

Liquid-surface interactions often have been underestimated and considered insufficiently compared with other physical parameters of the membranes, such as, pore size distribution and pore distance. The latter parameters become irrelevant when the surface chemistry is not adequately adjusted [79]. Importance of interactions between liquid-liquid and liquid-solid can be seen in other two phase systems processes such as emulsion separation using membranes [33].

G. K. Auernhammer and his co-workers used a rotating drum setup for studying velocity-dependent wetting/dewetting processes of complex (surfactant) solutions between a solid-gas-liquid interface [80-83]. This was considered a novel approach with the potential to be correlated in this work with the membrane emulsification process where the gas phase can be replaced by an immiscible phase allowing the investigation of wetting properties between two (immiscible) liquids and solid phase, dynamically. Two immiscible liquids can be placed in contact with an identical surface to the porous membranes used in membrane emulsification experiments. In Figure 2.4, a schematic diagram from the side view of the drum is presented.

This in-house built setup allows observation of both sides of the drum (advancing and receding contact angles) when half immersed into two immiscible liquids.

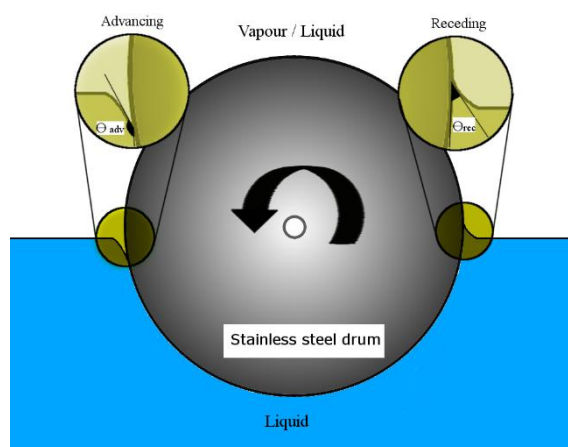


Figure 2.4. Schematic side view of the rotating drum and the resultant advancing and receding contact angle in a half-filled chamber by one (or two, immiscible) liquid(s).

The setup was designed in order to be enable the use of different drums (with same geometries) and be dismantled, or reassembled, with relative ease allowing the full cleaning of the different parts that are in contact with the fluids (see chapter 3.4.1.1).

The natural forms of stainless steel and nickel surfaces are mildly hydrophilic. Therefore, membranes made out of these materials are appropriate to obtain o/w emulsions (or, w/o/w emulsions) without surface treatment. On the other hand, surface properties of stainless steel or nickel membranes can be changed, rendering them hydrophobic, lowering the surface free energy, making them also suitable to produce w/o emulsions (or, o/w/o emulsions) [24, 55, 84].

It is normally postulated that a membrane that is not wetted by the dispersed phase, and ideally fully wetted by the continuous phase, is needed to have control over the droplet formation. Surfactants, used to stabilise the drop formed by the membrane, are complex molecules that may also act as wetting agents for the membrane and, therefore, change the surface properties of that membrane in a way that could be unwanted for the purpose of membrane emulsification. Due to their amphiphilicity, surfactants will diffuse and adsorb to interfaces where they orientate hydrophilic groups towards hydrophilic sites while hydrophobic groups will be towards hydrophobic sites. Surfactant molecules with multiple hydrophilic and hydrophobic sites can rearrange their molecule structure, influenced by concentration [80, 85]. So, these molecules can adsorb to liquid-gas, liquid-liquid interfaces and liquid-solid interfaces.

Therefore, a good knowledge of the interaction of the dissolved components that may help the dispersed phase wet the membrane, and careful control to prevent this, is important. Several authors observed that contact angle depends on both surface properties and on the surfactant used [75, 86, 87]. In this work, different surfactants with different surfaces were studied and investigated to see how they can affect the membrane emulsification process.

#### 2.1.4 Viscosity effects

Fluid behaviour knowledge of both phases during membrane emulsification is important, namely their viscosity, i.e., the resistance to flow of the fluid itself. Viscosity of the dispersed phase will have a great impact on the resultant flux obtained and consequently on the drop formation. In order to allow the use of high viscous liquids, the injection temperature can be raised, but this may promote droplet instability [88].

In addition, viscosity of the continuous phase will also play an important role in the drop formation and its stabilization. In this phase, surfactant is commonly present which is responsible to stabilize the droplets and, therefore, avoid coalescence. Under quiescent i.e. stationary fluid flow conditions, surfactant is transferred by diffusion. This is determined by the concentration gradient and the molecular diffusion coefficient (Ficks Law, Equation 2.6). The diffusion coefficient is inversely proportional to the bulk phase viscosity and the surfactant characteristic length according to the Stokes-Einstein equation (Equation 2.7).

$$J = -D \frac{\partial \varphi_c}{\partial x} \quad \text{eq. 2.6}$$

$$J = \frac{k_B T}{6\pi\mu r} \quad \text{eq. 2.7}$$

where  $J$  is the diffusion flux,  $D$  is the diffusion coefficient,  $\varphi_c$  is the surfactant molecule concentration,  $x$  is the diffusion length,  $K_b$  is Boltzmann's constant,  $T$  is the absolute temperature,  $\mu$  is the viscosity and  $r$  is the characteristic length of the sphere particle. If fluid is flowing, advective transport will enhance the surfactant mobility. Advection depends on the fluid velocity and the concentration of surfactant. In general, advection is more dominant than

diffusion. However, the two mechanisms of diffusion and advection provide an overall convective transport. Advection and diffusion can be related by a dimension number, Péclet number, and is defined as:

$$Pe = \frac{\text{advective transport rate}}{\text{diffusive transport rate}} \quad \text{eq. 2.8}$$

Continuous phase viscosity may vary during the process since the dispersed phase is gradually added over time. So, it can be theorised that the viscosity may increase and, therefore, droplets formed towards the end of process operation experience a higher drag force to those formed within pure surfactant solution at the very beginning. Thus, this can be avoided if single pass is used, i.e., drops are constantly being formed within “fresh” continuous phase solution.

Thus, it is worth to bear in mind that viscosity affects drop formation but, the resultant drop size may not be affected. For example, in the case of continuous phase viscosity increase, the diffusion coefficient will decrease, possibly resulting in higher interfacial tension, which should lead to larger droplets. However, increasing the continuous phase viscosity will result in higher drag force at the membrane surface, leading to small droplets. So, this makes it very difficult to estimate the expected behaviour as it is very dependent on the formulation being used and impossible to generalise for all systems.

Viscosity ratio is a parameter that can be used to characterise and compare the vast variety of formulations used in membrane emulsification. Viscosity ratio is determined by the ratio between the viscosity of the dispersed phase ( $\eta_d$ ) and viscosity of the continuous phase ( $\eta_c$ ). Generally, it is expected that working at high viscosity ratio the droplet size is not influenced. However, the droplet size can be affected at low viscosity ratio where the droplet size increases with decreasing viscosity ratio, until a minimal viscosity ratio at which droplet formation is no longer possible [89]. Van Dijke *et al.* [89] were not able to form droplets below a minimal value of the viscosity ratio 0.48 and above a critical viscosity ratio value of 2, the droplet size was not influenced by the viscosity ratio, for the different formulations tested.

### 2.1.5 Dispersed phase flow and membrane active pores

The superficial velocity, or approach velocity of the dispersed phase, during membrane emulsification can be determined in case dispersed phase flow rate and membrane surface area are known. However, determining the velocity in a pore (interstitial velocity), or “pore velocity”, is far more complicated because many variables (porosity, wetting, dynamic interfacial tension, shear, number of active pores, etc.) of the system may influence the result of this important feature. It is important to determine pore velocity as it will determine whether working conditions are within dripping regime (drops sheared off tangentially to the membrane surface) rather than jetting regime (drops formed by micro-jet break-up). Usually, to provide greater control over drop formation in membrane emulsification, the dripping regime is preferred: formation of drops on the membrane surface and contact angle continuous phase to solid surface  $< 90^\circ$ , where drops are sheared off [44]. However, if pore velocity is increased above a certain threshold, a change occurs from the dripping to the jetting regime. In the jetting regime, a micro-jet of dispersed phase is discharged from the pore, the continuous-membrane contact angle can approach  $90^\circ$  and droplet size is no longer necessarily dependent on the interfacial tension. Transition from dripping to jetting regime occurs above a certain critical capillary number, which is independent of the contact angle [33], but still depends on the formulation used, e.g., viscosity of the continuous phase.

Throughput of the dispersed phase in membrane emulsification is key to the implementation of this process at commercial scale. The throughput is primarily dependent on the transmembrane pressure, pore size, membrane porosity, number of active pores and fluids viscosity. For lower value systems, productivity could be raised by increasing the porosity of the membrane, changing the geometry of the system, or simply injecting at a higher rate accepting a likely loss of uniformity.

Pore size distribution affects the number of active pores and overall system performance. During membrane emulsification process, larger pores will firstly be activated and in case higher transmembrane pressures are experienced, smaller pores will also become active [45]. However, this is difficult to confirm. There is evidence that pore activation occurs randomly, some pores might become active while others may stop [67, 90]. Estimation of number of active pores is of great importance for process design (i.e. productivity) evaluation and modelling purposes.



In this study, a method is developed to estimate the number of active pores based on the dynamic interfacial tension. The objective is to determine, for a set of conditions, when the expansion rate of the drop is equal to the surfactant adsorption rate (see section 5.2). A larger flow rate of dispersed phase will lead to a faster expansion rate of drop formation which will increase the interfacial tension experienced by the drops in their detachment moment, for a given surfactant concentration. However, a larger concentration of the surfactant may reduce that interfacial tension for a given drop formation rate.

### *2.1.6 Shear stress control*

Conventionally, in membrane emulsification, the membrane remains stationary and shear stress is used, to control the drop formation, at the membrane/continuous phase interface by applying crossflow of the continuous phase [91]: higher shear stress provides smaller drops and is obtained by increasing continuous phase flow, which in general, leads to lower dispersed phase concentrations of a product for a “single pass” of the continuous phase over the membrane surface. To overcome this productivity restriction, recirculation of the emulsion can be used. However, when it is desired to produce large droplets, recirculation is likely to result in droplet damage within the pump and other fittings present in the system, leading to poor control over the droplet size distribution, limiting the use of this particular membrane emulsification technique to small emulsion sizes [92], typically less than 10  $\mu\text{m}$ . Alternative methods for generating shear at the membrane surface have been described, using stationary membrane systems where shear stress results from stirring [45], or using pulsed (oscillatory) flow of the continuous phase [44]. Other membrane emulsification systems have been reported using non-stationary membranes, in which case droplet detachment from the membrane surface is promoted by rotating [29, 46, 47, 50, 93] or vibrating [49, 68] the membrane. In non-stationary membranes, shear stress on the membrane surface is controlled by the speed of membrane rotation, or the frequency and displacement of membrane oscillation/vibration. A major advantage of using a non-stationary mechanically driven membrane is that it “de-couples” the control of the drop size by the applied shear from the crossflow of the continuous phase used to remove the product. Hence, in a single pass of continuous phase it is possible to achieve high dispersed phase concentrations of 38% v/v, or more, without recirculation through pumps and fittings [94]. However, the nature of the mechanically driven membrane does have other

consequences. For example, in the case of a fully rotating membrane a centrifugal field will be induced around a rotating membrane; in the most common case of an oil drop being less dense than the surrounding aqueous phase this will induce flow of the oil drop towards the membrane surface, which is not desirable as the concentration of drops at the membrane surface will increase leading to greater chance of coalescence and wetting of the membrane by the oil phase. Furthermore, having high shear consistently applied in one direction will cause deformation of the emerging oil drops, distorting them in one direction, something highly visible in Computational Fluid Dynamic modelling of drops emerging during emulsification [95], which is again likely to lead to membrane surface wetting and poor drop size control.

### 2.1.7 Modelling

#### 2.1.7.1 Dispersed drop size modelling

Earlier studies [48, 49, 94] have showed a good agreement between Equation 2.9 (below) and drop size obtained for low injection rates using membrane emulsification. That modelling is the result of a force balance between drag force and capillary force assuming complete wetting of the continuous phase ( $\Theta = 0^\circ$ ) of the pores by the continuous phase.

$$x = \frac{\sqrt{18\tau^2 r_p^2 + 2\sqrt{81r_p^4 \tau^4 + 4\gamma^2 r_p^2 \tau^2}}}{3\tau}, \quad \text{eq. 2.9}$$

where  $r_p$  is the pore radius,  $\tau$  is the shear stress applied,  $\gamma$  is the interfacial tension and  $x$  is the droplet diameter. Nevertheless, it can be expected that the contact angle will play a considerable role in the droplet formation mechanism and consequently on the resultant droplet size (Figure 2.5). Therefore, in the case of partial wetting of the continuous phase ( $0^\circ > \Theta > 90^\circ$ ) the resultant equation is as follows:

$$x = \frac{\sqrt{18\tau^2 r_p^2 + 2\sqrt{81r_p^4 \tau^4 + 4\gamma^2 r_p^2 \tau^2 \cos^2(\theta)}}}{3\tau}, \quad \text{eq. 2.10}$$

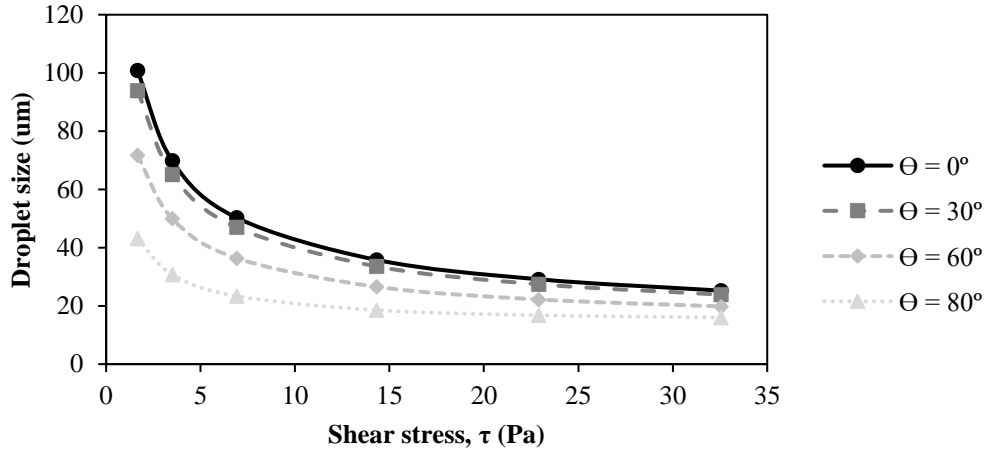


Figure 2.5 Influence of the contact angle on the final drop size

The force balance model (Equation 2.9 and 2.10) does not take into account the influence of the flux of the injecting material through the membrane. Earlier investigations empirically found that higher flux leads to bigger droplet sizes in the dripping regime [24, 48, 69, 94, 96]. For the simple paddle-bladed system (Figure 3.1), the shear stress must be determined in order to predict the drop size (Equation 2.9). Equation 2.11 is used to calculate the location of the transition radius along the paddle blade radius which is needed to determine the shear stress at the base of a paddle stirred vessel. The transitional radius is the point at which the rotation changes from a forced vortex to a free vortex.

$$r_{trans} = \frac{S}{2} 1.23 \left( 0.57 + 0.35 \frac{S}{T} \right) \left( \frac{b}{T} \right)^{0.036} n_b^{0.116} \frac{Re}{1000 + 1.43Re}, \quad \text{eq. 2.11}$$

where  $b$  is the blade height,  $T$  is the tank width,  $S$  is the stirrer width and  $n_b$  is the number of blades. The Reynolds Number is defined by:

$$Re = \frac{\rho\omega S^2}{2\pi\eta}, \quad eq. 2.12$$

where  $\rho$  is the continuous phase density,  $\omega$  is the angular velocity and  $\eta$  is the continuous phase coefficient of dynamic viscosity.

The boundary layer thickness,  $\delta$ , is defined by the Landau-Lifshitz [97] Equation:

$$\delta = \sqrt{\frac{\eta}{\rho\omega}}, \quad eq. 2.13$$

The shear stress,  $\tau$ , in the boundary layer above the membrane surface varies according to Equations 2.14 and 2.15, for radial positions less than the transitional radius and greater than the transitional radius, respectively [98].

$$\tau = 0.0825\eta\omega r \frac{1}{\delta}, \quad r < r_{trans}, \quad eq. 2.14$$

$$\tau = 0.0825\eta\omega r_{trans} \left(\frac{r_{trans}}{r}\right)^{0.6} \frac{1}{\delta}, \quad r > r_{trans}, \quad eq. 2.15$$

In the following work, the maximum shear stress is calculated using Equation 2.14, or 2.15, with  $r = r_{trans}$  for a given rotation speed and continuous phase viscosity. The maximum shear stress is then used in Equation 2.9 to provide the predicted drop size, which is then compared to the experimental values obtained in the following work where this membrane emulsification device was used.

## 2.1.7.2 Membrane oscillation

When considering an oscillation of the membrane (either vertically or azimuthally), the resultant shear stress is determined differently. In this study two different oscillation systems were used: vertical oscillation, represented in Figure 3.3 and azimuthal oscillation, represented in Figure 3.4.

In oscillatory flow it is known that the Stokes boundary layer forms. It is within this boundary layer that the drops will be generated during membrane emulsification. The Stokes boundary layer thickness ( $\delta$ ) is given by:

$$\delta = 2\pi \sqrt{\frac{\mu}{\pi f \rho}} \quad \text{eq. 2.16}$$

So, in water systems using a frequency of 10 to 50 Hz the Stokes boundary layer thickness would be expected to be 1100 to 500 micrometres. If generating drops significantly with diameters below these values one may conclude that the drops will be produced in a quiescent boundary layer and the bulk turbulence is not important, provided it is not sufficient to damage the drops after they have been formed. If the occurrence of turbulence and ‘turbulent bursts’ near the membrane surface can be neglected, then it may be possible to correlate drop size with the shear stress at the membrane surface based on the wave equation for shear stress [99]:

$$\tau = v_o \left( \frac{\omega_f \mu \rho}{2} \right)^{1/2} [\sin(\omega_f t) - \cos(\omega_f t)] \quad \text{eq. 2.17}$$

where  $\omega_f$  is the angular frequency, determined by:

$$\omega_f = 2\pi f \quad \text{eq. 2.18}$$

where  $f$  is the frequency of the oscillation and  $v_o$ , is the peak velocity related to both the angular frequency and the amplitude ( $a$ ) of oscillation by the equation:

$$v_o = \omega_f a \quad \text{eq. 2.19}$$

A ‘peak shear event’ occurs when the value of wall shear provided by Equation (2.20) is at a maximum:

$$\tau_{max} = 2a(\pi f)^{3/2}(2\mu\rho)^{1/2}, \quad \text{eq. 2.20}$$

The maximum shear occurs twice per cycle, and the maximum shear has been used in Equation (2.9) for drop size in previous publications investigating vertical oscillation of the membrane and pulsation of the liquid over an otherwise stationary membrane [43]. Clearly, in order to employ Equation (2.9) the value of shear stress at the membrane surface must be known and in the case of oscillatory motion that shear will vary from zero to a maximum value.

### 2.2.8 Outlook for industrial implementation

Membrane emulsification has potential to offer many advantages over conventional processing methods. This is predominantly associated with low energy consumption and the high control level over the emulsification process, capable of producing high-value products with minimal losses. However, its adoption for industrial applications has been slower than other disruptive technologies and this can be speculated due to a number of different reasons. In the first years of its appearance, the membranes used were not suitable for certain formulations, resulting in poor results, and therefore its disbelief among various industry leaders; unlike conventional emulsification methods, lack of knowledge and no straightforward procedure to scale-up a membrane emulsification device can be viewed as a risky decision from trusted technologies to a relatively unknown. However, Morinaga Milk Industry (Japan) is an example of a manufacturer that is publicly known to produce a product using membrane emulsification [73].

Looking at industrial applications, membrane emulsification is more appropriate for production of “high technology” products and uses, for example in chromatography resins, medical diagnostic particles, drug carriers, food and flavour encapsulation, i.e. in fields where there is a need for a high degree of droplet size uniformity, and above the 10  $\mu\text{m}$  threshold below which simple crossflow with recirculation of the dispersion could be used to generate the drops. The liquid droplets obtained by membrane emulsification could become solid through widely known polymerization, or coacervation methods of the drops and potentially turning them into specialized particles.

Considering the general configuration of the process, there are multiple different approaches that can potentially be adopted at the time of up-scaling. Ideally, throughput demand should be estimated in order to start designing the process. One of the greatest advantages of membrane emulsification is that this technique is suitable to be designed to run continuously which would decrease drastically labour time and, in theory, eliminate batch variability. However, the emulsification process would need to be monitored, over that certain period of time, to assure product consistency (drop size and drop size distribution for instance) over a long period of time. Even if continuous emulsification is successful, continuous post-processing may be challenging in certain application. This can also present an obstacle in the mindset of certain professionals in certain areas, who may prefer to eliminate any foreseen risks delaying the use of this technology in commercial applications.

During upscaling other aspects will come in place that need to be addressed such as high-volume handling. For instance, a low emulsion concentration may be interesting and suitable at a R&D stage, but it may be incompatible once in commercial production. Low emulsion concentrations will necessarily require larger volumes in the case when the final product is the dispersed phase content. Therefore, some other commitments may be needed to be taken in to account during upscaling. Another example can be the quality of the emulsion. When high productivities are required, dispersed phase flow may have to be increased further than recommended to meet the demands, but the quality of the emulsion may be compromised. Unlike processes such as rotor-stator mixers, or homogenizers, engineers specialized in scaling up may have limited relevant experience. For instance, choice of suitable pumps for the dispersed and continuous phases. In membrane emulsification, pumps should provide a pulseless flow to not disturb the drop formation, or the velocity profile of the continuous phase at the membrane surface.

## 2.2. Spontaneous Emulsification

In general, emulsification is a process that requires energy input, generally mechanical, to disperse the dispersed phase in the continuous phase and to create the additional interfacial area. Alternatively, for the spontaneous formation of emulsions,  $\Delta G$  should be negative, hence, the interfacial tension ( $\gamma$ ) should be very low (Equation 2.1).

The extent of surfactant adsorption at a liquid surface is expressed in terms of its surface excess concentration,  $\Gamma$ . Surface excess concentration is related to surface tension by the Gibbs Equation, which for a non-ionic surfactant takes the form [100]:

$$\Gamma = -\frac{c}{RT} \frac{d\gamma}{dc} = -\frac{1}{RT} \left( \frac{d\gamma}{d \ln c} \right) s \quad \text{eq. 2.21}$$

where  $c$  is the surfactant concentration. It becomes possible to estimate the area occupied by each adsorbed surfactant molecule at known  $\Gamma$  [100]. In systems containing high surfactant concentration, such as a membrane emulsification process using high concentration to enhance the rate of adsorption of surfactant at the emerging drop interface, there is the possibility that over time other emulsification processes may occur, such as spontaneous emulsification and the formation of microemulsions.

### 2.2.1 Microemulsions

Microemulsions are an example of thermodynamically stable and macroscopically homogeneous mixtures of water, oil and surfactant. They form spontaneously, and they are characterised by ultra-low interfacial tension ( $<0.1$  mN/m) between water and oil, thus minimising the required amount of energy to form the new surface area as shown in Equation (2.1). Microemulsions can be opaque or transparent depending on the size and concentration of droplets in the emulsion. In the case of ultralow interfacial tension this type of emulsification does not require energy input, as the ultralow interfacial tension leads to a spontaneous emulsification when the phases are brought in to contact [101]. The full mechanism behind this



phenomenon is still under investigation and is a matter for discussion despite the fact that microemulsions were first recorded in the XIX century [102-109].

Spontaneous formation of a new type of emulsions in the presence of relatively high surfactant concentration and high enough interfacial tension was discovered earlier [11]. According to Shinoda and Kunieda [110] these systems were erroneously considered as microemulsions, however, they are “solubilized solutions” and for such systems “swollen micellar solution” may be a more adequate term [11]. Usually, very large concentrations (10-25% w/w) of a non-ionic surfactant are required to produce these so-called microemulsions [110, 111]. Solubility of water in hydrocarbons and vice versa has been studied extensively due to the high interest that the energy industry has in this technology. Equations of state have been used to describe mutual solubility of water and several types of hydrocarbons at a wide range of pressures and temperature [112, 113].

In the section 4.5, spontaneous formation of w/o emulsion, at sufficiently high interfacial tension in the presence of high concentration of oil soluble surfactant is investigated. From the beginning, it was suspected that such microemulsions were swollen reverse micelles [110].

Control of spontaneous emulsification is important in a number of applications where there is a demand for nano-sized droplets in an emulsion such as in personal care, cosmetics and health, care industry [114]. Alternatively, this process can be undesirable in certain processes. An excess of surfactant is commonly used in a semi-batch process where the amount of dispersed phase increases with time and an “over use” of surfactant takes places in order to avoid the depletion of surfactant at the end of the process. The existence of this spontaneous process should be taken in to consideration in processes where the main goal is to have great control over the droplet size and size distribution (e.g. in membrane emulsification). Processes operated over a long period of time are more vulnerable to swollen micelles.

An interesting possible application of spontaneous microemulsions is the fuel industry. There is an interest in w/o emulsions, which can play a substantial role in reducing emissions and improving engine performance: diesel fuel emulsions have been shown to reduce NO<sub>x</sub>, CO, soot, hydrocarbons and particulate matter emissions when used in a compression ignition engine [115], and better overall efficiency [116]. In the production of uniform particles there are a number of w/o processes where hydrogel particles are formed by dispersing an aqueous phase into an oil phase, typically low odour kerosene, using membrane emulsification to form uniform droplets and, therefore, particles after reaction [30]. This reaction is often a

condensation polymerisation in which water is one of the reaction products, thus emulsion containing nano-sized water drops become evident during the reaction often detected by the haziness of the solution (i.e. ‘Span haze’).

The spontaneous process studied, see section 4.5, was performed using sessile droplet experiments where a single (large) water drop (surrounded by the organic phase) was monitored. To confirm the presence of aqueous nano-droplets in the organic phase, with a varying concentration of oil soluble surfactant, a set of experiments were designed to evaluate the drop size and concentration at equilibrium conditions using a NanoSight<sup>®</sup> nano-droplet tracking analysis characterisation technique. Kerosene was chosen as the organic phase because it is both an example of a common fuel and it is used as the continuous phase in a number of emulsification processes [30] for hydrogel particles.

## Chapter 3 EXPERIMENTAL

### 3.1 Emulsification devices

#### 3.1.1 Dispersion Cell

The Dispersion Cell was supplied by Micropore Technologies Ltd. Figure 3.1 illustrates a 3D sketch of this device, which consists of a base made out of Poly Ether Ether Ketone (PEEK) where a flat membrane disc is located below a glass cylinder and a stirrer with a flat paddle. Stirring speed is controlled by voltage applied from a power supply. A syringe pump is used to pump the dispersed phase through the membrane without providing any pulsing to the flow as other pumps may, e.g. a peristaltic pump. A “vortex breaker” made of PTFE is attached to the stirrer to assure that the vortex generated by the stirrer does not approach the membrane surface and influence the drop formation.

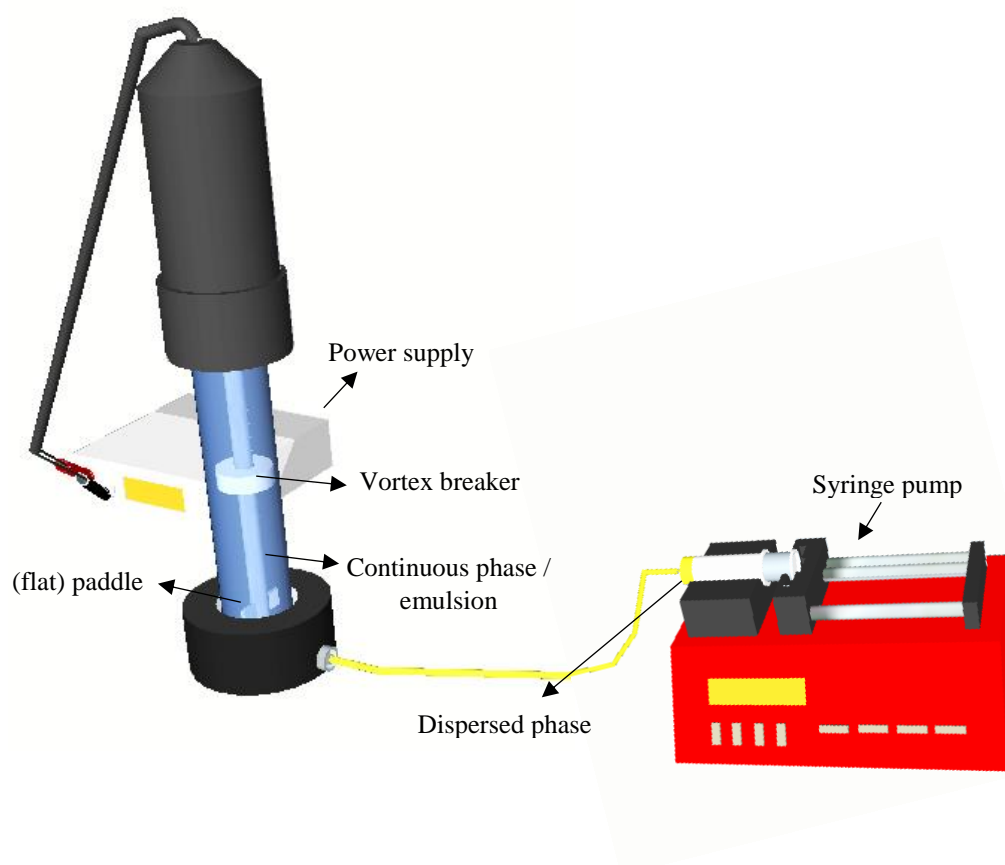


Figure 3.1 3D illustration of all the components from the Dispersion Cell.

### 3.1.1.1 Formulation and experimental procedure

#### a) w/o emulsions

A solution of 13.5% wt. PVA ( $M_w$  13 000 – 23 000 87-89% hydrolysed Sigma Aldrich, UK) was used as the dispersed phase, while the continuous phase was kerosene (reagent grade, low odour, Sigma Aldrich, UK) containing an (oil soluble) surfactant - Span<sup>®</sup> 80 (Sigma Aldrich, UK), which was used at various concentrations between 5-100 mM. The Dispersion Cell uses a 24 Volt DC motor to drive a paddle stirrer, which provides shear at the membrane surface (Figure 3.2). A stirring speed of 800 RPM (8 volts) was used for all the experiments providing a maximum shear at the membrane surface of 5.8 Pa. The method used to determine the maximum shear is described in section 2.1 using a density value of  $780 \text{ kg m}^{-3}$  and a viscosity of  $1.64 \times 10^{-3} \text{ Pa s}$  for the continuous phase. A syringe pump (World Precision Instruments, Florida, USA) was used to provide the pulseless flow. Two different injection rates were tested: 0.2 and 0.5  $\text{mL min}^{-1}$ . The continuous phase volume was 100 mL, and 5 mL of dispersed phase was injected through the membrane for each experiment. A flat disc membrane containing uniform cylindrical pores of 10  $\mu\text{m}$  and pore spacing of 200  $\mu\text{m}$  was used and the membrane surface was not treated, it was bare 316 stainless steel. The membrane used had an annular ring of open pores as presented in Figure 3.2c where the transitional radius will be located and shear reaches its maximum (Figure 3.2b). Regarding the experimental equipment used:  $H = 110 \text{ mm}$ ,  $S = 30.0 \text{ mm}$ ,  $b = 11.8 \text{ mm}$  and  $T = 34.3 \text{ mm}$ .

Before each experiment the membrane was cleaned (section 3.1.1.2). After cleaning, the membrane was immersed into the continuous phase for about 30 min after being ultra-sonicated for about 1 min. This is important to ensure that the membrane was wetted by the continuous phase and no air was entrapped in the pores. Then, the membrane was placed into the base of the Dispersion Cell, and after assembly of this device, about 100 mL of continuous phase was placed inside the glass cylinder. To ensure that no air was present, continuous phase was pulled through the membrane using a three-way valve and syringes. Finally, a syringe was loaded with dispersed phase, placed in the syringe pump and connected to the three-way valve. The three-way valve was turned, and the injection started monitoring that no air bubbles were present between the interface dispersed phase/continuous phase.

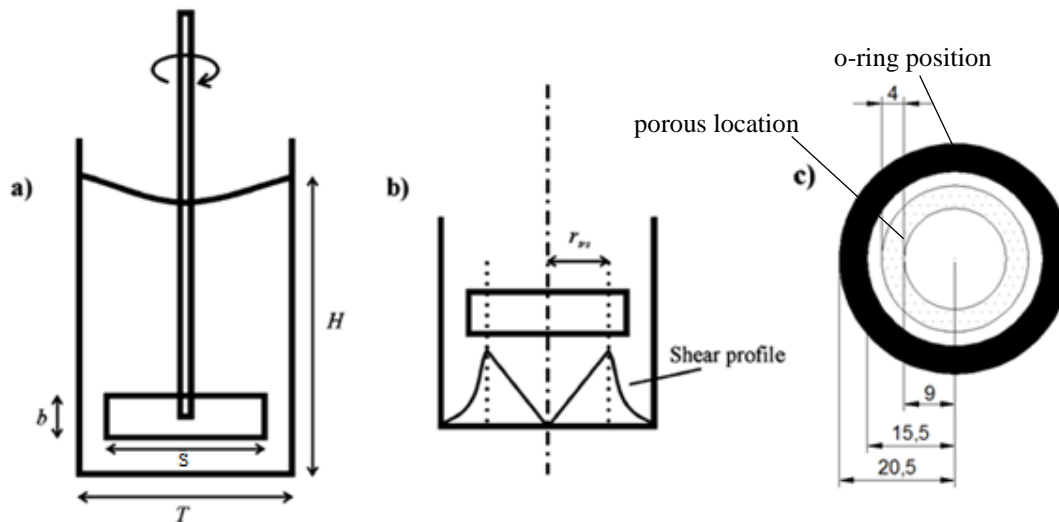


Figure 3.2 Schematic diagrams showing (a) the stirred cell, (b) the shear profile under the stirrer, and (c) the annular radial ring membrane for dispersion. Adapted from [48].

#### b) o/w emulsions

PLGA microspheres were produced from a 20% wt. polymer (PLGA,  $M_w$  24 000 - 38 000 g/mol) dispersed phase using dichloromethane (DCM) as solvent. The PLGA polymer was Resomer RG 503H purchased from Evonik industries. For all the tests, the continuous phase was an aqueous solution of PVA (MW 13 000 – 23 000 87-89% hydrolysed Sigma Aldrich, UK) and two different concentrations were used: 0.5% wt. and 4% wt. Prior to the injection, the continuous phase was saturated with DCM (1 mL of DCM per 100 mL of continuous phase) and chilled (5°C) overnight. Each batch test of emulsion from a Dispersion Cell comprised of 5 mL of dispersed phase injected into 100 mL of continuous (aqueous) phase. The dead volume associated with each injection was approximately 5 mL, taking the total dispersed phase volume consumed per test injection to 10 mL. The same approach was used to ensure that no air was entrapped in the system as described above (see section 3.1.1.1).

Each emulsion produced was transferred to a simple stirred beaker and diluted about 3 times (with 0.5% wt. PVA solution) for hardening by solvent evaporation inside a fume cupboard. PLGA particles were washed after hardening, which took approximately 2 hours. Washing the particles consisted of several cycles (at least 3) of letting the particles settle, decant the excess of liquid phase, followed by addition of distilled water. After separating the PLGA particles from the continuous phase, the particles were re-suspended in distilled water and freeze dried.

A sample of particles were observed with a Field Emission Gun Scanning Electron Microscope (FEGSEM), Zeiss Ultra plus.

#### 3.1.1.2 Membrane cleaning

The membrane cleaning procedure for the flat disc membranes is dependent on the formulations used. However, the standard cleaning procedure was effective for both formulations (w/o and o/w emulsions) and consisted of soaking the membrane in 4M NaOH solution for 10 minutes, followed by rinsing with tap water and then placing in distilled water for 1 minute. Afterwards, the membrane was soaked in 2% wt. citric acid solution for 10 minutes, rinsed with tap water and again placed in distilled water for 1 minute. Finally, the membrane was dried and stored, or pre-soaked in the continuous phase, getting ready for the next experiment. Every time that the membrane solution was changed, an ultrasonic bath was used for 1 minute to promote the cleaning and/or remove any air bubbles that may be present in the membrane pores.

## 3.1.2 Vertical oscillating membrane system

The vertical oscillating membrane system is presented in Figure 3.3. This system uses tubular membranes which are coupled to a motor that oscillates a drive shaft up and down, i.e., parallel to the membrane tube axis. The tubular membrane used had a working (outside) diameter of 15 mm and a length of 60 mm. To reduce the turbulence resulting from oscillation, at the bottom end of the membrane, a stainless-steel cap in the shape of a cone was used, as can be observed in Figure 3.3, which sealed off the tubular membrane. The metal membrane had a thickness of 100  $\mu\text{m}$ .

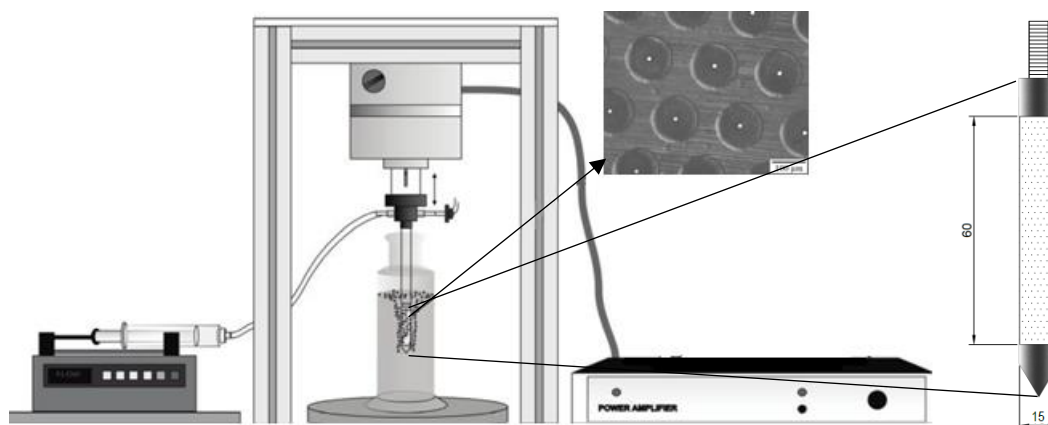


Figure 3.3 Representation of the vertical oscillating membrane emulsification device used with an inset showing the regular pore pattern of the membrane (triangular array) and the shape of the tubular membrane used. Adapted from [49].

The oscillation could be controlled via a LabView executable program running on a PC. The oscillation signal was provided by a PC via a National Instruments interface which needed to be amplified, by a power amplifier (LDS PA 100E, Brüel & Kjaer), in order to drive the electro-mechanical oscillator. An accelerometer (PCB Piezotronics model M352C65) was used to provide the information from the oscillation: frequency, was determined by the direction of travel, and amplitude, was deduced from the acceleration measurement. This accelerometer was connected to the National Instruments Analogue to Digital converter (NI eDAQ-9172) which was interfaced to the LabView executable program. This system enabled a wide range of frequencies (1-99 Hz) and amplitudes (0.1 to 7 mm) to be tested.

### 3.1.2.1 Formulation and experimental procedure

A solution of 13.5% wt. PVA (MW 13 000 – 23 000 87-89% hydrolysed Sigma Aldrich, UK) in distilled water was used as the dispersed phase, while the continuous phase was kerosene (reagent grade, low odour, Sigma Aldrich, UK) containing an (oil soluble) surfactant - Span<sup>®</sup> 80 (Sigma Aldrich, UK) - which was used in various concentrations between 5-100 mM. The tubular membrane used was hydrophobized as described in section 3.3. The membrane had 10  $\mu\text{m}$  diameter pores and they were spaced equidistantly 200  $\mu\text{m}$ , providing a surface porosity of 0.23%. The distance between pores is 20 times higher than the pore size ensuring that contact of emerging droplets is unlikely to occur.

The oscillation was parallel to the membrane tube axis. For the experiments reported below, a frequency of 35 Hz and displacement of 2 mm was used. The resultant maximum shear for these conditions was 3.25 Pa. Section 2.1.6 describes how the maximum shear stress can be calculated for this system.

The same approach was used to ensure that no air was trapped in the system as described previously in section 3.1.1.1. It is critical to verify that the membrane was (still) completely immersed in the continuous phase after oscillation starts. During the experiment 10 mL of dispersed phase was passed through the membrane into 200 mL of continuous phase, achieving a 5% (v/v) concentration emulsion in all experiments reported using this system.

### 3.1.2.2 Membrane cleaning

The membrane cleaning procedure for the hydrophobic tubular membranes, after use in the vertical oscillator, consisted of soaking in 4M NaOH solution for 10 minutes, followed by rinsing with tap water and then placing in distilled water for 1 minute. Afterwards, the membrane was soaked in acetone solution for 10 minutes. The membrane was then dried and stored or pre-soaked in the continuous (organic) phase getting it ready for the next experiment. Every time that the membrane solution was changed, an ultrasonic bath was used for 1 minute to promote the cleaning and/or remove any air bubbles that may be present in the membrane pores.



## 3.1.3 Azimuthally oscillating membrane system (Micropore Technologies Ltd)

The azimuthally oscillating membrane system is presented in Figure 3.4. This system uses tubular membranes which are coupled to a motor that oscillates back and forwards, i.e., perpendicular to the membrane tube axis.

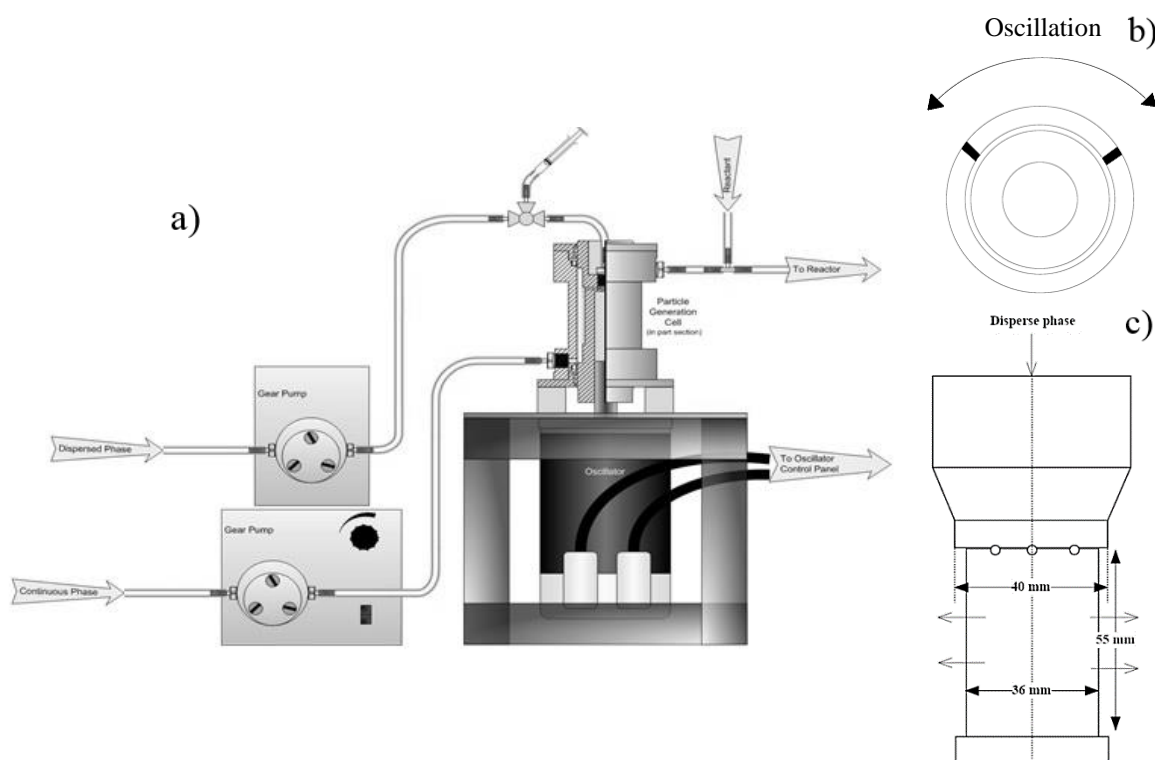


Figure 3.4 a) Schematic illustration of the Micropore Technologies Ltd Oscillating Membrane Emulsification system; b) Overhead view of the shaft that contains the membrane, illustrating the oscillatory movement of the membrane; c) Side view of the shaft with membrane covering lower parallel sided section (55 mm high and 40 mm diameter).

The oscillation signal was provided by a control panel which was connected to the oscillator motor providing separate control over the frequency and membrane displacement (defined as being the peak to peak distance in the cycle and therefore twice the amplitude of the oscillation). This device is able to generate frequencies up to 50 Hz and displacements up to 7 mm. A single sieve-type membrane was used, which had uniform laser drilled pores (5  $\mu\text{m}$  or 15  $\mu\text{m}$ ) with a distance between the pores of 200  $\mu\text{m}$ . The membrane was laser welded to a cylindrical stainless steel body (36 cm diameter), Figure 4.3b, with a working diameter of 40 mm and height of 45 mm. The membrane surface area was 52  $\text{cm}^2$ . The geometric characteristics of the membrane are also given in Figure 4.3c.

The dispersed phase was injected using a gear pump (Ismatec<sup>®</sup>, IDEX Health & Science, Wertheim, Germany) while the continuous phase was injected using a peristaltic pump (Watson-Marlow<sup>®</sup> 505, Cornwall, U.K).

### 3.1.3.1 Formulation and experimental procedure

Different formulations were used using the azimuthally oscillating membrane system:

- a) Oil droplets of sunflower oil in water stabilized by Tween<sup>®</sup> 20
- b) PCL droplets in water stabilized by PVA
- c) w/o/w emulsion – encapsulation of Bovine Serum Albumin (BSA) using polycaprolactone particles as the carrier.

#### 3.1.3.1 a Single (o/w) emulsion - Floating droplets

Food grade sunflower oil was used as the dispersed phase and a solution of 2% wt. Tween<sup>®</sup> 20 (Sigma Aldrich, UK) in distilled water was used as the continuous phase. The measured viscosities for 2% wt. Tween 20 solution in water and sunflower oil are 0.001 and 0.039 Pa s, respectively. The tubular membrane used contained uniform cylindrical pores of 5  $\mu\text{m}$  and pore spacing of 200  $\mu\text{m}$ , providing a porosity of 0.05%. The distance between pores is 40 times higher than the pore size ensuring that contact of droplets being formed will not occur. The membrane surface was not treated, it was bare 316 stainless steel. The sunflower oil was pre-filtered before trials using Minisart<sup>®</sup> syringe filters (Sartorius stedim biotech GmbH, Germany) of 1.2  $\mu\text{m}$ .

After setting up the equipment, the system was filled up with continuous phase ensuring that there was no air entrapped in the system and membrane was wetted by the continuous phase. Then, dispersed phase was injected from the top of the membrane shaft Figure 4.3c, filling the dead volume behind the membrane. Once this volume was filled, the dispersed phase permeates through the pores of the membrane, into the continuous phase which was gently cross-flowing in the upward direction to collect the droplets and transfer them to a downstream vessel. It is notable that this system is designed to operate in continuous flow mode, without the need to

recycle the emulsion phase over the membrane as would be the case for a simple crossflow membrane emulsification system, such as an SPG membrane tube. Thus, it is a highly flexible system where the shear at the membrane surface is decoupled from the crossflow rate and the emulsion is generated in a single pass of continuous phase. This system used in this thesis was a pre-production prototype from Micropore Technologies Ltd., and no prior publications had been made on it before the work reported here.

#### 3.1.3.1 b Single (o/w) emulsion - Sinking droplets

A solution of 15% wt. PCL Mw 50 000, Polysciences, Inc, UK) dissolved in DCM, Sigma Aldrich, UK) was used as the dispersed phase, while the continuous phase was a solution of 4% PVA (MW 13 000 – 23 000 87-89% hydrolysed Sigma Aldrich, UK) dissolved in distilled water. Prior to the testing, continuous phase was saturated with DCM (10 mL of DCM per 1000 mL of continuous phase) overnight.

The tubular membrane used contained uniform cylindrical pores of 15  $\mu\text{m}$  and pore spacing of 200  $\mu\text{m}$ , providing a surface porosity of 0.44%. The membrane surface was not treated as stainless steel is naturally hydrophilic. Filtration of the dispersed phase was not carried out. In the initial tests performed the flow rates of the dispersed and continuous phases were kept constant, 5  $\text{mL min}^{-1}$  and 80  $\text{mL min}^{-1}$ , respectively. The same approach was used to ensure that no air was trapped in the system as described previously in section 3.1.3.1 a. The azimuthally oscillating membrane emulsification system was ran at controlled temperature due to the presence of a water jacket. This was employed in order to assure that the dispersed phase (DCM which is very volatile) would not evaporate during injection, leading to polymerization and consequently blockage on the membrane surface. Chilled water was used to keep the temperature of the dispersed phase inlet below 25°C. Chilled water temperature was about 5°C.

The different emulsions produced were transferred to a simple stirred beaker and diluted about 3 times (with 0.5% wt. PVA solution) for hardening by solvent evaporation inside a fume cupboard. PCL particles were washed after hardening which could take approximately 2 hours. Particles were washed during several cycles (at least 3) of letting the particles settle, decanting the excess of liquid phase, followed by addition of further distilled water. After washing the

PCL particles from the continuous phase, they were resuspended in distilled water and freeze dried.

#### 3.1.3.1 c Multiple (w/o/w) emulsion – BSA encapsulation

A two-step emulsification was adopted to produce a multiple w/o/w emulsion and encapsulate a water-soluble model protein. A homogenizer (T18 digital Ultra Turrax®, with head S 18N-10G, IKA) was used to carry out the first emulsification (w/o) and the azimuthal oscillating system was used to carry out the second emulsification (w/o/w). The w/o emulsion preparation consisted of adding 10 mL of an aqueous solution of 10% wt. BSA (Fraction V Roche LOT 155 652 26) into 90 mL of 15% wt. PCL dissolved in DCM and homogenized at 24 000 rpm for 5 minutes which ensured that the mean droplet size was smaller than 0.5  $\mu\text{m}$ . In order to minimize evaporation of the solvent, homogenization occurred at low temperatures, where the emulsion beaker was kept in ice to prevent heating. Then, the w/o emulsion was used as the dispersed phase in the second emulsification and the continuous phase was a solution of 4% wt. PVA (MW 13 000 – 23 000 87-89% hydrolysed Sigma Aldrich, UK) dissolved in distilled water. Prior to testing, the continuous phase was saturated with DCM (10 mL of DCM per 1000 mL of continuous phase) overnight. The operational conditions were chosen according to the best results obtained during PCL particle tests (section 3.1.3.1.b) and injection was performed during 45 minutes in order to evaluate its quality over time. The same approach was used to ensure that no air was trapped in the system, and to harden the particles, as described in the previous section 3.1.3.1 b.

#### 3.1.3.2 Membrane cleaning

The standard cleaning procedure was effective for the systems used and consisted of soaking the membrane in 4M NaOH solution for 10 minutes, followed by rinsing with tap water and then placing in distilled water for 1 minute. Afterwards, the membrane was soaked in 2% wt. citric acid solution for 10 minutes, rinsed with tap water and again placed in distilled water for 1 minute. Finally, the membrane was dried and stored, or pre-soaked in the continuous phase getting it ready for the next experiment. Every time that the membrane solution was changed,

an ultrasonic bath was used (for 5-10 seconds) and membrane cleaning solution was pulled, carefully, avoiding the collapse of the membrane, through the membrane.

### 3.2 Determination of mean droplet size and droplet size distribution

Throughout this work different techniques were adopted to determine the droplet size and droplet size distribution. The droplet diameter is expressed as the volume median diameter  $D(V, 0.5)$ , which is the diameter corresponding to 50% on the cumulative volume distribution curve. Droplet size uniformity is expressed in terms of coefficient of variation (CV):

$$CV = \frac{\sigma}{\mu} \times 100, \quad \text{eq. 3.1}$$

where  $\sigma$  is the standard deviation and  $\mu$  is the mean of the volume distribution curve. Different techniques were available, and they were used according to the experimental needs and demands: Coulter Counter, static image analysis, dynamic image analysis and The Malvern Instruments Nanosight LM10.

For example, in section 5.3, the CV and  $D(V,0.5)$  values reported were obtained by using three analytical methods: a stereoscopic microscope (static image analysis), Vision 500<sup>TM</sup> (dynamic Image Analysis) by Micropore Technologies Ltd., and a Multisizer<sup>TM</sup> 3 Coulter Counter<sup>®</sup>. A large number (typically several hundred) drops were counted and measured using the microscope and Image J (image processing software) to confirm the data obtained from the Vision 500 and Coulter Counter. Once the preliminary sizing tests were completed, and robust sizing techniques confirmed, data from the Vision 500 was used when the  $D(V,0.5)$  was above 45  $\mu\text{m}$  and for  $D(V,0.5)$  below 45  $\mu\text{m}$ , the Coulter Counter data is reported. The Coulter and Vision 500 systems gave identical results around these sizes, but for sizes with a significant amount of the distribution below 20  $\mu\text{m}$  the on-line Vision system thresholding was not reliable, hence off-line tests using the Coulter was used for the smaller drops. In all cases: static and dynamic image analyses as well as Coulter electric zone sensing, are well known ‘primary’ techniques directly measuring the drop size distribution, which is deemed to be more reliable than ‘secondary’ techniques such as laser diffraction.

### 3.3 Surface modification

Hydrophobization of metal surfaces were performed based on silanization reactions. The hydrophobic surface treatment of metal substrates made out of 316 stainless steel (0.1x25x25 mm, purchased from GoodFellow Ltd) is described in this section. Various parameters were experimented and explored, with evaluation of the contact angle, such as: temperature of the reaction, exposure of a metal sheet in HCl solution, type of silane chemical, concentration of the silane chemical, solvents, reaction time, multiple appliances of the silane chemical, etc. After extensive experimental tests, the procedure below is the ultimate one used to provide hydrophobic behaviour on both metal bodies: stainless steel and nickel.

#### 3.3.1 Developed procedure

Firstly, the substrates were cleaned by soaking in 4 M NaOH solution for 10 minutes, followed by rinsing with tap water and then placing in distilled water for 1 minute. Afterwards, the membrane was soaked in 10% wt. HCl solution for 10 minutes, rinsed with tap water, and again placed into distilled water for 1 minute. The substrates were then dried at 50°C for 1 hour. For hydrophobization the substrates were placed in a solution of 0.01M 1H,1H,2H,2H-Perfluorododecyltriethoxysilane (FAS) which was dissolved in undecane (aprotic solvent). It was empirically found that the metal sheet should be allowed to soak in the solution for a minimum of 4 hours at 45°C to achieve a desirable hydrophobicity. The same procedure was applied to treat the tubular membrane which was then rinsed with acetone, dried and ready to be used in the experiments. The FAS chemical (Figure 3.5) was purchased in Fluorochem<sup>®</sup> while undecane was obtained from Sigma Aldrich, UK.

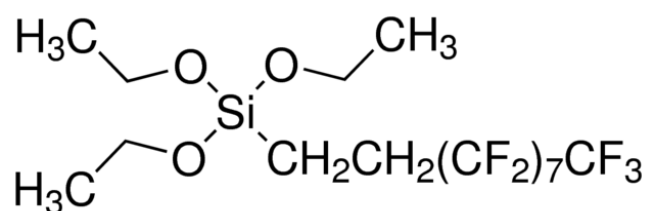


Figure 3.5 Chemical structure of 1H, 1H, 2H, 2H-Perfluorododecyltriethoxysilane (FAS)

### 3.3.2 Durability and stability tests

Five metal sheets (treated to be hydrophobic) with a known contact angle were placed in the standard solutions used to clean the metal porous membranes: distilled water, 4M NaOH and 2% wt. citric acid for 24 hours. After this period, all the metal sheets were rinsed with distilled water and dried at 50°C for 1 hour. Then, contact angle measurements (sessile droplets experiments) were carried out in order to check if the hydrophobic treatment remained stable after being in contact for long a period (24 hours) with the standard membrane cleaning solutions.



### 3.4 Contact angle, surface and interfacial tension measurements

#### 3.4.1 Sessile droplet experiments

Observing sessile droplets is a common method for measuring static (apparent) contact angles,  $\Theta_{\text{app}}$ . In this work, either a direct determination of the contact angle with a drop shape analyser (DSA 100, Kruss, Germany), or with a custom built experimental setup was performed.

##### 3.4.1.1 Home built setup

Sessile droplet experiments with the home-made setup (Figure 3.6) were carried out to monitor time evolution of aqueous droplet height, radius and dynamic contact angle. The substrate used was a 316 stainless steel sheet (0.1x25x25mm) purchased from GoodFellow Ltd. The substrates were chemically hydrophobically coated (see section 3.3). A DMK 23G 445 GigE monochrome industrial camera (Imaging source, Germany), coupled with Bi-telecentric lenses (OPTO Engineering, Italy), was used for monitoring the side view of the droplet. On the opposite side a light source was mounted parallel to the camera – telecentric HP Illuminator (OPTO Engineering, Italy) as shown schematically in Figure 3.6. Thereby a light source is positioned behind the drop, so that it appears dark.

The experimental protocol was as follows: a water droplet was deposited on the hydrophobic stainless steel sheet which was surrounded by the organic phase (kerosene). The volume used of organic phase was about 20 mL, contained in a (optical) glass chamber of 40x40x30 mm. During experiments the chamber was covered in order to avoid dust deposition. The cleaning of the substrate consisted of placing the SS sheets in an organic solvent (methanol and/or acetone) followed by drying at 50°C for at least 30 minutes before the start of a new experiment. The drop deposition was performed using a micro-syringe (500  $\mu\text{L}$ ) mounted in a support designed to improve the drop placement accuracy. The drop volume used during sessile droplet experiments was not larger than 9  $\mu\text{L}$  to avoid influence of gravity forces. These measurements were performed in triplicate. The organic phase was low odour kerosene purchased from Sigma Aldrich. The surfactant Span<sup>®</sup> 80, purchased from Sigma Aldrich, was dissolved in the organic phase.

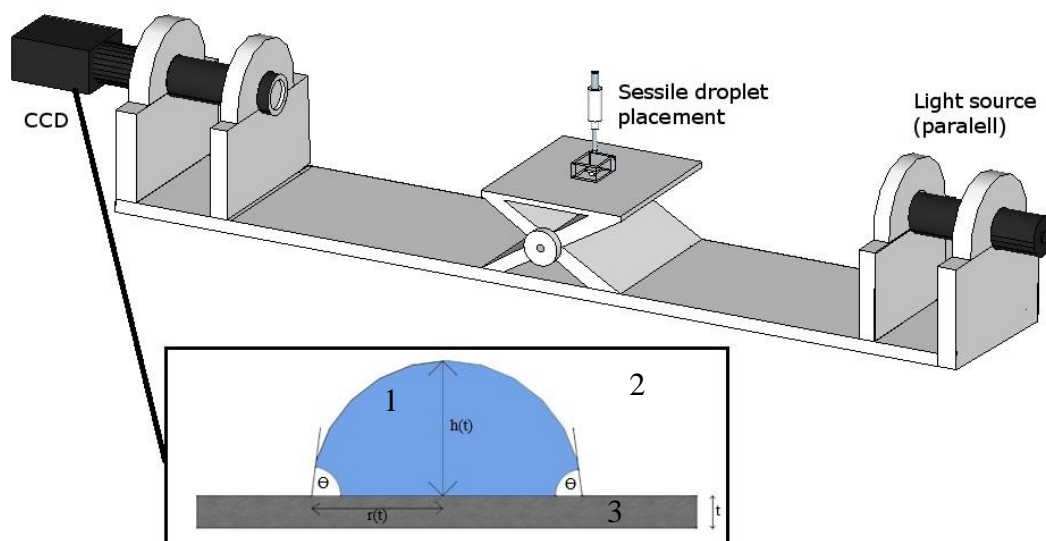


Figure 3.6 Diagram of the experimental set up for sessile droplet experiments: 1 - aqueous droplet with (or without) added salt; 2 - organic phase with (or without) Span<sup>®</sup> 80 surfactant, 3 - hydrophobic support.

Image analysis was undertaken using a feature called Vision Builder from LabView (National Instruments). A script was programmed to acquire the following measurements of the droplet: height ( $h$ ), contact angle ( $\Theta$ ) and radius ( $r$ ) of the droplet base. So, the drop volume ( $V$ ) could be determined using well-known Equations 3.2 or 3.3. The two equations allow calculation of the droplet volume in two different ways. These two different ways of calculation of the drop volume were compared in order to evaluate the image analysis reliability, estimating the measurement error. The drop volume was normalised according to Equation 3.4. The droplet was formed in the organic phase with surfactant (Figure 3.6). Various amounts of surfactant used in the system changed the interfacial tension, up to the Critical Micelle Concentration (CMC). However, spontaneous droplet formation was observed only at concentrations above the CMC, which resulted in different droplet sizes.

Drop volume was determined using measured values of height ( $h$ ) and radius of the base ( $r$ ):

$$V = \frac{\pi h}{24} (3r^2 + h^2), \quad \text{eq. 3.2}$$

Alternatively, the drop volume was also determined using measured values of the radius of the base ( $r$ ) and contact angle ( $\Theta$ ):

$$V = \frac{\pi r^3}{3} \left( \frac{2 - 3 \cos(\theta) + \cos^3(\theta)}{\sin^3 \theta} \right), \quad \text{eq. 3.3}$$

The reduced droplet volume was calculated according to the following equation:

$$V_n = \frac{V(t)}{V_0}, \quad \text{eq. 3.4}$$

Results of experiments using this setup are showed in section 4.4.

#### 3.4.1.2 Droplet shape analyser

Static (apparent) contact angle measurements were obtained from sessile droplets with a droplet shape analyser (DSA -100, Kruss, Germany). Young fitting was used to contour the drop and obtain the contact angle. This fitting gives an identical contact angle on both sides of the drop observed. These experiments were performed at room temperature ( $22 \pm 2^\circ\text{C}$ ). The experiment was deemed to have finished when the measurements achieved an equilibrium value. These measurements were performed in triplicate. The substrate used was a 316 stainless steel sheet (0.1x25x25mm) purchased from GoodFellow Ltd and cleaned using the procedure described in section 3.1.1.2. Various systems were characterised following the protocol described in section 3.4.1.1, using an identical (optical) glass chamber: water (distilled) against vapour and kerosene in the presence of Span<sup>®</sup> 80 (bulk phase), saline solution (10% wt. NaCl) against vapour and kerosene in the presence of Span<sup>®</sup> 80 (bulk phase) and 13.5% wt. PVA solution (drop phase) against vapour and kerosene in the presence of Span<sup>®</sup> 80 (bulk phase).

## 3.4.2 Rotating drum experiments

A home built rotating drum system (Figure 3.7) was used for measurements of the dynamic advancing and receding contact angles. In these experiments, one planar exchangeable drum was used, made of stainless steel with the following dimensions: 6 cm diameter and 2 cm width (Figure 3.7b).

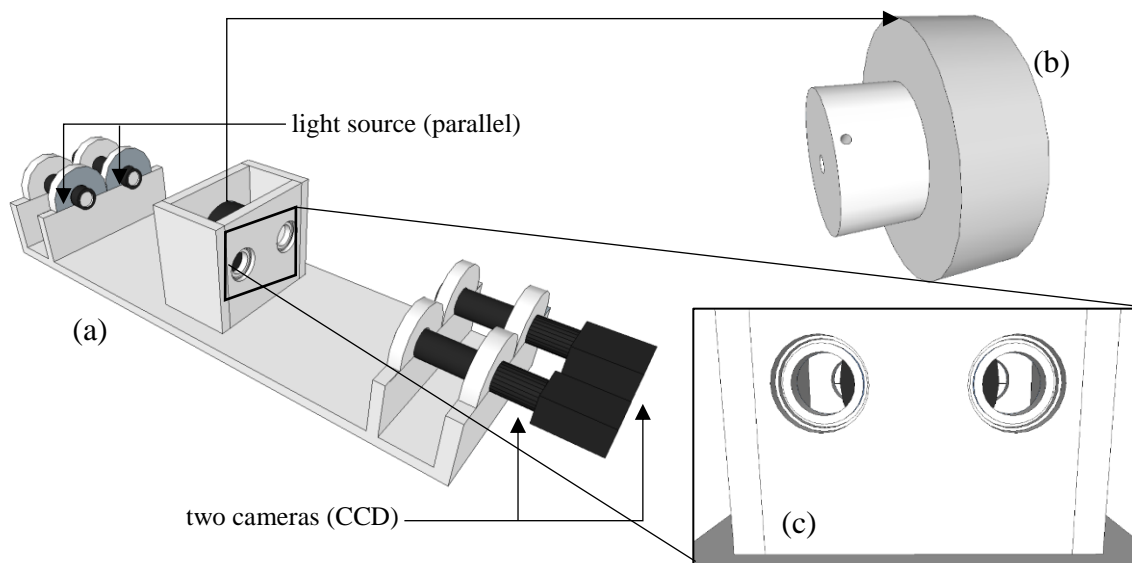


Figure 3.7 Rotating drum system (a) setup 3D view; (b) stainless steel drum; (c) cameras view

The DC motor rotated the drum with peripheral speeds of between  $1 \text{ mm s}^{-1}$  and  $10 \text{ mm s}^{-1}$ . The maximum velocity depends on the capillary number of the system which should not be higher than  $10^{-4}$  in order to avoid the dominance of viscous forces over the capillary forces. Two cameras were mounted on each side of the drum to capture the side view. One of them was an ImagingSource DMK 23G445 and the other one was a Baumer EXG50. Both cameras had Bi-telecentric objective lenses TC23009 from Opto Engineering, with a magnification of 1.000x. Two blue Telecentric HP illuminators from Opto Engineering were used as light sources.

Advancing and receding contact angles were observed simultaneously, via side-view, using a low frame rate ( $<10 \text{ fp s}^{-1}$ ). Cameras were mounted on a movable (horizontally) frame to focus on the three-phase contact line. The light source was mounted on the same frame at the opposite window, to achieve a black and white image. Light source and camera were mounted in the

same frame to ensure that they are parallel to each other, which is important for higher accuracy of contact angle measurements. Therefore, other light present in the laboratory would not interfere with the experimental measurements.

Two different drums, made out of 316 stainless steel, were tested. One of them was hydrophobized following the procedure described in section 3.3 while the other was subjected to the standard (membrane) cleaning procedure described in section 3.1.3.

In the initial experiments, the hydrophobized drum was used, which was half immersed with water solutions containing surfactants: Tween<sup>®</sup> 20 or Pluronic<sup>®</sup> L-35. So, the three phase contact consisted of a solid surface, a water based solution and the vapour phase. Then, further experiments were performed using two immiscible liquids where the vapour phase is replaced by an organic phase (kerosene, with or without presence of surfactant: Span<sup>®</sup> 80). In these experiments, firstly is introduced the water based solution to half of the height of the rotating drum and, later, the organic phase (kerosene) is added, very carefully, until the drum is fully submerged in liquid. In combination with the two immiscible liquids, both 316 stainless steel drums were used. All measurements were performed at room temperature (about 21°C).

#### 3.4.3 Surface and interfacial tension measurements

Surface and interfacial tension measurements were obtained with a drop shape analyser (DSA-100, Kruss, Germany) by drop shape analysis using the pendant drop method. To perform interfacial tension measurements, two different needles were needed depending on the density of the liquids, i.e., for case of rising drops ( $d_{\text{drop}} < d_{\text{bulk}}$ ) hook needles were used, but if drop density is higher than bulk density, then, a standard needle is used (both needles were supplied by Kruss, Germany). For surface tension measurements only standard needles were used. These experiments were performed at room temperature ( $22 \pm 2^\circ\text{C}$ ). As soon as a drop was created, snapshots were taken every 0.5 seconds and the drop shape was evaluated with respect to time [117] to determine “dynamic” interfacial tension. The experiment was deemed to have finished when the measurements achieved an equilibrium value. These measurements were performed in triplicate. The systems characterised were: water in the presence of Tween<sup>®</sup> 20 (drop phase) against vapour (bulk phase), water (drop phase) against kerosene in the presence of Span<sup>®</sup> 80 (bulk phase), 13.5% wt. PVA solution (drop phase) against kerosene in the presence of Span<sup>®</sup> 80 (bulk phase) and sunflower oil (drop phase) against water in the presence of Tween<sup>®</sup> 20.

### 3.5 Spontaneous emulsification experiments

Six solutions of an aqueous phase with different NaCl concentrations (0%, 0.1%, 1%, 2%, 5% and 10% w/w) and four kerosene solutions with different Span<sup>®</sup> 80 concentrations were prepared. In each 10 mL of kerosene Span<sup>®</sup> 80 solutions were added to 10 mL of aqueous NaCl solutions and left undisturbed in hermetically closed vials (clear glass 28 mL capacity) for several hours. In total 24 vials were prepared in such a way. After reaching equilibrium by both phases the presence of water droplets in the organic phase was checked, and the concentration and size of droplets were determined using a NanoSight LM10 (NanoSight/Malvern, Amerbury, United Kingdom), equipped with a sample chamber with a 640-nm laser and a Viton fluoroelastomer O-ring. The device employed Nano-particle Tracking Analysis (NTA) software. The samples were injected in to the sample chamber with sterile (5 mL) plastic syringes (BD Discardit<sup>®</sup> II) until the liquid reached the tip of the nozzle. All measurements were carried out at room temperature 25°C. NTA 3.0 software was used for capturing and analysing the data. Samples were measured for 60 seconds with manual shutter and gain adjustments. Five measurements of each sample were repeated and the averaged values were used.

## Chapter 4 MEMBRANE PROPERTIES AND COMPLEX FLUIDS BEHAVIOUR

### 4.1 Membranes characterization

In this work, multiple metal porous membranes were used for the emulsification tests. Regarding the membrane emulsification device, membranes have different forms, i.e., using the Dispersion Cell (section 3.1.1) the membrane is a flat disc with a diameter of 41 mm while the vertical and the azimuthally oscillating system uses tubular membranes with diameters of 10 mm (section 3.1.2) and 40 mm (section 3.1.3), respectively.

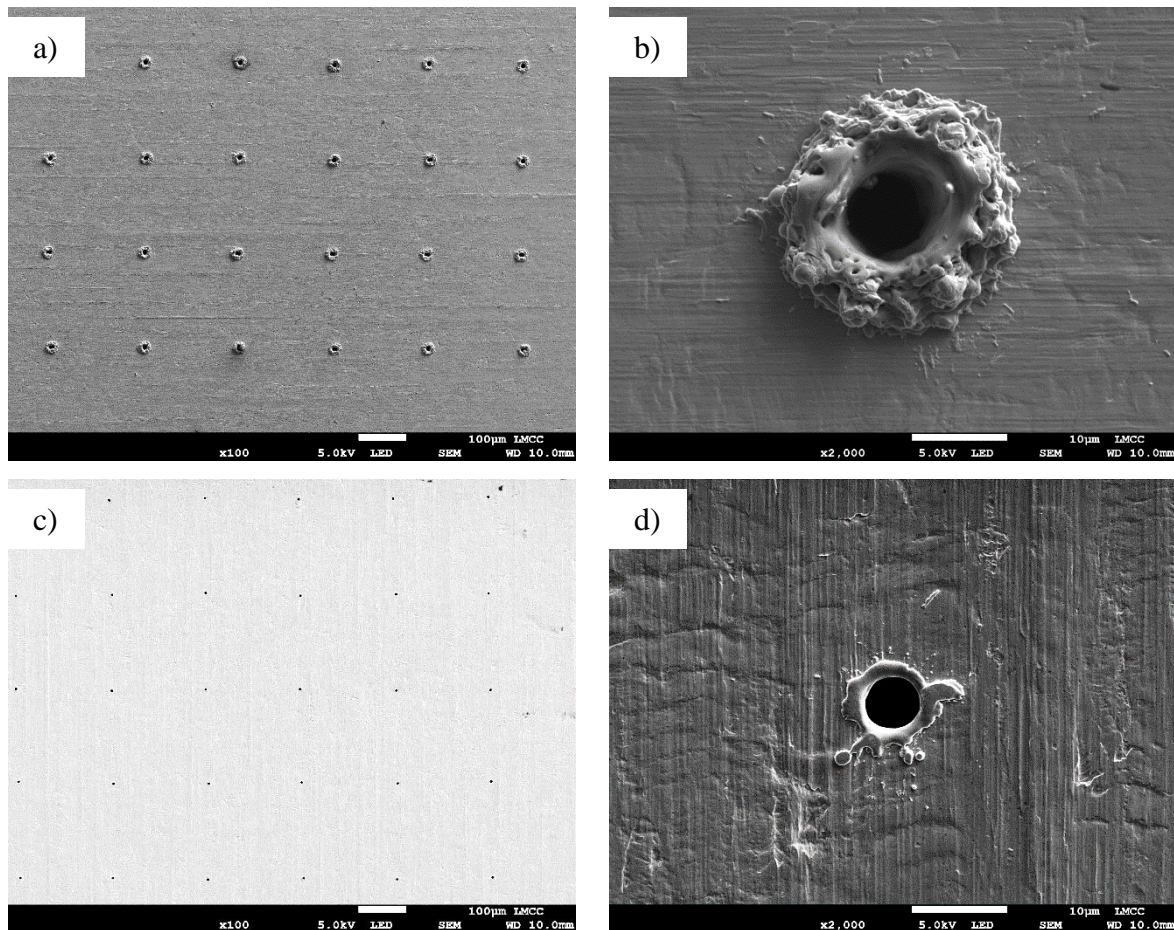


Figure 4.1 Top view of the entry and exit side of a stainless steel membrane with pores of 5  $\mu\text{m}$  (a) entry side – square pore pattern (b) single pore on the entry side (c) exit side – square pore pattern (d) – single pore of the exit side. These pictures were obtained using a SEM – JEOL JSM 7100F.

Nonetheless, all the membranes used have a well-defined pore size, a narrow pore size distribution (section 4.1.1.) and a very regular matrix, rather than the usual tortuous pore channel depth filter commonly used for membrane emulsification. The pore channel length of these membranes is the membrane thickness (100  $\mu\text{m}$ ). In this study, two types of metal membranes were used: nickel and stainless steel. Pore pattern and pore shape are the main differences between the two as can be observed in Figure 4.1, Figure 4.2 and Figure 4.3.

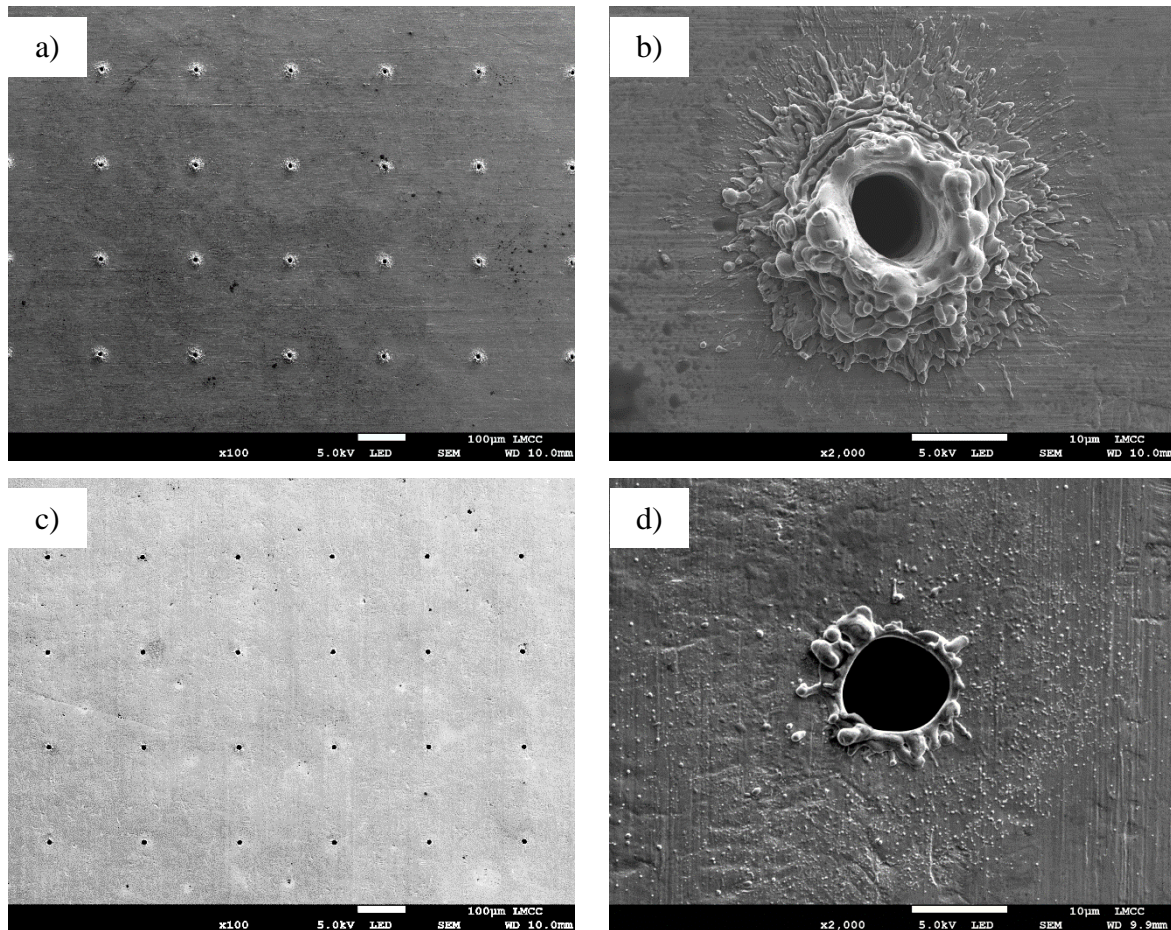


Figure 4.2 Top view of the entry and exit side of a stainless steel membrane with pores of 10  $\mu\text{m}$  (a) entry side – square pore pattern (b) single pore on the entry side (c) exit side – square pore pattern (d) – single pore on the exit side. These pictures were obtained using a SEM – JEOL JSM 7100F.

The pores of the stainless steel membranes are displaced in a square (200  $\mu\text{m}$ ) array while pores of the nickel membranes have a triangular array and are all equidistant (200  $\mu\text{m}$ ). The two sides of the membrane can be distinguished looking at the pore shape. For membrane emulsification purposes, the most relevant side is where drops are formed and the surface should be as flat as possible. Therefore, looking at the membranes made of stainless steel, the side showed in



Figure 4.1a-b and in Figure 4.2a-b is used as the entry side of the dispersed phase and, in Figure 4.1c-d and in Figure 4.2c-d, the side showed is the exit side where (dispersed phase) drops are formed. On the other hand, looking at nickel membranes type (Figure 4.3), pore has a conical shape and the side used as the exit side is observed in Figure 4.3d-f).

Pores of the stainless steel membranes are laser drilled. Therefore, to obtain different pores sizes, laser settings need to be adjusted such as laser aperture, power, time, etc. Thus, looking at the entry side of the membranes a higher residue amount is leftover which surrounds the pore. Comparing the two stainless steel membranes with different pore sizes, it is possible to observe that larger pores are likely to have higher amount of residue due to the larger drilled area. In section 4.1.1, quality of these membranes is evaluated by determining pore size distribution for different membrane pore sizes available.

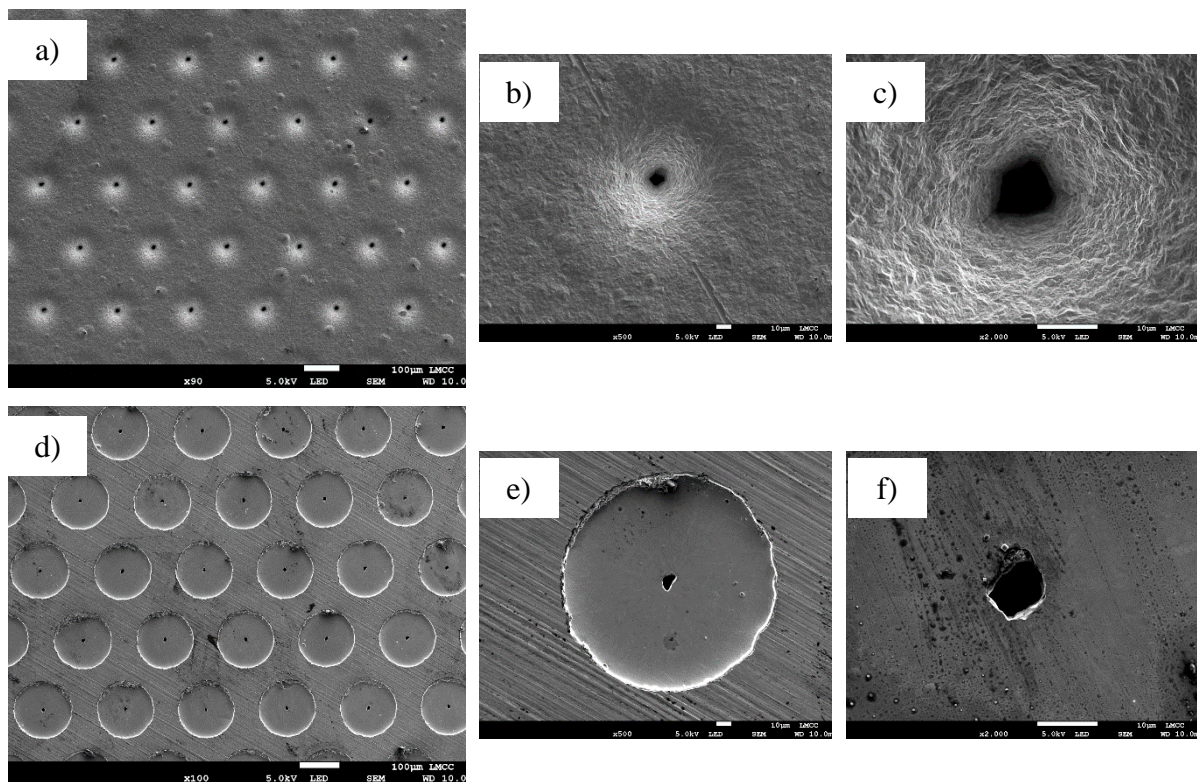


Figure 4.3 Top view of the entry and exit side of a nickel membrane with pores of 10 µm (a) entry side – triangular pore pattern (b, c) single pore on the entry side (d) exit side – triangular pore pattern (e, f) – single pore on the exit side.

Furthermore, by handling both types of membranes it was noticeable that stainless steel membranes are less flexible and more resistant to bending but no technical analyses were carried out to characterize this aspect.

#### 4.1.1 Pore size distribution

Final droplet size is proportional to the pore size as shown in the modelling (section 2.1.7). Thus, pore size distribution is very important and subsequently, a narrow pore size distribution will contribute to narrower drop size distributions emulsions. Therefore, some pore size analysis were carried out on the available membranes (flat discs): 5, 10 and 20  $\mu\text{m}$  (see Table 4.1 and Figure 4.4).

Table 4.1 Pore size characterization of a 5, 10 and 20  $\mu\text{m}$  membrane determined by optical microscopy and Image J analysis

Membrane pore size	D50 ( $\mu\text{m}$ )	Mean ( $\mu\text{m}$ )	D10 ( $\mu\text{m}$ )	D90 ( $\mu\text{m}$ )	D90 – D10 ( $\mu\text{m}$ )	CV (%)
5	4.4	4.2	3.7	4.9	1.2	12.1
10	12.1	12.2	11.4	13.4	2.0	7.8
20	21.6	21.4	19.8	23.6	3.8	7.1

In Figure 4.4 the pore size distribution of three stainless steel membranes is analysed. The mean pore sizes obtained are slightly shifted from what was expected and absolute variation in size between D90 value and D10 value is about 20% of the mean size (Table 4.1). But, overall, these membranes present a narrower size distribution relative to other types of membranes commonly reported in the literature for membrane emulsification purposes such as ceramics [35, 37], silicon or glass [41, 42]. Besides that, these metal membranes are more robust and less fragile being more likely to be adopted at industrial scale.

In principle, during membrane emulsification, due to the capillary pressure, the larger pores are the first to be activated. Capillary pressure is the minimum transmembrane pressure required for the dispersed phase to go through the membrane structure, forming droplets. Capillary pressure is inversely proportional to the pore size. Therefore, use of different transmembrane pressure may result in different number of “active” pores. Thus, many pores

may not be “active” during membrane emulsification. Consequently, this explains that resultant emulsion size distribution can be narrower than pore size distribution of the membrane.

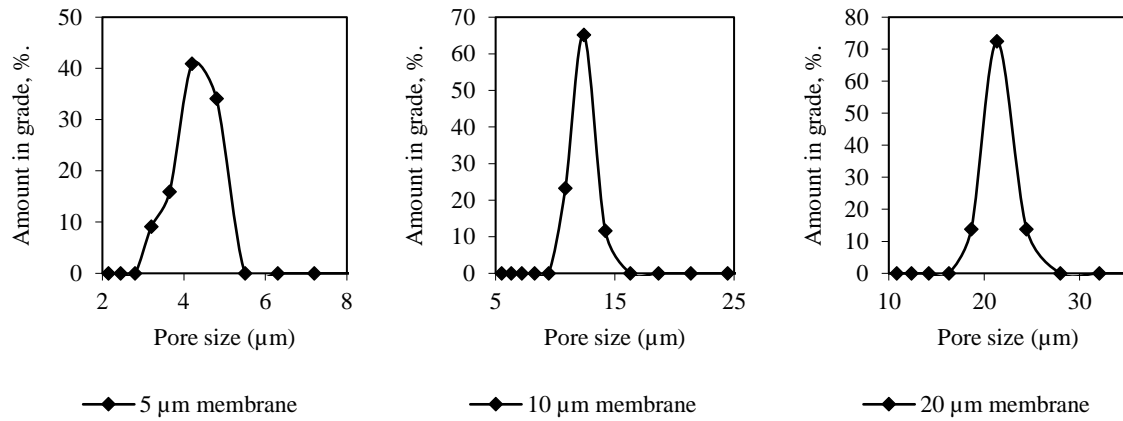


Figure 4.4 Pore size distribution of a 5, 10 and a 20 μm stainless steel membrane determined by optical microscopy and Image J analysis

## 4.1.2 Surface modification

Metal surfaces have a natural moderate hydrophilic behaviour. Therefore, to use these membranes for w/o emulsions it is required to make them hydrophobic. Therefore, in this work, a physicochemical treatment was developed on these metal porous surfaces to render them hydrophobic. Micropore [57] developed successfully, a modification of these surfaces which consisted of a physical bonding of polytetrafluoroethylene (PTFE) nanoparticles to the surface. PTFE is a material energetically stable, highly inert and has a low surface free energy of  $19.4 \text{ mN m}^{-1}$  [56]. In this section, a hydrophobic treatment is described using a FAS compound which is chemically absorbed to the metal surface. These compounds have a lower surface free energy than PTFE ( $8\text{-}9 \text{ mN m}^{-1}$ ), which makes them suitable for rendering hydrophobic surfaces [118].

As can be seen in Figure 4.5, regardless the pre-treatment/cleaning of the metal sheet the apparent contact angle gradually transitions over the drying period (at  $45^\circ\text{C}$ ) for about 1-2 hours from  $30 \pm 5^\circ$  to  $85 \pm 5^\circ$ . Similar behaviour was found in [119], suggesting a contact angle  $< 30^\circ$  for a clean steel surface, which increases to a value of  $\sim 75^\circ$  as the oxide layer is restored in vapour (air). Therefore, for this type of substrate (metal, susceptible to oxidation when exposed to vapour) the reported contact angle will depend on how it has been handled as well as its storage conditions.

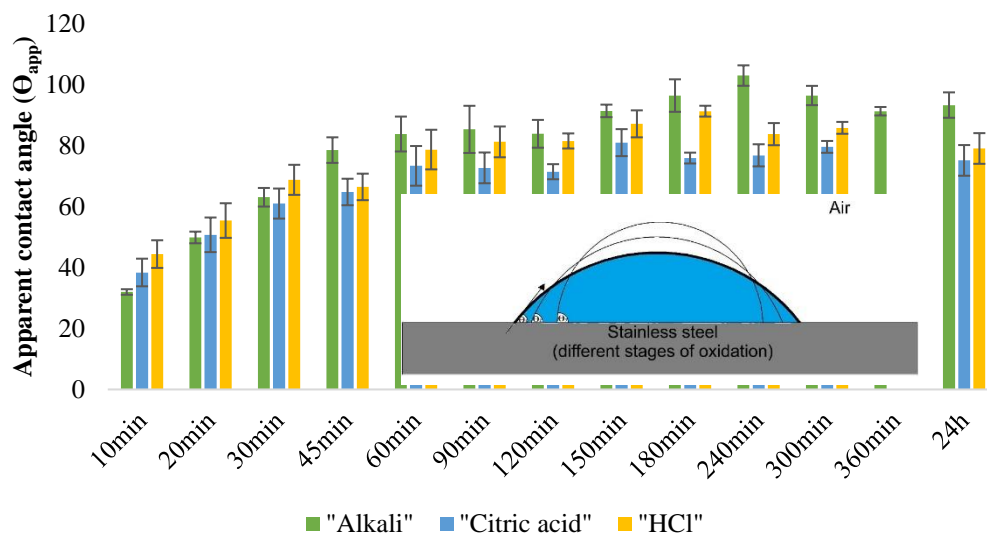


Figure 4.5  $\Theta_{app}$  monitoring water drop contact angle on metal sheets that were exposed to 4M NaOH (“alkali”), 2% wt. citric acid or 10% wt. HCl over a variable drying period.

It is apparent from Figure 4.5 that the contact angle, and therefore degree of surface oxidation, remains roughly constant after about one hour. Thus, in order to provide a consistent surface for the silanization stage, see Figure 2.2, a procedure of leaving the metal for a minimum of one hour after cleaning before treating with FAS solution was adopted.

Initial experiments indicated that a minimum soaking time required to achieve a contact angle around  $110^\circ$  at room temperature using a concentration of 0.01 M 1H,1H,2H,2H-Perfluorododecyltriethoxysilane. Therefore, a series of experiments were designed in order to optimise the process by possibly enhancing the contact angle.

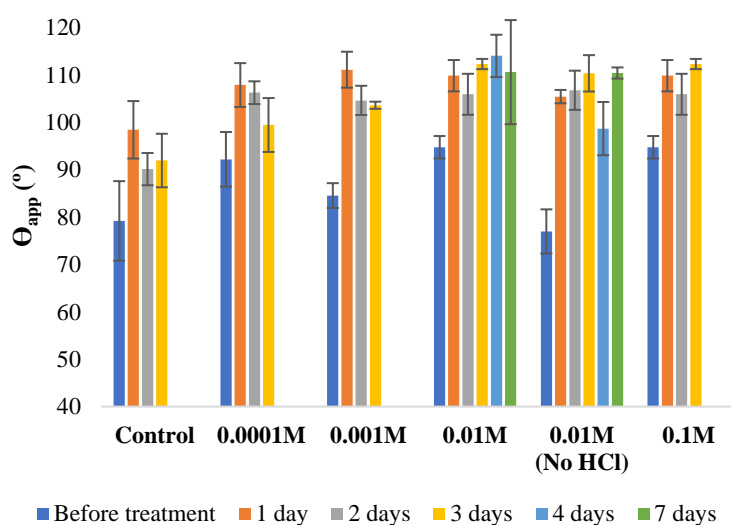


Figure 4.6. Apparent contact angle ( $\Theta_{app}$ ) measurements of sessile water drops on stainless steel sheets that were “FAS treated” using different concentrations of 1H,1H,2H,2H-Perfluorododecyltriethoxysilane (0.0001M, 0.001M, 0.01M and 0.1M) in undecane for various periods of time (1-7 days) at room temperature. As control, the presence of FAS chemical was avoided, exposing the surface only to undecane. The stainless steel used in the set named “0.01M No HCL” was not cleaned using HCl, all the others were.

Contact angles reported in Figure 4.6 were obtained from a series of experiments where a metal (stainless steel) sheet was treated in order to obtain a hydrophobic metal surface. A FAS chemical (1H,1H,2H,2H-Perfluorododecyltriethoxysilane) was used and bonded to the surface through the silanization reaction (see 2.1.1.1) lowering the surface free energy. Overall, the maximum contact angle achieved is about  $110^\circ$ . So, a (minimum) concentration of 0.01M is

suitable to achieve that level of hydrophobicity within 1-3 days. The need of exposing the metal surface to cleaning using HCl is not conclusive based on the contact angle evaluation. However, the metal (nickel) porous membrane treated to perform the drop formation experiments was exposed to HCl following the procedure described in section 3.1.1.1. The reason for exposing the metal body to HCl is to remove any impurities that may be absorbed to the surface, in a process known as pickling.

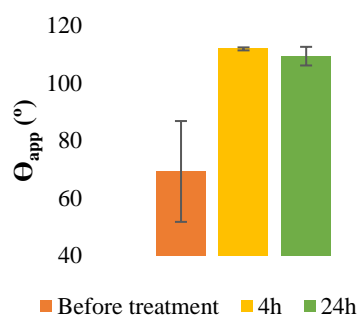


Figure 4.7. Apparent contact angle ( $\Theta_{app}$ ) measurements of sessile water drops on stainless steel sheets that were “FAS treated” using a concentration of 0.01M of 1H,1H,2H,2H-Perfluorododecyltriethosylsilane in undecane for 4 hours and 24 hours at 45°C.

As can be seen in Figure 4.7, silanization reaction time can be reduced to 4 hours at 45°C, achieving a contact angle of about 110° which is equivalent to the maximum contact angles observed in Figure 4.6.

In Figure 4.8, there are two images of a water droplet sitting on a FAS treated metal sheet surrounded by vapour (a),  $\Theta_{app} = 110 \pm 8^\circ$ , and by kerosene (b),  $\Theta_{app} = 150 \pm 5^\circ$ . This increase in the  $\Theta_{app}$  was expected according to the Young equation (Equation 2.5), i.e. the lower interfacial tension between drop phase and surrounding phase will lead to a higher contact angle. The contact angle achieved in vapour,  $110 \pm 8^\circ$ , is very similar to the reported contact angle for polytetrafluoroethylene [120-122], which is a material commonly used for hydrophobic applications. In ME apart from the degree of hydrophobicity, it is important to

achieve a surface that will maintain its characteristics over the emulsification period, to avoid any change of the contact angle and therefore change of the resultant droplet size, widening the drop size distribution [33].

The developed treatment was simple to apply and, in principle, could be easily applied at bigger scales to hydrophobize a metal membrane for the purpose of membrane emulsification to produce water-in-oil emulsions. It is also simple to reapply the FAS treatment to a surface.

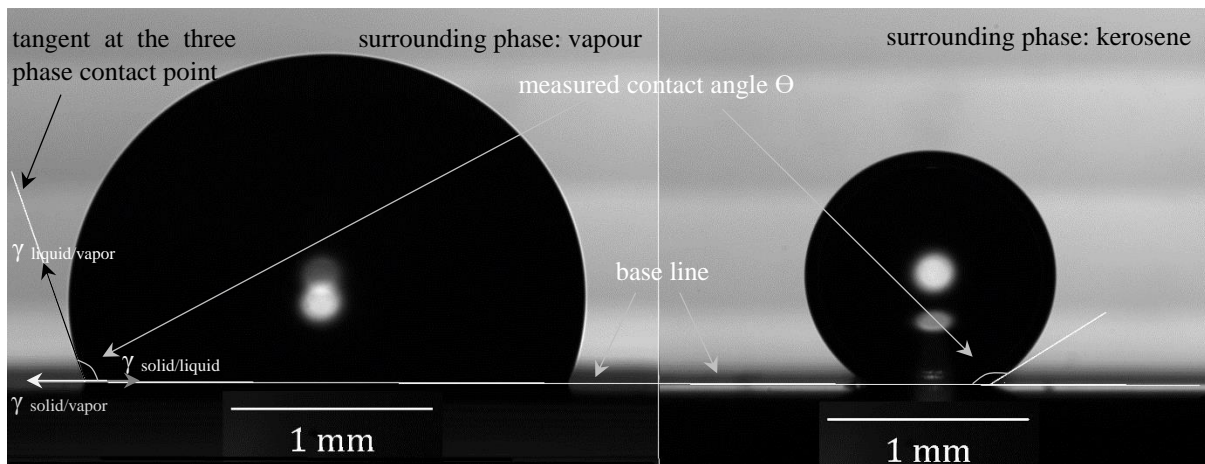


Figure 4.8. Image of a sessile water drop on a hydrophobic stainless steel (FAS treated) surface: (a) in vapour and (b) in kerosene, illustrating the interfacial tensions involved.

The stability of the surface treatment was evaluated by exposing the metal sheets hydrophobically treated for 24 hours to the standard membrane cleaning solutions. Contact angle measurements shown in Figure 4.9 indicate that hydrophobicity is kept after being exposed to water and a strong alkali (4M NaOH) solution but decrease when is exposed to citric acid. The loss of hydrophobicity is potentially explained by the fact that stainless steel is reduced when in contact to citric acid and therefore the siloxane bonds can be removed by hydrolyses [65]. Therefore, a hydrophobically treated membrane should not be cleaned with reducing agents such as citric acid, otherwise it must be recoated.

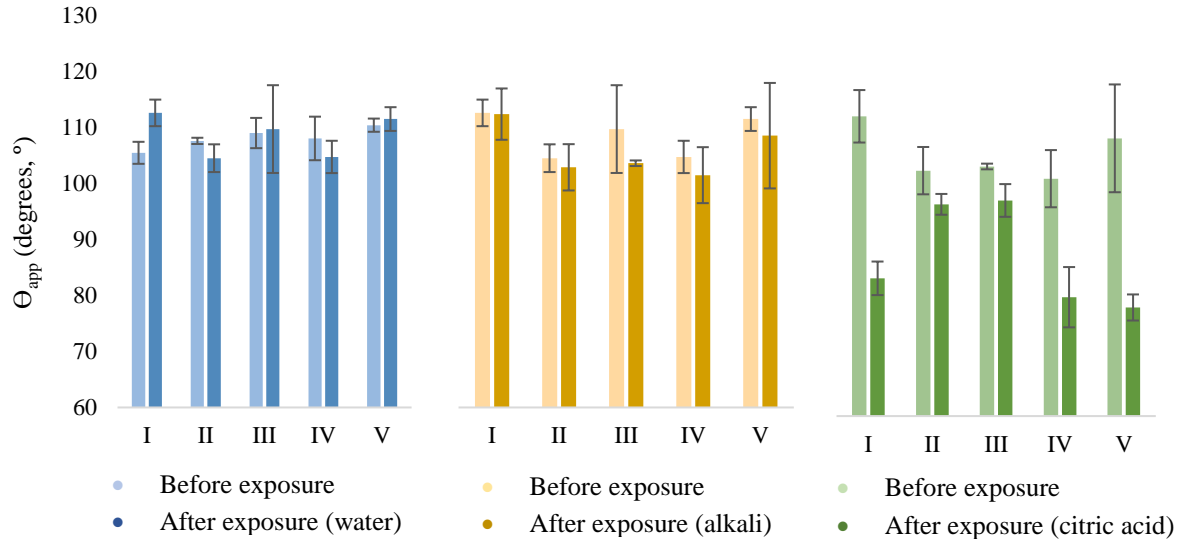


Figure 4.9 Contact angle measurements before and after of 5 stainless steel sheets being exposed for 24 hours to different aqueous solutions: water, 4M NaOH and 2% wt. citric acid.

In previous work by S. Morelli *et. al.* [32], two types of hydrophobic nickel membranes were used: PTFE coated (supplied by Micropore Technologies Ltd.) and FAS treated (with the optimised process that is described in this work). Uniform w/o emulsions were produced using both membranes, however further details, disclosed here, show that FAS treatment is an effective and reliable method for producing multiple uniform w/o emulsions. In Figure 4.10, water based droplets are shown with a formulation reported previously [32], in order to evaluate the performance of a PTFE coated and a FAS treated membrane for multiple emulsions. Operating parameters and cleaning cycles between the runs were equal in order to allow a direct comparison. Figure 4.10 shows the pictures of emulsions obtained using a new PTFE or FAS coated membrane (Figure 4.10a and c) and “used” PTFE or FAS coated membranes (Figure 4.10b and d), after they have been used 4 times.

From Figure 4.10a it is visible that the emulsion obtained with the new PTFE coated membrane was uniform (CV=18%) while a reduction of the uniformity is visible after multiple uses: the fourth emulsion produced using the same membrane had a CV= 35% (Figure 4.10b). Uniform drops were produced with a new FAS coated membrane with a measured CV of 22% (Figure 4.10c), and a CV of 24% was measured for the fourth emulsion produced using the same FAS coated membrane (Figure 4.10d). It is noticeable that a new PTFE coated membrane gives smaller droplets than a new FAS coated membrane. In fact, this is an indication that the new



PTFE membrane presented a higher level of hydrophobicity than the new FAS. However, after multiples uses, the PTFE coating is rendered less effective, producing larger droplets and resulting in a wider size drop distribution. Thus, FAS treated membranes are shown to be more stable, durable and reliable for producing multiple emulsions.

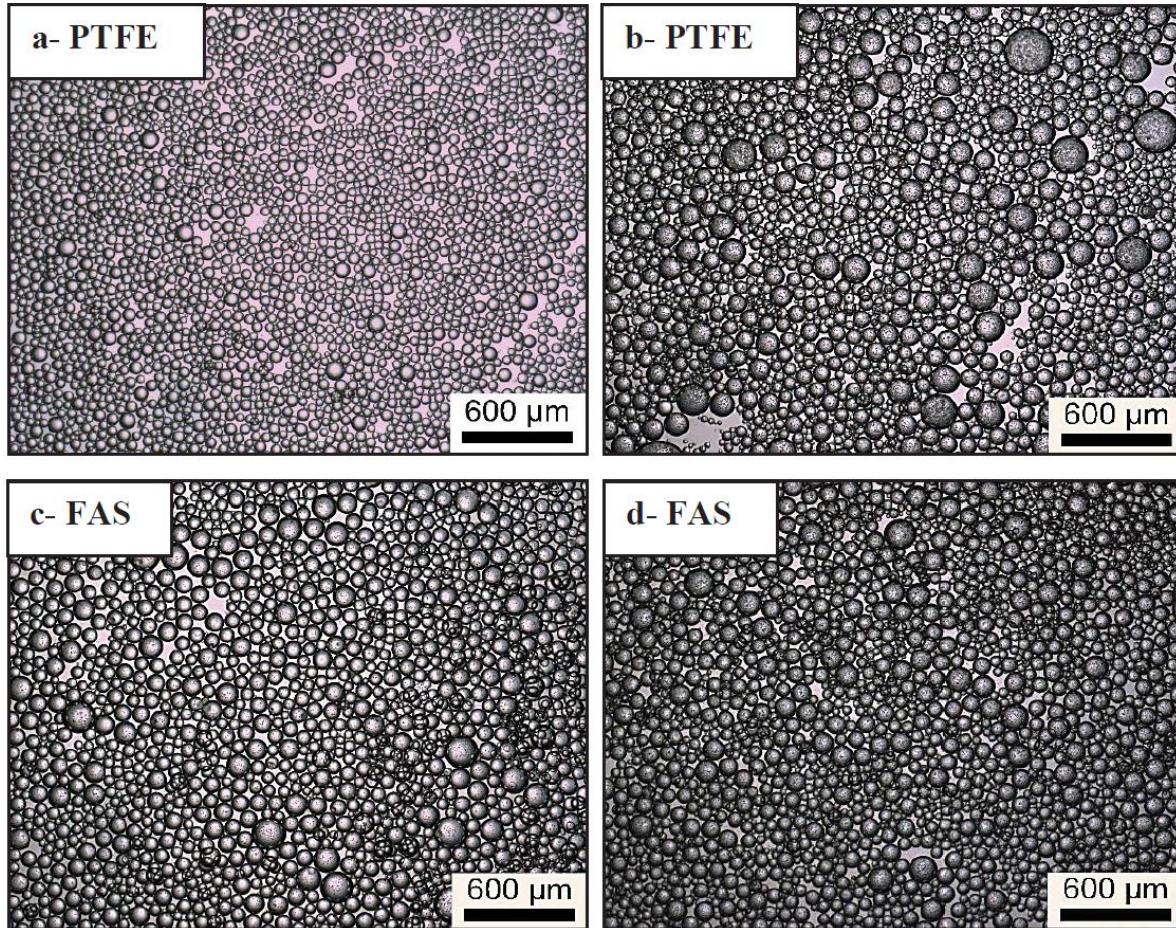


Figure 4.10. w/o emulsions produced using (a-PTFE) a new PTFE coated membrane, (b-PTFE) PTFE coated membrane after 4 uses, (c- FAS) a new FAS treated membrane and (d- FAS) a FAS treated membranes after 4 uses.

## 4.2 Surface and Interfacial tension measurements

In this work, mainly two surfactants were commonly used: Tween<sup>®</sup> 20 and Span<sup>®</sup> 80. Those are the common commercial names for these two non-ionic surfactants. Tween<sup>®</sup> 20 is a polysorbate type surfactant (see Figure 4.11a) with a high HLB number (16.7) [123] while Span<sup>®</sup> 80 is a sorbitan monoester (see Figure 4.11b with a low HLB number (4.3) [124]. Both are very commonly used in industry as emulsifiers in a number of domestic and scientific applications. As expected from their HLB number, Tween<sup>®</sup> 20 is used to stabilize o/w emulsions while Span<sup>®</sup> 80 is used to stabilize w/o emulsions. In this section, the interfacial properties of both surfactants by performing surface and interfacial tension measurements was investigated.

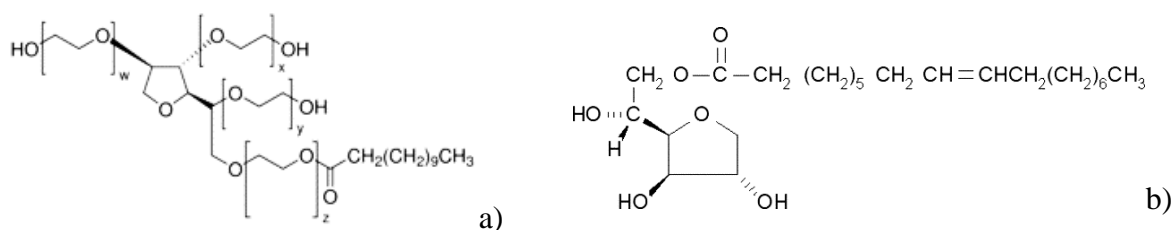


Figure 4.11 The structures of surfactants: a) Tween<sup>®</sup> 20 and b) Span<sup>®</sup> 80.

In Figure 4.12, the equilibrium surface tension ( $\sigma$ ) and interfacial tension ( $\gamma$ ) were determined by using the pendant drop method. As the concentration of surfactant increases, adsorption takes place at the interface until it is fully overlaid, which corresponds to the minimum value of surface tension. A knowledge of the CMC is very important for systems when using surfactants, and this feature was determined for Tween<sup>®</sup> 20 (Figure 4.12) and Span<sup>®</sup> 80 (Figure 4.13).

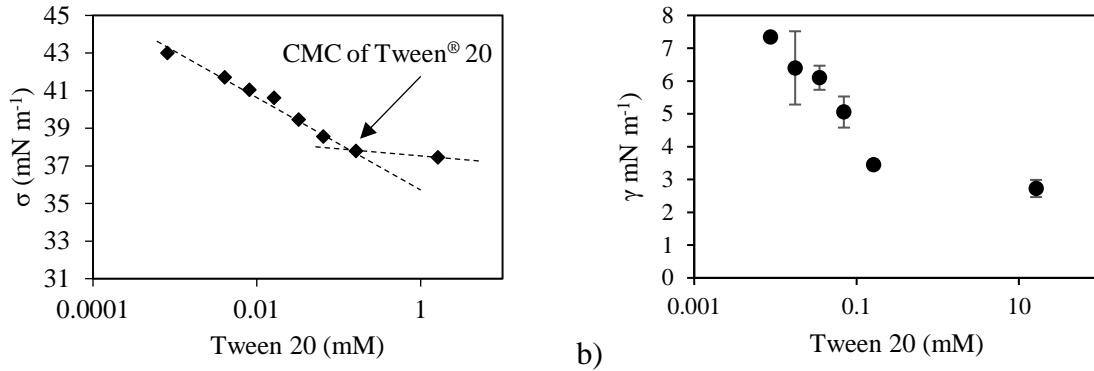


Figure 4.12 a) CMC determination of Tween 20 by measuring equilibrium surface tension using the pendant drop method. b) Equilibrium interfacial tension measurements between (commercial) sunflower oil and water with different Tween<sup>®</sup> 20 concentrations.

To determine the CMC of a surfactant dissolved in an oil by determining the minimum surface tension, a hydrophilic phase (like water) at the interface instead of vapour is needed, otherwise surfactant molecules will not adsorb to the interface as both phases are hydrophobic (e.g.: oil and vapour). The determined CMC of Tween<sup>®</sup> 20 is  $0.06 \pm 0.01$  mM and of Span<sup>®</sup> 80 is  $0.51 \pm 0.07$  mM.

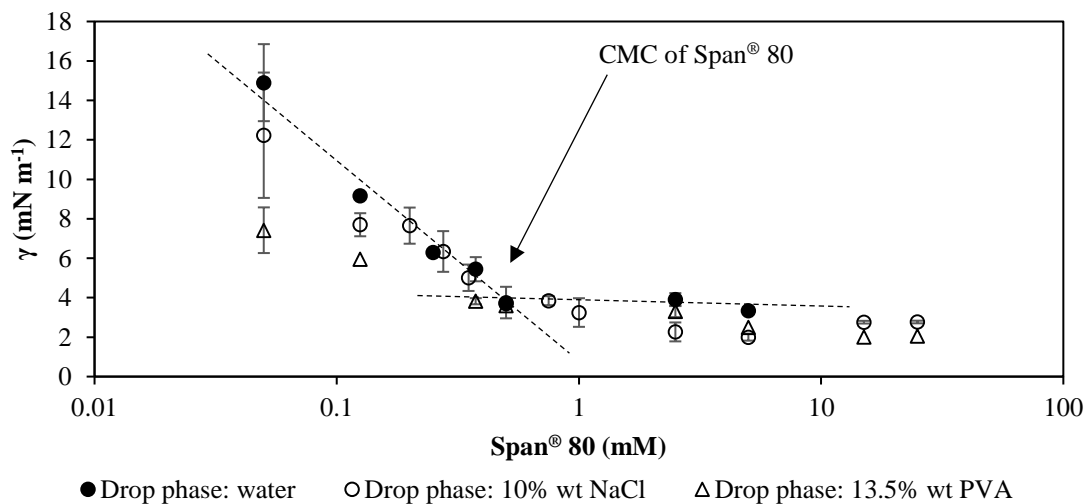


Figure 4.13 Interfacial tension between drop phases: ● pure water; ○ saline water (10% (w/w) NaCl) and △ 13.5% (w/w) PVA in water) and surrounding phase that contained different surfactant (Span<sup>®</sup> 80) concentrations present in kerosene using pendant drop technique.

Dynamic interfacial tension measurements were undertaken between water and kerosene with various concentrations of Span<sup>®</sup> 80 dissolved (Figure 4.14a) as well as between 13.5% PVA in water and kerosene with same concentrations of Span<sup>®</sup> 80 (Figure 4.14b). Looking at Figure 4.14, it is possible to conclude that the polymer PVA is surface active. In fact, this polymer is used in section 5.1.2 and 4.3.2 as a surfactant stabilizing the organic droplets and due to its high molecular weight provides a good stabilization by steric repulsions. So, in the case that PVA and Span 80 are present there is dynamic adsorption competition at the interface, PVA diffuses from the bulk of the aqueous phase while Span<sup>®</sup> 80 diffuses from the bulk of the organic phase.

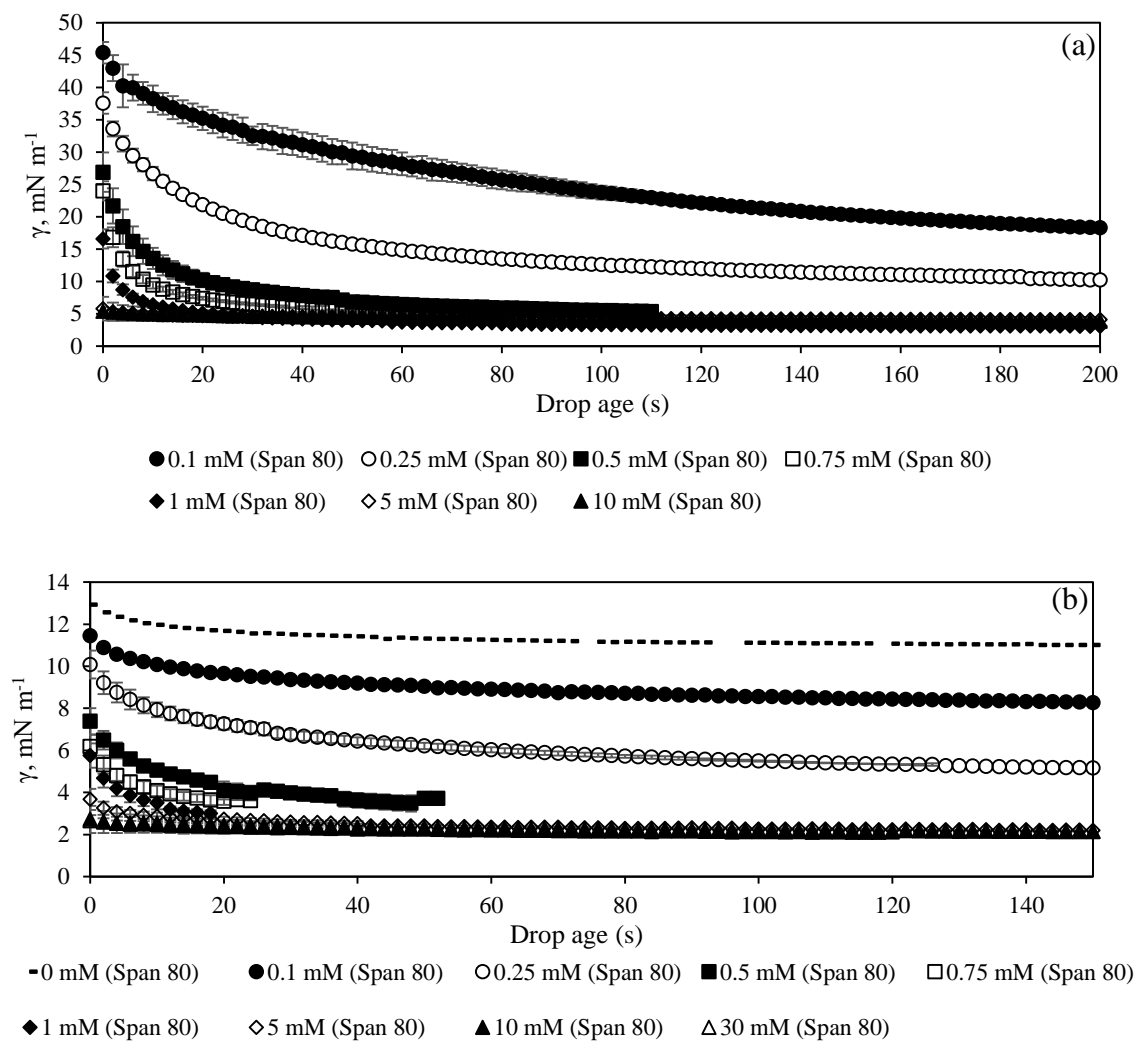


Figure 4.14 Dynamic interfacial tension determined by pendant drop method between distilled water (a) or 13.5% wt. PVA in water (b) and kerosene that contained different concentrations of Span<sup>®</sup> 80 dissolved: 0.1, 0.25, 0.5, 0.75, 1, 5, 10 and 30 mM plotted as a function of aging drop time.

Dynamic interfacial tension measurements were used to determine the surfactant dynamics in the system, which was needed in the method developed during this work, to determine the number of active pores in membrane emulsification using certain operational conditions (see section 5.2.2).

### 4.3 Static contact angles

Sessile droplet experiments were carried out to characterize the wetting properties, mimicking the drop formation contact angle, using similar substrates (stainless steel) to the membranes used for emulsification experiments and the same liquid solutions (water, 10% wt. NaCl, 13.5% wt. PVA, Span<sup>®</sup> 80 in kerosene and so on).

Initially, spreading of aqueous drops on the metal surface without presence of either surfactant or immiscible liquid, i.e., just vapour phase surrounding the metal sheet, was investigated; and later with presence of surrounding liquid phase: kerosene with, or without, surfactant. Table 4.2 summarises the apparent static contact angle obtained for these experiments.

Table 4.2: Static contact angles obtained from sessile drop experiments using the DSA 100. The error value reported is the standard deviation from at least three measurements performed.

Drop phase	Surrounding phase	$\Theta$ (°)
(Pure) water	Vapour	$46 \pm 10$
	Kerosene	$55 \pm 9$
10 % NaCl	Vapour	$52 \pm 5$
	Kerosene	$69 \pm 9$
13.5 % PVA	Vapour	$37 \pm 4$
	Kerosene	$44 \pm 4$

Table 4.2 shows that stainless steel is partially wetted by the three-different water based drops tested ( $\Theta < 90^\circ$ ), showing hydrophilic behaviour when the surrounding phase is vapour. Similar results are obtained when kerosene is present (instead of vapour): all drops tested showed partial wetting behaviour ( $\Theta < 90^\circ$ ).

Figure 4.15 shows that apparent contact angle increased, with the presence of surfactant Span<sup>®</sup> 80 in the surrounding phase, for the three-different water based drops, reaching a constant value when surfactant concentrations were slightly above critical micelle concentration (0.5 mM).

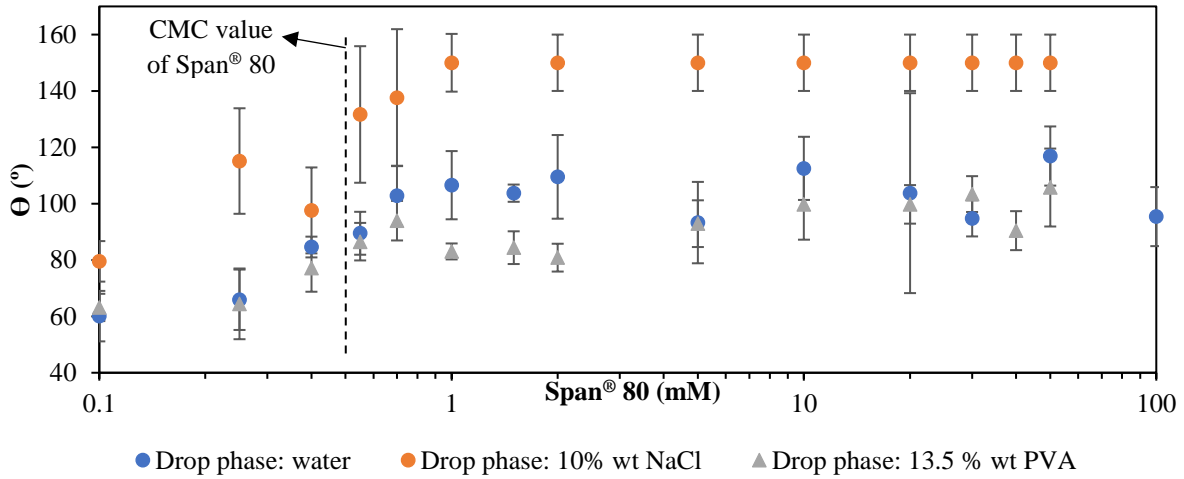


Figure 4.15 Contact angles of three different drop phases (● pure water; ○ salty water (10% (w/w) NaCl) and ▲ 13.5% (w/w) PVA in water) surrounded by different surfactant concentrations present in kerosene on a non-treated (hydrophilic) stainless steel sheet. These measurements were performed using the DSA 100.

Overall, increasing the surfactant concentration, the (equilibrium) interfacial tension liquid-liquid lowers (till CMC value) which explains the increase of the contact angle (since contact angle is higher than 90°) as is predicted by Young equation:

$$\gamma_{sv} = \gamma_{sl} + \gamma_{lv} \cos \theta \tag{eq. 4.1}$$

where  $\gamma_{sv}$  is the solid-vapour (or immiscible liquid) energy,  $\gamma_{sl}$  is the solid liquid interfacial energy,  $\gamma_{lv}$  is the liquid vapour (or immiscible liquid) interfacial energy, i.e., surface (or interfacial) tension and  $\theta$  is the resultant contact angle (see Figure 4.16):

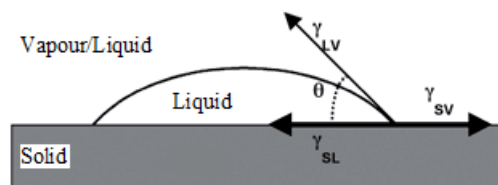


Figure 4.16 Liquid drop on a solid surface showing the interfacial tensions at the three phase contact line.

In experiments when the concentrations above CMC were used, a lag time was observed before spreading starts. This lag time increased with higher surfactant concentration and it could take several seconds, or even minutes before spreading starts. However, this lag time was difficult to determine because it varied between experiments using identical conditions. Once the spreading starts, resultant contact angle is nearly constant and experiments proved to be very reproducible (see Figure 4.15). The presence of PVA decreased the contact angle as was expected since, it was concluded from data showed in Figure 4.14, that PVA is surface active. On the other hand, using salty water contact angles observed were overall higher compared to pure water. These results cannot be explained by change of the interfacial tension, since interfacial tension measured, practically, did not change in the presence of salt in the drop (see Figure 4.13).

Contact angle measurements with 13.5% wt. of PVA ( $90^\circ < \Theta < 110^\circ$ ) show that droplets formed during emulsification experiments should not wet membrane surface at concentrations of Span<sup>®</sup> 80 above CMC (between 10 and 100 mM) (see Figure 4.15). Another important observation is the presence of the lag time: which means that in the course of membrane emulsification (which occurs faster than the lag time) the droplet does not have enough time to spread over the membrane surface. However, wetting may occur because generation of drops in membrane emulsification is a very dynamic process: after the drop forms and detaches from the membrane surface, surfactant must diffuse from the bulk to the membrane surface. The latter process may result in a partial wetting of the membrane surface.



#### 4.4 Dynamic contact angles

A rotating drum setup was used to characterize wetting and dewetting of the surface when in contact with two immiscible liquids. Data acquired with this setup was obtained monitoring the interface from both sides of the rotating drum between water (with and without presence of surfactant) and kerosene (with and without presence of surfactant). Advancing and receding contact angles were determined for different rotation speeds (0-12 mm/s, at the periphery of the drum). Dynamic contact angles depend on the rotating velocity of the substrate and here they are represented in contact angle versus velocity and scaled by per cent of the CMC value of the surfactant used.

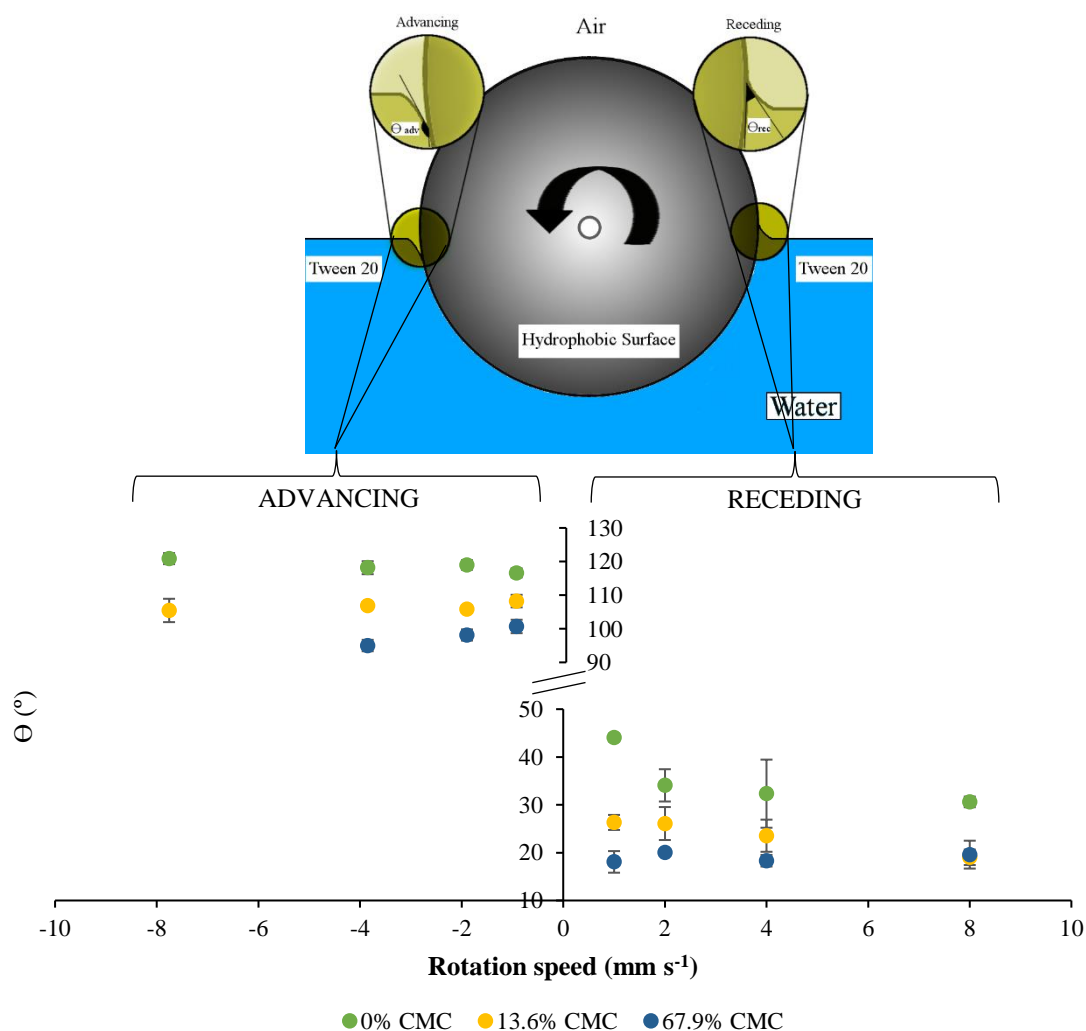


Figure 4.17 Dynamic advancing and receding contact angles against rotation speed for different surfactant concentrations (three phase contact: hydrophobic drum, vapour and water in the presence of Tween<sup>®</sup> 20).

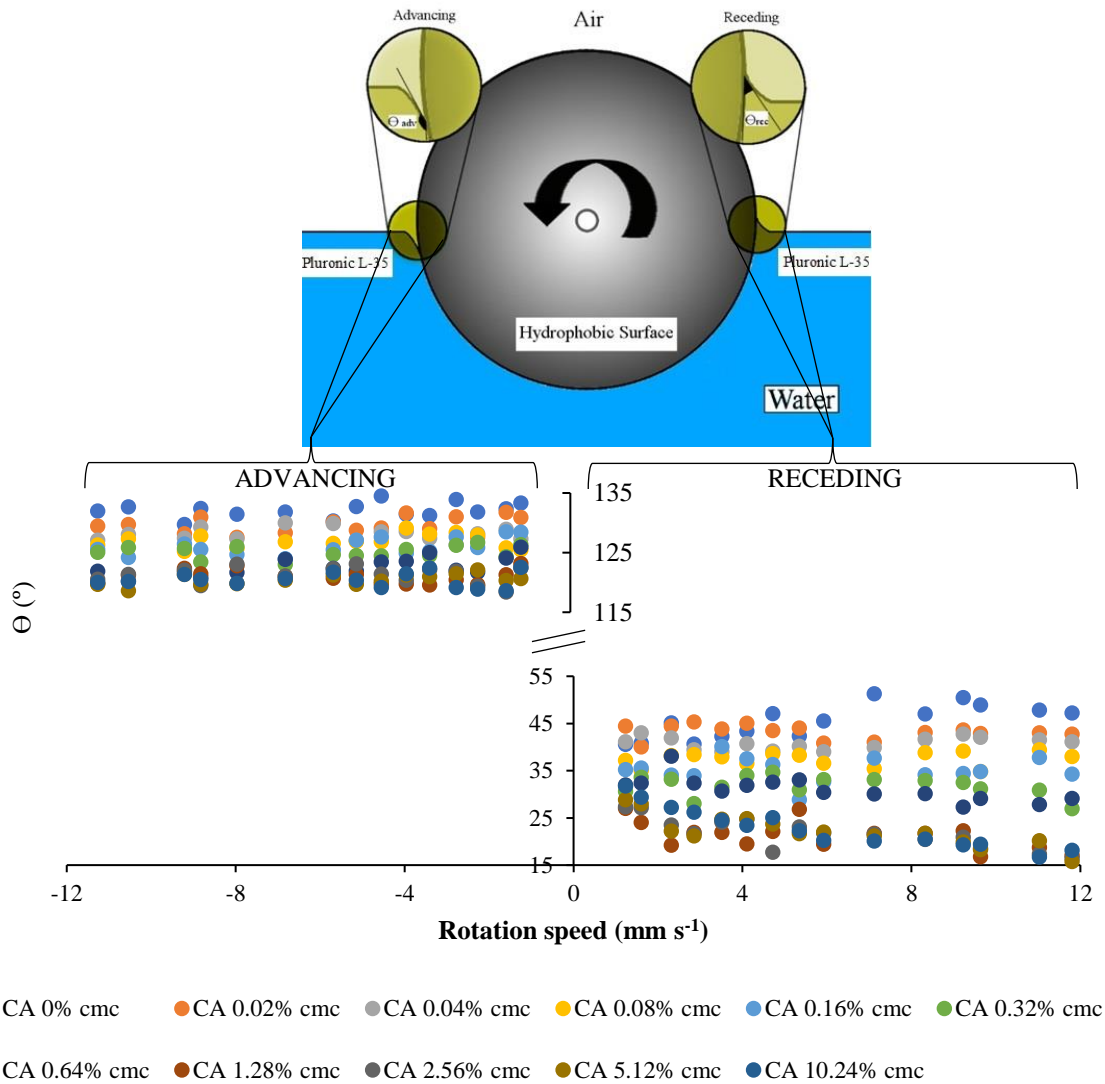
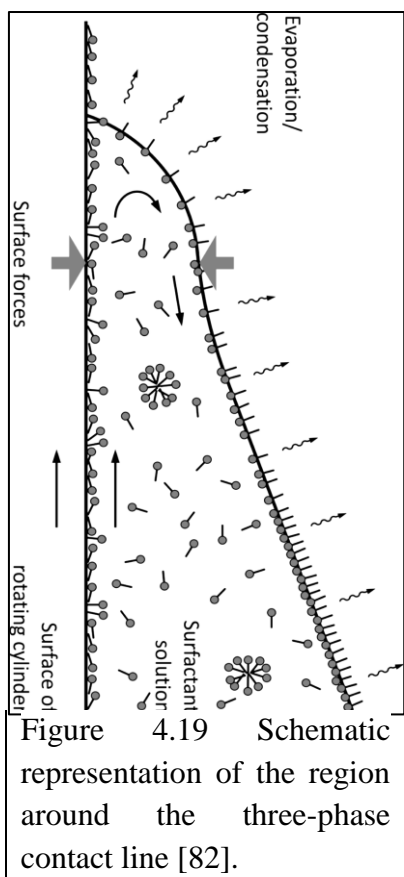


Figure 4.18 Dynamic advancing and receding contact angles against rotation speed for different surfactant concentrations (three phase contact: hydrophobic drum, vapour and water in the presence of Pluronic<sup>®</sup> L-35).

The dynamic contact angles reported in Figure 4.17 and Figure 4.18 are using a single liquid phase with presence of Tween<sup>®</sup> 20 and Pluronic<sup>®</sup> L-35, respectively. So, the (three phase) interface in these experiments is constituted by a hydrophobic surface (drum), water (with surfactant) and vapour phase. Drum surface has been (hydrophobically) treated using the same procedure as the metal membranes with FAS (see section 3.3). Both dynamic contact angles are rotation velocity and surfactant concentration dependent. Increasing the drum velocity, the difference between the advancing and receding contact angle, so-called hysteresis, increased. In general, it was observed that an increase in the advancing contact angle coincided with a

decrease in the receding contact angle. However, for the range of velocities tested, that difference is just a few degrees ( $\sim 5^\circ$ ), but it would be expected to be greater if higher velocities would be tested as in work performed by G. K. Auernhammer and his colleagues (0-250 mm/s) [83]. Nonetheless, the main aim was to characterize the system with two liquids and for this purpose use of speeds above 10 mm/s would not be recommended because viscous forces would overcome the capillary forces (Capillary number of the system should not be higher than  $10^{-4}$ ).

With increase of surfactant concentration, advancing and receding contact angle decreased, as expected, due to the lower surface tension. However, it is noticeable that the decrease of the receding contact angle ( $25-30^\circ$ ) is higher than the decrease of the advancing contact angle ( $\sim 15^\circ$ ) resulting in higher contact angles hysteresis as surfactant concentration increased. Results showed in Figure 4.18 is a good example of this behaviour. For the Pluronic L-35 concentrations tested, the total decrease of the advancing contact angle is about  $15^\circ$  while the receding contact angle decreased about  $25-30^\circ$ . This behaviour has been observed previously [82] (see Figure 4.19) and explained by the presence of a surface tension gradient near to the three phase contact on the “receding” side. On this side, liquid is being pulled up with the substrate and fresh surface is created near to the three-phase contact, resulting in a lower



concentration of surfactant molecules close to this fresh interface. Therefore, a gradient of surfactant molecules means a gradient in surface tension resulting in a Marangoni force in the direction of the contact line contributing to the decrease of the contact angle. This phenomenon is not observed in the advancing side, where liquid is being pulled down, because the concentration of surfactant molecules near to the three-phase contact is equal to the concentration at the interface elsewhere. So, these results are in agreement with work performed previously with a similar setup [80, 82, 125]. To the thesis author's knowledge, no experiments were carried out before using two immiscible liquids. In this current work, this approach was explored in order to gain better understanding which can be correlated to systems where it is important to know about wetting and dewetting properties

of the substrates in contact with immiscible liquids (with, or without, the presence of surfactant) such as membrane emulsification.

Four different combinations were tested using the rotating drum system with two immiscible liquids:

- a) hydrophilic drum, water with surfactant and kerosene;
- b) hydrophobic drum, water with surfactant and kerosene;
- c) hydrophilic drum, water and kerosene with surfactant;
- d) hydrophobic drum, water and kerosene with surfactant.

Using combination (a), it was only possible to determine the dynamic contact angles without presence of surfactant for different rotation speeds (see Figure 4.20). As soon as Tween<sup>®</sup> 20 is present in the aqueous phase, the hydrophilic drum is wetted by the aqueous phase (forming a film surrounding the drum surface) and the three phase contact line is lost. Using combination (d), it was only possible to determine the dynamic contact angles without presence of surfactant (see Figure 4.20). As soon as Span<sup>®</sup> 80 is present in the organic phase, the hydrophobic drum is wetted by the organic phase forming a film that surrounds the drum surface and the three phase contact line is no longer seen. During the performance of the experiments, it was evident the formation of the aqueous film using combination a) and formation of the organic phase film using combination d) after only half turn of the drum. So, for these combinations, a) and d), it was only possible to determine the dynamic contact angles without presence of surfactants for different rotation speeds (see Figure 4.20).

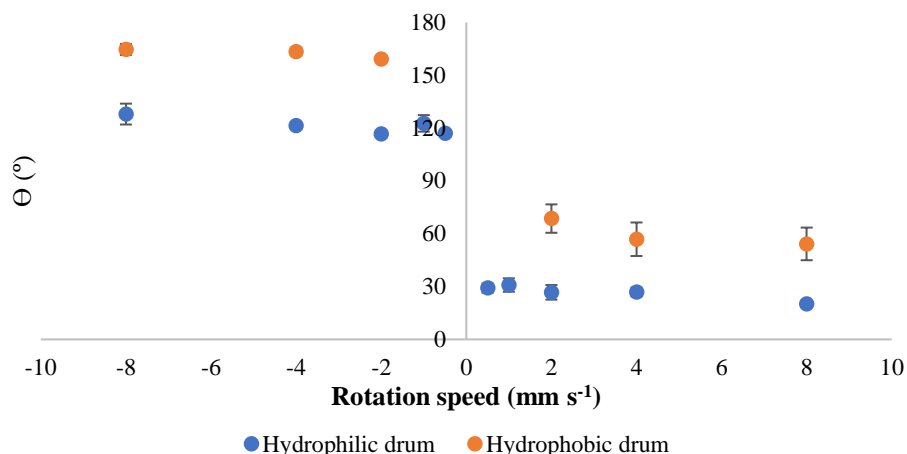


Figure 4.20 Dynamic advancing and receding contact angles against rotation speed using two different drums (hydrophilic, no modification, and hydrophobic treated) half immersed in water and kerosene without presence of surfactants.

Wetting (advancing side) and dewetting (receding side) properties of two different drums used in this work were compared using the same liquids and same rotation speeds without presence of surfactants. It is possible to observe in Figure 4.20 a difference of about 40° between the two drums which is quite encouraging regarding the effectiveness of the hydrophobic treatment applied.

Contact angle hysteresis observed is quite large (80-100°). This feature is influenced by the setup geometry chosen that can affect mainly flow profiles as well by the roughness of the substrate. These aspects are well described in the PhD thesis of D. Fell in the fourth chapter: “Influence of the setup geometry on dynamic wetting/dewetting” [125].

Results obtained with combinations b) and c) are showed in Figure 4.21 and Figure 4.22, respectively.

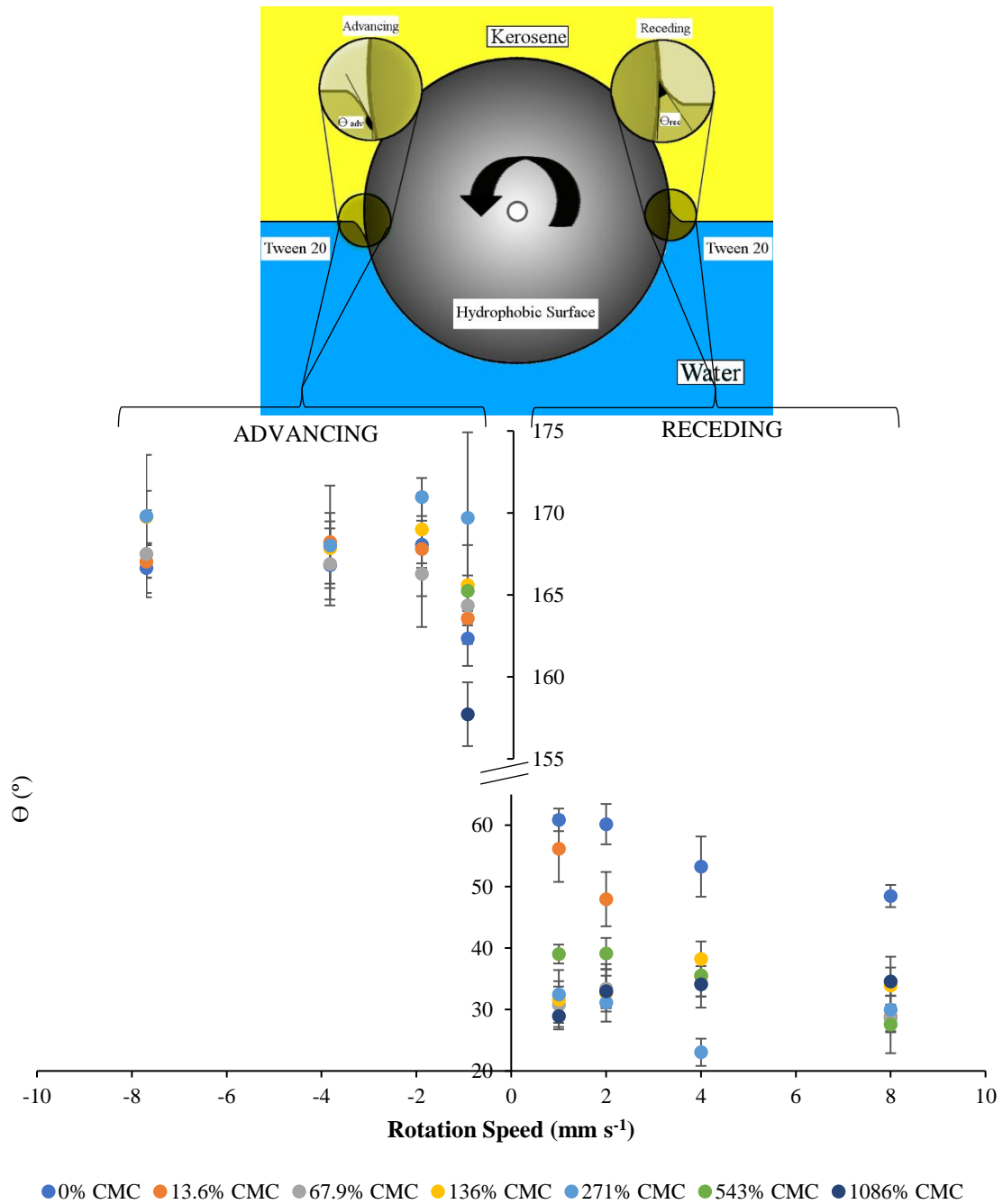


Figure 4.21 Dynamic advancing and receding contact angles against rotation speed for different surfactant concentrations (three phase contact: hydrophobic drum, kerosene and water in the presence of Tween<sup>®</sup> 20).

With the presence of the organic phase instead of the vapour phase similar dynamic contact angle behaviour was observed, i.e., both dynamic contact angles decreased with surfactant concentration while increase of rotation velocity led to the decrease of the receding contact angle and increase the advancing contact angle.

Comparing Figure 4.21 and Figure 4.22, it is possible to identify a major difference between those experiments: the larger decrease in the contact angle in Figure 4.21 is observed on the receding side while in Figure 4.22 this larger decrease is observed on the advancing side. Previously, in the presence of a single liquid, a Marangoni flow would enhance the decrease of the contact angle on the receding side. With two immiscible liquids, the presence of Marangoni flow is noticed in both configurations as shown by the data.

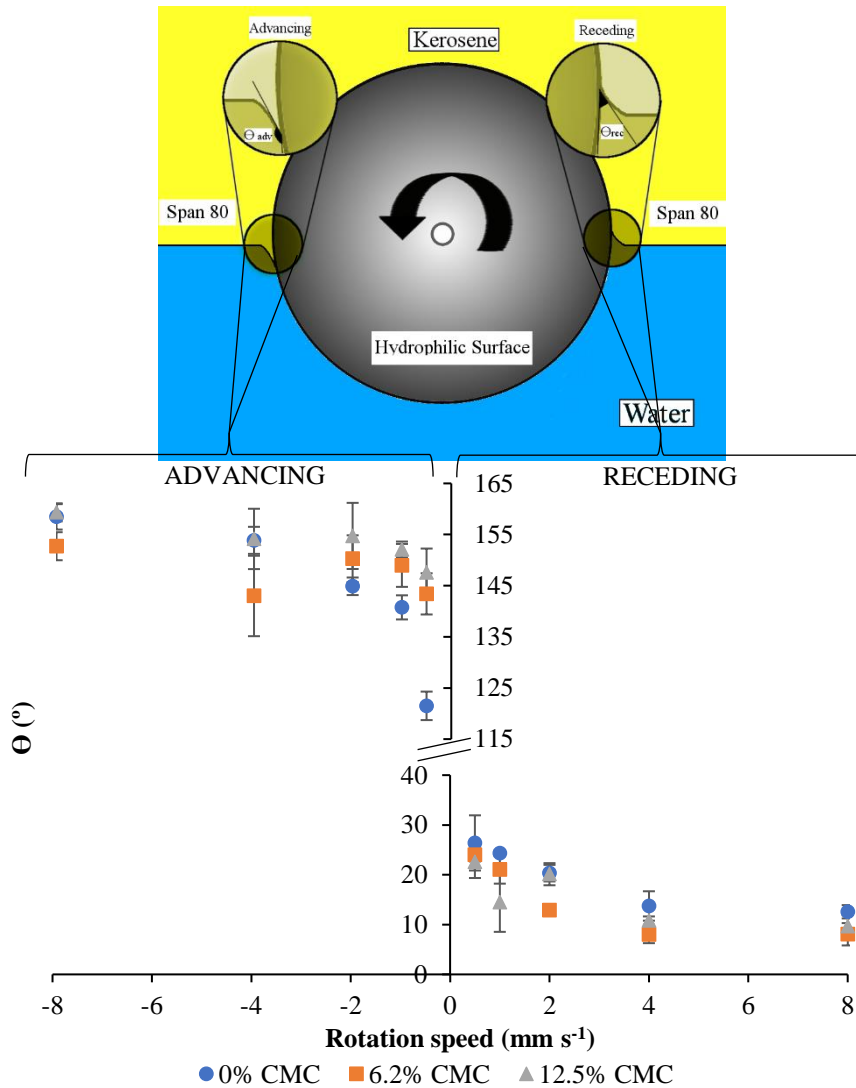


Figure 4.22 Dynamic advancing and receding contact angles against rotation speed for different surfactant concentrations (three phase contact: hydrophilic drum, kerosene in the presence of Span<sup>®</sup> 80 and water).

Essentially, when surfactant is present in the aqueous phase, on the “receding side” there is created a fresh (aqueous) surface at the three-phase contact line which creates a gradient of

interfacial tension, caused by the gradient of surfactant concentration molecules, “pulling up” the aqueous liquid which contains the dissolved surfactant. On the other hand, when surfactant is present in the organic phase (Figure 4.22), on the advancing side there is created a fresh (organic) surface at the three-phase contact line which creates a gradient of interfacial tension “pulling down” the top organic liquid which contains the dissolved surfactant. It is worth mentioning that the “receding side” is being referred relative to the aqueous phase, but in fact the receding side for the organic phase (top liquid) would be the opposite side. However, for consistency in this work, receding side always refers to the bottom liquid where the substrate is moving upwards.

In both scenarios, Figure 4.21 and Figure 4.22, a film was observed being formed around the drum above a critical surfactant concentration. In the case of experiments shown in Figure 4.21 this film is formed by the aqueous phase (advancing and receding contact angles were below  $90^\circ$ ) while in case of Figure 4.22, this film is formed by the organic phase (advancing and receding contact angles were above  $90^\circ$  - see Figure 4.23).

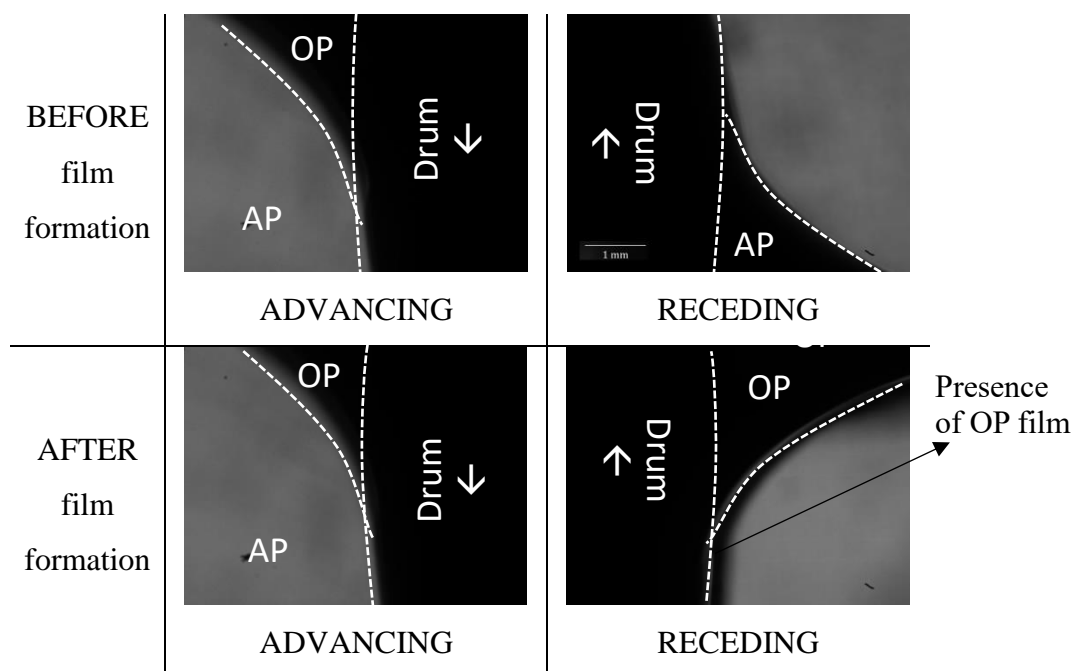


Figure 4.23 Pictures of advancing and receding contact angle between the organic phase (OP) and the aqueous phase (AP) before and after film formation for concentrations above 12.5% of the CMC in the OP using a hydrophilic drum.



Figure 4.23 shows the images obtained by the developed rotating drum setup, by both cameras located at each side of the drum which are focused at the interface between the two liquids interface while the drum is being rotated at a certain rotation speed. It can be observed that advancing and receding contact angle are distinct before film formation while after film formation (by the organic phase) advancing and receding contact angle are identical, in this case, well above  $90^\circ$ . Therefore, these observations support the fact that this substrate will preferably wet by the phase that contains surfactant, even at very low concentrations, 12.5% CMC, well below to the surfactant concentrations used in membrane emulsification processes.

Measurements of the reported dynamic contact angles provide valuable information which can be applied to membrane emulsification, or other processes using two liquid systems in which surfactants are present. To give a practical example, many membranes used in membrane emulsification have a natural hydrophilic behaviour and conventionally, these membranes need to receive a hydrophobic treatment when the aim is to produce w/o emulsions. However, the experiments reported above show that an organic phase can wet a hydrophilic surface completely, using very low surfactant concentrations, without dewetting in presence of an aqueous phase. So, these are encouraging results when the aim is to produce w/o emulsions using an hydrophilic membrane (see Section 5.1.1).

## 4.5 Spontaneous emulsification of water in oil at appreciable interfacial tensions

In this section, a dynamic phenomenon observed during sessile drop experiments and interfacial tension measurements when water and organic phase (kerosene) with high concentrations of Span<sup>®</sup> 80 was in contact for relatively short times (< 5 min) is reported. Basically, it was observed that formation of very small droplets at the interface between water and organic phase occurred. These small droplets had the similar look as an emulsion (white fog) providing a certain haziness to the organic phase solution after a short time. This phenomenon became more evident for longer periods of contact between water and organic phase loaded with surfactant (Span<sup>®</sup> 80). Therefore, this interesting phenomenon was studied further by designing a set of experiments using glass vials (section 4.5.1) and sessile droplets (section 4.5.2).

### 4.5.1 Characterization of the water droplets present in the organic phases

After suspecting the presence of spontaneous formation of aqueous droplets in kerosene, facilitated by the presence of a micelle forming organic phase surfactant, the influence of both salt concentration in the aqueous phase and surfactant concentration of Span<sup>®</sup> 80 in the organic phase was investigated.

Figure 4.24 shows that microemulsions of water were formed only if the concentration of surfactant in the kerosene was higher than a critical value, which according to the experimental results was either equal to CMC or slightly above CMC. Observations performed during the experiments indicated that the turbidity in the organic phase was clearly influenced by the amount of surfactant present (Figure 4.25). The influence of salt concentration in the aqueous phase on the microemulsion formation was also investigated. These experiments showed that the higher the salt concentration in the aqueous phase the lower the turbidity is (low concentration of droplets inside the kerosene). Characterization of this process was carried out, using a Nanosight size analyser: concentration of the aqueous microdroplets and their size was determined. Table 4.3 and Table 4.4 summarise the data collected from these experiments. Higher concentration of surfactant promotes the self-emulsification of water in kerosene, while higher concentration of salt retards, or even stops, this phenomenon from happening.

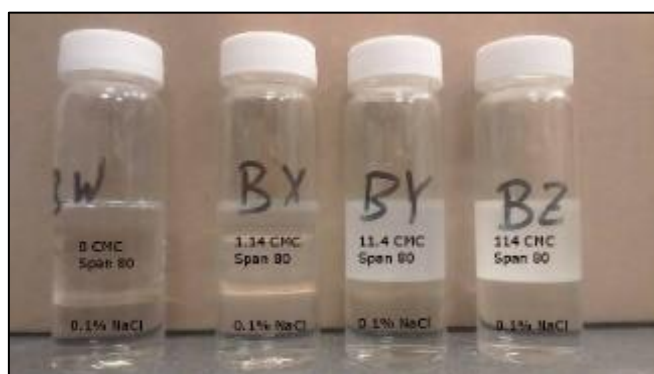


Figure 4.24 Example of the surfactant concentration influence on the self-emulsification process: each vial contains 10 mL of water (lower liquid layer) and 10 mL of kerosene (top liquid layer) with different concentration of Span<sup>®</sup> 80: samples BW, BX, BY and BZ contain pure water, 1.14, 11.4 and 114 times the CMC, respectively. There is no visible detection of microemulsion formation in vials BW and BX, but they are present in vials BY and BZ.

Table 4.3 Droplet concentration with salt and surfactant concentration during the spontaneous formation of aqueous droplets in kerosene determined by Nanosight size analyser.

Concentration of NaCl (% w/w)	Concentration of drops (number/mL) at the following CMC values:			
	0x	1.14x	11.4x	114x
0	0	$6.0 \times 10^8$	$2.5 \times 10^{12}$	$7.0 \times 10^{12}$
0.1	0	0	$1.19 \times 10^{12}$	$3.5 \times 10^{12}$
1	0	0	$2.7 \times 10^8$	$1.9 \times 10^{11}$
2	0	0	$7.6 \times 10^8$	$1.2 \times 10^{11}$
5	0	0	$7.05 \times 10^8$	$9.1 \times 10^{10}$
10	0	0	$2.5 \times 10^8$	$1.1 \times 10^{10}$

The data presented in Table 4.3 shows that the concentration of drops formed in the organic phase decreases rapidly with increasing of salt concentration. In the absence of any salt in the aqueous phase the maximum water drop concentration reaches  $7.0 \times 10^{12}$  drops per mL, when using a Span 80 concentration 114 times that of the CMC value. Table 4.4 illustrates a wide range of droplet sizes found in the samples that contained aqueous droplets in the organic phase, but the reported drop sizes are generally between 200 and 300 nm.

Table 4.4 Aqueous droplet size with salt concentration in the aqueous phase and surfactant concentration in the organic phase determined by Nanosight size analyser.

Concentration of NaCl		Drop size (nm) at the following CMC values:			
(% w/w)	0x	1.14x	11.4x	114x	
0	0	226	190	320	
0.1	0	0	190	290	
1	0	0	230	270	
2	0	0	210	210	
5	0	0	220	270	
10	0	0	420	240	

The data suggests that self-emulsification does not occur when the surfactant concentration is below the CMC and that even a very low concentration of salt will stop the self-emulsification process when operating at a surfactant concentration close to the CMC. When operating at a surfactant concentration of 114 times CMC then 200 to 300 nm aqueous drops were formed at all concentrations of salt used in the aqueous phase, but with much reduced resulting drop concentration at increasing salt concentration.

#### 4.5.2 Sessile droplets experiments

According to the procedure described previously (two ways of determining droplet volume (Equation 3.2 and Equation 3.3) the experimental error in the drop volume calculations is less than 7%. Experiments on time evolution of aqueous droplets deposited on a hydrophobic substrate surrounded by an organic phase (kerosene) with a high amount of surfactant (Span<sup>®</sup> 80) in the organic phase are reported in this section. The concentration of surfactant used was 114 times above the CMC. Five seconds after placing the water drop on the hydrophobic substrate (SS), some cloudiness was observed at the bottom of the droplet (Figure 4.25a). After 125 seconds (Figure 4.25b), the cloudiness became more visible and a film started to form on the substrate in the vicinity of the three-phase contact line. After around 1 hour (Figure 4.25d), the film became large enough to be observed using the top camera. The film had a circular shape around the droplet base and its diameter increased with time (see Figure 4.25). It was

observed after 8 h that the main droplet was becoming noticeably smaller and the film thicker with time. Hence, during this experiment spontaneous emulsification was happening over a prolonged period of time, transferring water from the main drop to the surrounding film via microemulsion droplets within the continuous phase (kerosene).

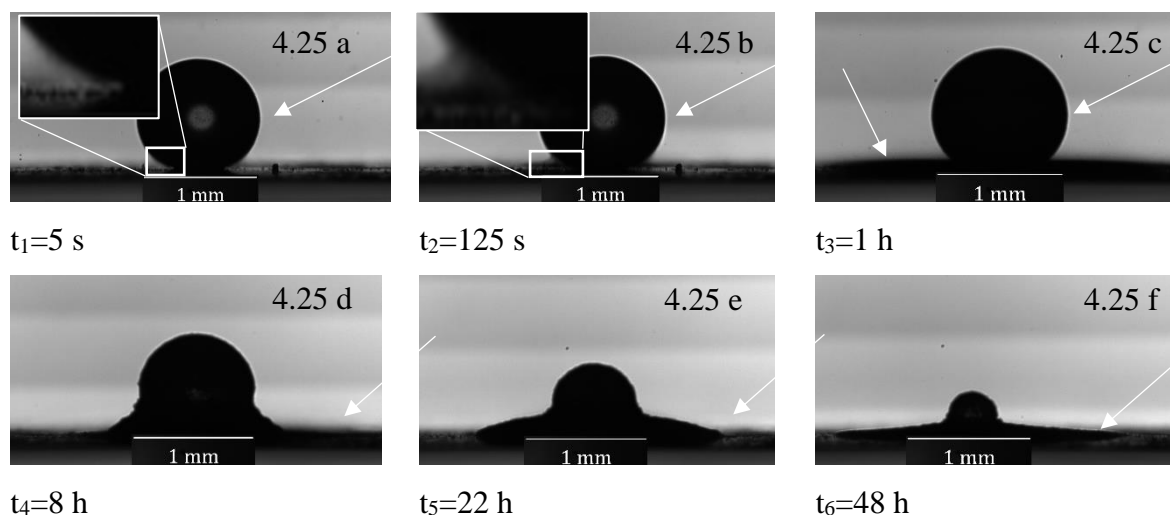


Figure 4.25 Formation of a cloud of nano-sized droplets and a film at the droplet base assisted by swollen micelles present in the organic phase (kerosene).

The critical micelle concentration of Span<sup>®</sup> 80 in kerosene was determined by interfacial tension measurements, and found to be  $0.51 \pm 0.07$  mM. The interfacial tension between water and kerosene at the CMC is  $4.0 \pm 0.1$  mN/m. This value agrees well with the literature data [126]. According to Peltonen measurements [124] this surfactant apparently has higher interfacial tension at the CMC using a pure alkane (hexane) instead of a mixture of alkanes and some residual aromatics hydrocarbons present in the low odour kerosene.

The water drop volume behaviour for four different Span<sup>®</sup> 80 concentrations was also investigated. The phenomenon described above (film formation around the droplet base) was only observed when Span<sup>®</sup> 80 concentrations used was above 11.4 CMC. After a certain time contact angle could not be measured anymore due to the presence of the surrounding water film. Therefore, the volume with time dependences presented in Figure 4.26 were determined using just the height of the droplet and assuming that radius of the droplet was constant.

It can be seen in Figure 4.26 that the decrease of the drop volume is faster when the number of micelles in the organic phase is higher. This implies that the mass transfer of water in the

organic phase is influenced by the presence of reverse micelles. The decrease of volume of aqueous droplet shows a linear behaviour when surfactant is not present in organic phase. The rate ( $dV/dt$ ) determined in this case was 1.8 nL/h. However, in presence of surfactants above the critical concentration (11.4 and 114 times its CMC), the water drop volume decreases logarithmically.

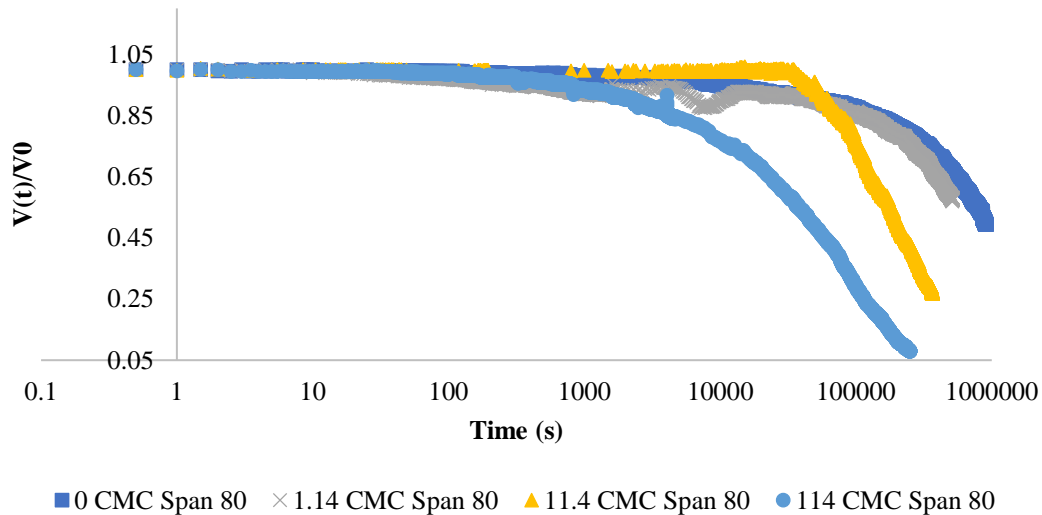


Figure 4.26 Influence of surfactant concentration on the water sessile droplet solubilisation in to the surrounding phase

In this system, the reverse micelles solubilise water molecules and transfer through the organic phase. The micelles swell over time and, eventually become large enough to scatter light ( $> 0.5 \mu\text{m}$  diameter) and sank to form the film of water around the main water drop. The process is shown schematically in Figure 4.27.

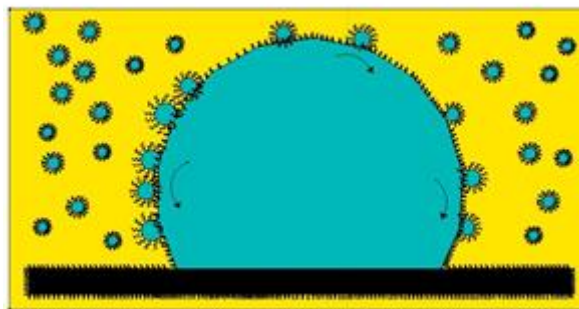


Figure 4.27 Schematic representation of spontaneous emulsification being driven by the swollen micelles.

As soon as the water molecules “escape” from the droplet they are surrounded by the micelles which solubilise them and swell. Due to the buoyancy effect, these swollen micelles roll down to the bottom forming a film. Different salt concentrations were tested in the aqueous phase. According to section 4.5.1, the increased salt concentration should inhibit the mass transfer of water into the organic phase. A range of NaCl concentrations in the aqueous drop was investigated, the results are shown in Figure 4.28.

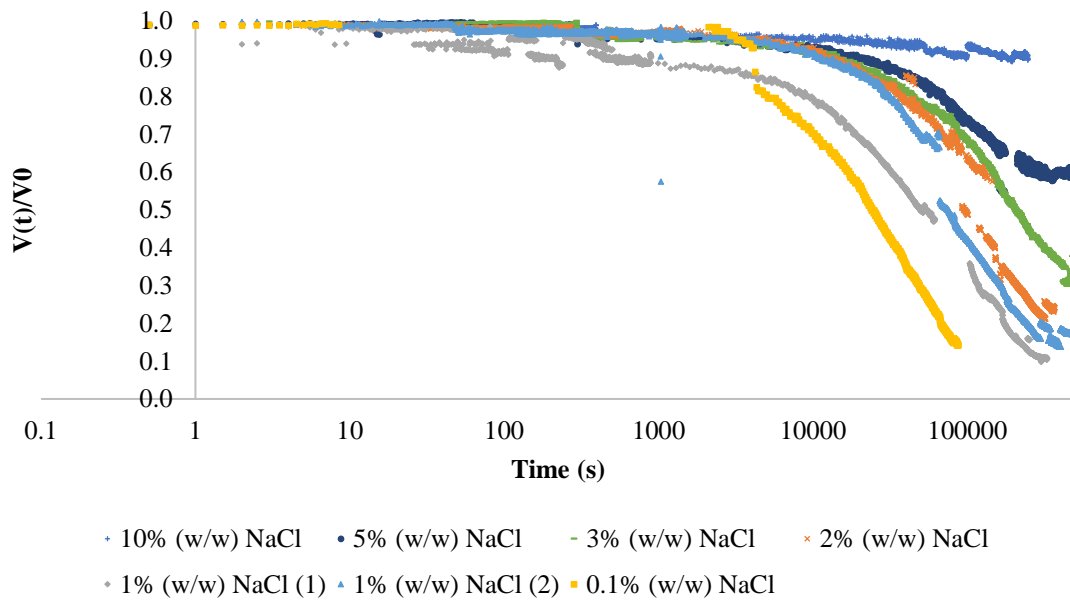


Figure 4.28 Influence of salt in the aqueous phase on the drop volume evolution

Figure 4.28 shows that different concentrations of NaCl in the water phase have a clear influence on the transfer of water molecules to swollen micelles. Higher concentrations of salt slow down the transfer process. At a concentration of 10% (w/w) NaCl the droplet barely changes its volume for almost 250000 seconds (70 hours). It is important to note that during mass transfer the salt concentration in the water droplet increases over time which explains the non-linear behaviour of the droplet volume shrinking with time for lower ratios of CMC.

## Chapter 5 CONTROLLED DROPLET FORMATION: DISTINCT FORMULATIONS AND APPLICATIONS

### 5.1 Different uniform emulsions using a hydrophilic membrane

This section was motivated to elucidate a conventional concept within the membrane emulsification community which is the need to use an hydrophobic membrane to produce uniform w/o emulsions. Results showed previously with sessile drops experiments (Figure 4.15) and with rotating drum setup (Figure 4.22) were encouraging in the sense that stainless steel non-treated (hydrophilic) is preferably wetted by the organic phase when surfactant (Span<sup>®</sup> 80) is present rather than by the aqueous phase. This presents a great advantage specially for processes where hydrophobic treatment is not advised due to health and safety approval, e.g., for the manufacture of food and pharma products. For these set of experiments, the Dispersion Cell was used, which is a lab equipment that enables the use of low volumes, feasible to develop emulsion formulations and its operational characteristics are well understood (see section 3.1.1).

In the section 5.1.2, o/w emulsion were produced using the same device and same membrane surface for drop size and drop size distribution comparison as well as showing the capabilities of producing uniform PLGA particles with this technique.

#### 5.1.1 Drop formation experiments with the Dispersion Cell (w/o emulsion)

Droplet size and droplet size distribution after emulsification using the Dispersion Cell for various concentrations of surfactant are presented in Figure 5.1, which shows a wide range of droplet sizes that can be obtained just by varying the surfactant concentration and using the same conditions, i.e., pore size, shear or injection rate. This demonstrates the importance of interfacial science in processes such as membrane emulsification. Not only surfactant concentration, but also type of surfactant plays a key role where surface activity would define the rate of surfactant adsorption to liquid interface, or liquid/solid interface. In addition, this has been acknowledged in different studies [76, 127, 128] enhancing the need of knowledge of



surfactant proprieties which would facilitate the process design and optimisation at production scale.

It is also seen in Figure 5.1 that for the two flow rates tested, higher surfactant concentration results in decrease of the resultant drop size, even when in excess of the CMC. This can be explained by dynamic interfacial tension, i.e., higher surfactant concentration increases the rate of adsorption to the fresh interface generated by drop formation and therefore reduction of interfacial tension is faster, and consequently, a smaller time for drop growth and detachment, producing smaller drops.

Figure 5.1 shows that a lower injection rate results in a narrower drop size distribution. These results fit very well with the observations and results obtained in the previous sections (particularly, section 4.4), where it was shown that surfactant present tends to adsorb to the solid surface facilitating its wetting. Narrower drop size distributions obtained with lower injection rate can be due to: expansion rate of the droplets is lower, allowing more time for the surfactant to adsorb to the drop and surface which could possibly contribute to avoid wetting and consequently more uniform drop size generation. A picture of some droplets formed at  $0.2 \text{ mL min}^{-1}$  (corresponding to a superficial velocity of  $43.4 \text{ L m}^{-2} \text{ h}^{-1}$ ) is shown in Figure 5.2 with the size distribution.

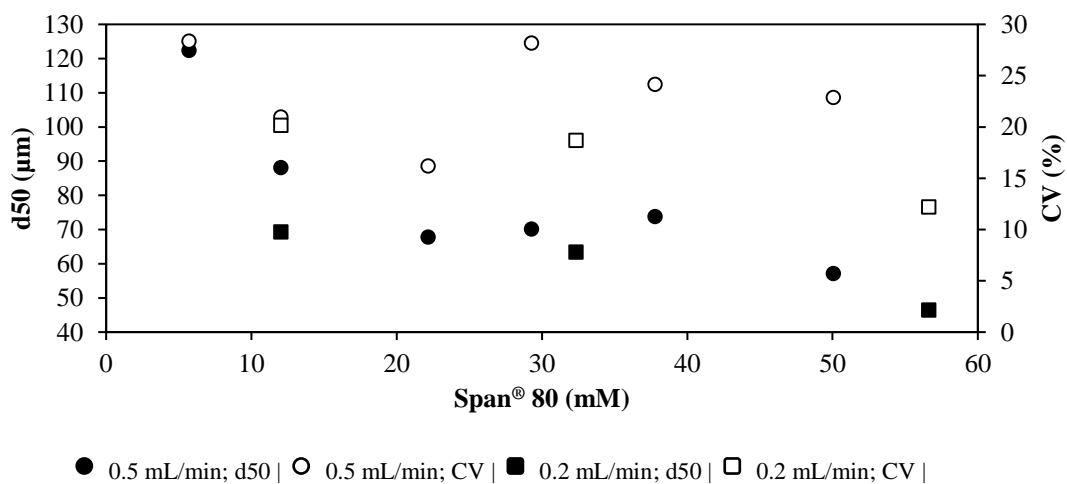


Figure 5.1 Influence of two different injection rate used on the droplet size (d50) and on droplet size distribution (CV) as a function of surfactant concentration.

The CV values obtained using a hydrophilic membrane to produce w/o emulsions are comparable to other studies where membrane emulsification process was adopted, but an hydrophobic membrane was utilised [24, 129-131] (section 5.1.2). Emulsion manufacturing using the Dispersion Cell is a batch process which means that during droplet formation surfactant will be depleted from the organic media. To prevent this being a major disadvantage, the ratio between dispersed and continuous phases should be kept low (e.g. 5% v/v).

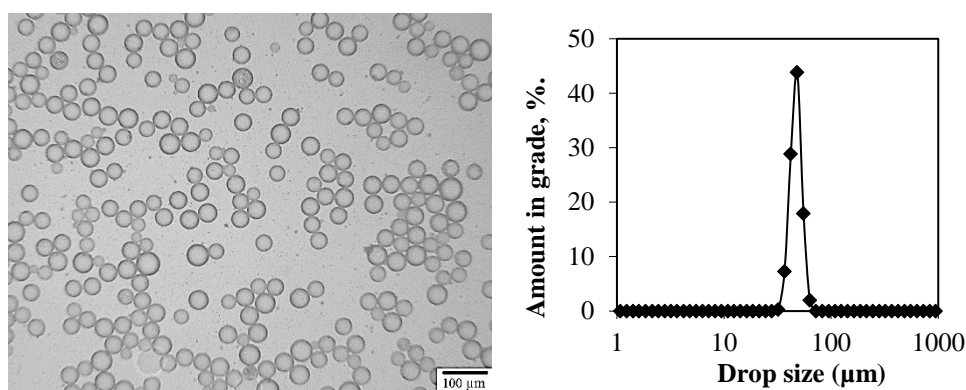


Figure 5.2 Droplets formed during injection of 13.5% PVA solution at  $0.2 \text{ mL min}^{-1}$  in to kerosene with 50 mM Span® 80 concentration using a surface shear of 5.8 Pa using a (non-treated) hydrophilic membrane, i.e., relying on the surfactant present in the organic phase to wet membrane and avoid its dewetting by the (aqueous) dispersed phase.

### 5.1.2 Drop formation experiments with the Dispersion Cell (o/w emulsion)

Even though the formulation used is different, this section is included in this thesis to give a direct comparison of drop size distribution to the results shown in section 5.1.1. using the same membrane surface (hydrophilic) but using the conventional approach, i.e., to produce an o/w emulsion membrane, use of a hydrophilic surface. The membrane used had the same design (ringed), pore size ( $10 \text{ }\mu\text{m}$ ) and pore distance ( $200 \text{ }\mu\text{m}$ ) as the one used in the experiments showed in the previous section 5.1.1.

PLGA microspheres were produced from a 20% wt. Poly(lactic-co-glycolic acid) (PLGA) polymer dispersed phase using dichloromethane (DCM) as solvent. The continuous phase was an aqueous solution of PVA dissolved in water and two different concentrations were used: 0.5% wt. and 4% wt.

In Table 5.1 are given the different parameters used to produce o/w emulsions with the Dispersion Cell. Injection rate of the dispersed phase was kept constant for all the tests.

Between test 1 and 2 the stirring speed is different and between test 2 and 3 the concentration of PVA in the continuous phase was increased.

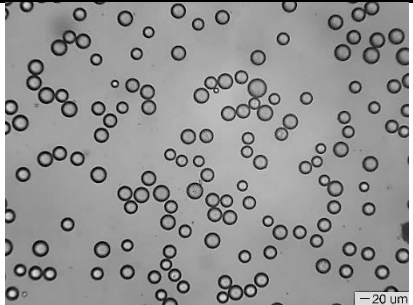
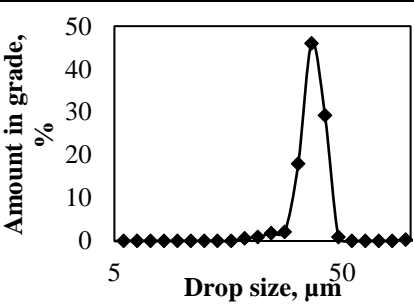
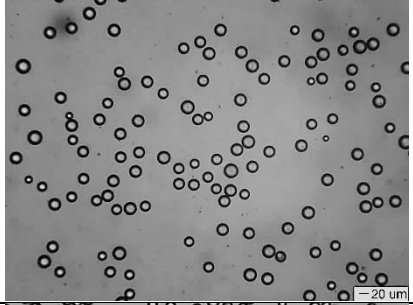
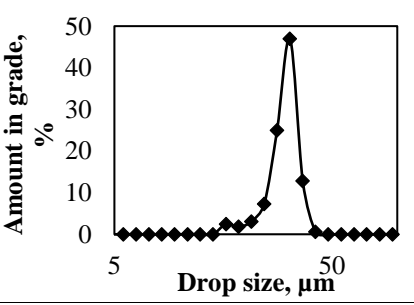
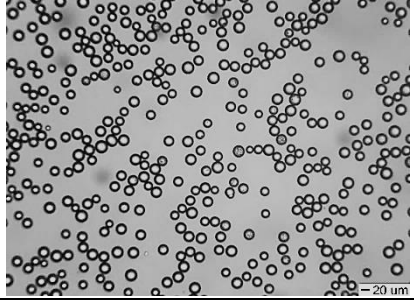
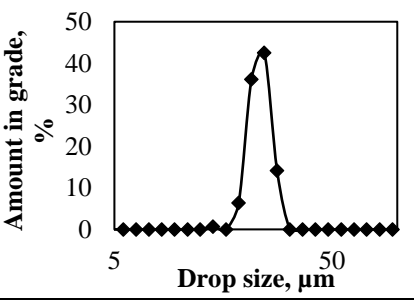
Table 5.1 Test parameters used to produce o/w emulsions with the Dispersion Cell

Test	Dispersed phase			Continuous phase	Operational conditions	
	Polymer (wt %)	Injection rate (L/h)	Superficial velocity (L/(m <sup>2</sup> .h))	PVA (% wt.)	Stirring speed (RPM)	Max Shear (Pa)
1	20	12 x 10 <sup>-3</sup>	43.4	0.5	800	6.1*
2	20	12 x 10 <sup>-3</sup>	43.4		1050	9.3*
3	20	12 x 10 <sup>-3</sup>	43.4	4	1050	13.0*

\* Viscosity values of 1.2 cp for a 0.5% wt. PVA solution and 4.0 cp for a 4% wt. PVA solution were used to determine the resultant maximum shear.

As can be seen in Table 5.1, resultant shear at the membrane surface can be manipulated by changing the stirring speed and/or increasing the viscosity of the continuous phase.

Table 5.2 Particle sizing analysis of the tests performed using conditions showed in Table 5.1

Test	Picture	Distribution	D50 (µm)	CV (%)
1			38.8	15.3
2			32.3	15.2
3			24.2	11.3

Final particle size characterization is showed in Table 5.2. It is estimated that polymeric particles had shrunk about 1.7 times due to solvent evaporation resulting in 41% size reduction. Expected shrinking is dependent on the initial polymer concentration, polymer density (PLGA: 1.3 g/ml) and solvent density (DCM: 1.33 g/ml). It is estimated that initial drop size was 66  $\mu\text{m}$ , 55  $\mu\text{m}$  and 41.2  $\mu\text{m}$  in the test 1, test 2 and test 3, respectively, using an initial 20% wt. PLGA/DCM solution

As observed before in other experiments, increasing the shear caused the decrease of the droplet size and CV values obtained are very similar (~15%). Furthermore, it can be observed that increasing the PVA concentration in the continuous phase caused the decrease of the droplet size and an improvement of the drop size distribution (CV value: 11%). PVA is present in this formulation as a polymer surfactant to stabilise the droplets. By increasing its concentration, the number of PVA molecules available to adsorb to the droplets increases (which increases the surfactant adsorption rate) and viscosity of this phase also increases which enhances the shear. On the other hand, diffusion coefficient of the surfactant is lower with rise of the viscosity. But, overall, increase of the PVA concentration resulted in smaller drop size, but it is difficult to judge if this is due to lower dynamic interfacial tension, or higher shear (viscosity increase).

Polymer droplets were hardened by solvent evaporation and a Scanning Electron Microscope (SEM) evaluation of the particles obtained in test 3 was performed. As can be seen in Figure 5.3, the produced PLGA particles with the Dispersion Cell are spherical, smooth and uniform. During SEM imaging particles are submitted to vacuum, which could have caused particle damage in case DCM was present/entrapped in the particles. Therefore, the good shape and form of the particles, after SEM imaging, indicates that the solvent removal conditions used were adequate and DCM is not present.

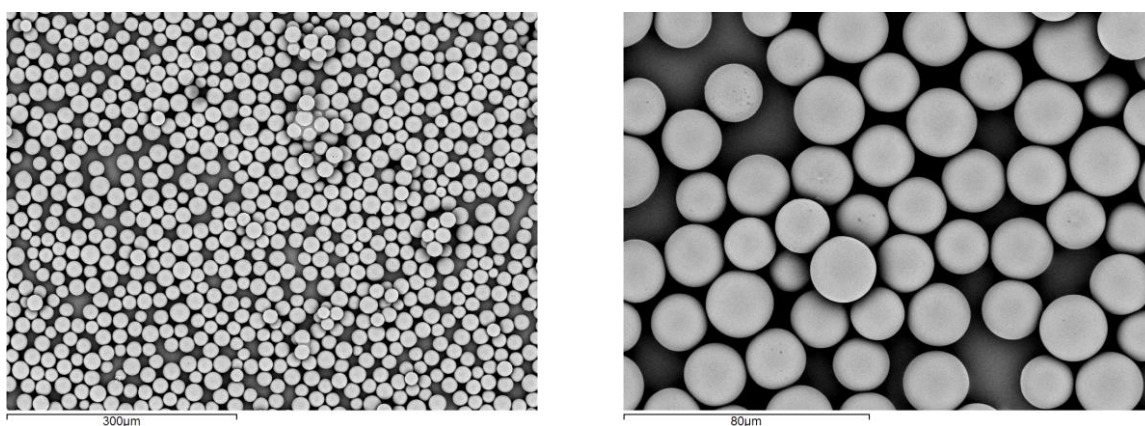


Figure 5.3 SEM pictures of freeze dried PLGA particles.

## **5.2 Influence of dynamic interfacial tension in membrane emulsification**

This section reports the role of the dynamic interfacial tension in the process of membrane emulsification and its knowledge can be useful to tune the drop size as well as to predict the number of active pores. This is a feature that is far from trivial to determine, which may delay and reduce the adoption of membrane emulsification in industrial processes, replacing other conventional emulsification methods that, in general, require higher amounts of energy and achieve lower yields, i.e., larger waste material is produced. The vertical oscillating membrane emulsification system was chosen to carry out these experiments, mainly, because, the continuous phase is not flowing or being stirred which would affect the surfactant rate adsorption to the drops formed at the membrane surface. In spite of continuous phase not being completely steady, this is the setup where the bulk continuous phase is left immovable and, therefore, the most suitable to run these experiments in order to evaluate the influence of dynamic interfacial tension in the drop formation from multiple pores.

### 5.2.1 Drop formation experiments with vertical oscillating membrane system

It can be seen in Figure 5.4 that droplet size decreased with surfactant concentration. Higher surfactant concentrations led to faster adsorption of surfactant on the emerging drop new interfaces, speeding the surface coverage and decreasing the time needed to achieve an equilibrium interfacial tension. In these experiments, oscillation conditions were kept at 35 Hz and 2 mm peak-to-peak, resulting in a maximum peak shear value of 7.3 Pa, and employing a constant dispersed phase flow of 1 mL min<sup>-1</sup>. Therefore, in these tests the only variable was the amount of surfactant available to cover newly formed interface formed by the drop as it emerged from the metal membrane pore.

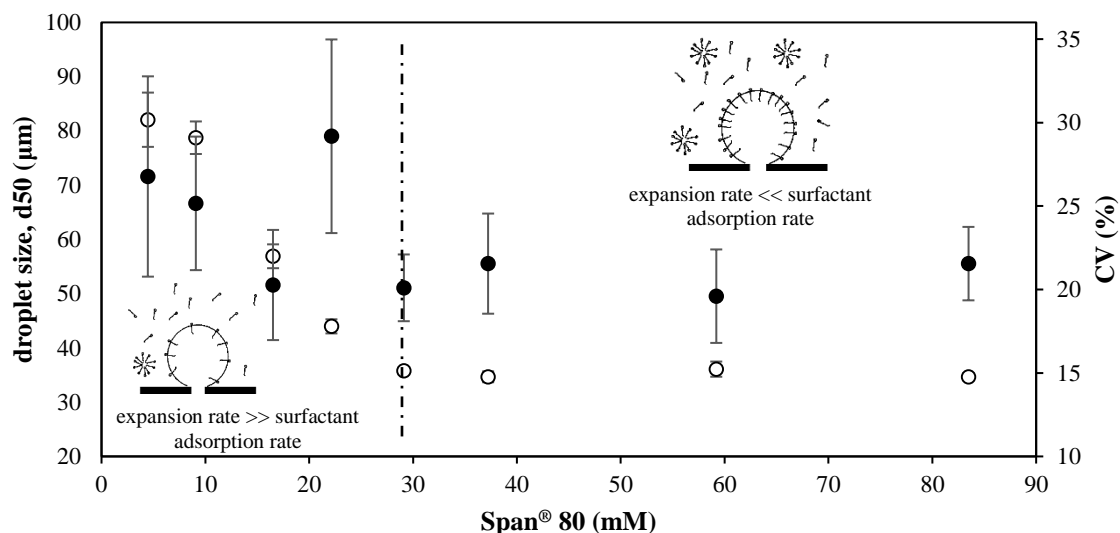


Figure 5.4. Median droplet diameters (○) and coefficient variation (CV) values (●) of PVA droplets in kerosene as a function of concentration of Span® 80 for a (constant) flow of  $1 \text{ mL min}^{-1}$  during membrane emulsification of a FAS treated metal (nickel) membrane. Error bars are reported showing the standard deviation of the measurements. Note the CMC of Span® 80 in kerosene is less than  $1 \text{ mM}$  (see section 4.5.2).

These tests were batch experiments and available surfactant concentration to stabilise freshly emerging drops will decrease with time during the experiment, as new interfaces will be created throughout. Any effect of this will be more noticeable for the lowest concentration of surfactant tests, as there is a lower amount of surfactant available at the beginning of the experiment. At high surfactant concentrations, surfactant depletion will not be significant. This phenomenon helps to explain the improving CV with respect to surfactant concentration.

A typical example of the resulting emulsion, and drop size distribution, is illustrated in Figure 5.5.

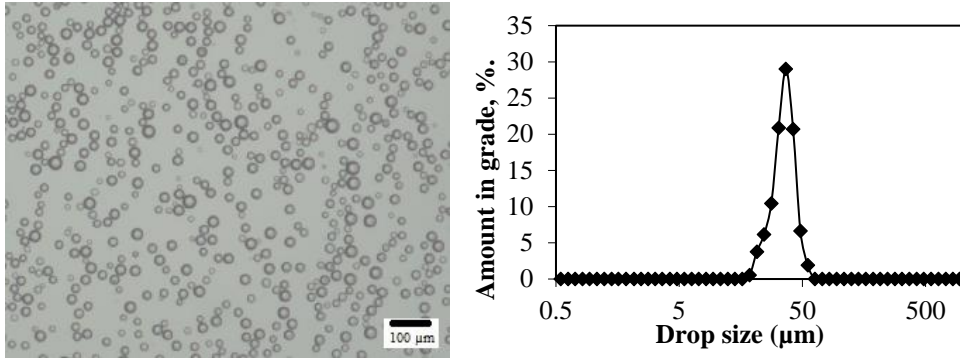


Figure 5.5. Droplets formed during injection of 13.5% wt. PVA solution at  $1 \text{ mL min}^{-1}$  in to kerosene with 40 mM Span<sup>®</sup> 80 surfactant concentration using a surface shear of 7.3 Pa.

Rearranging the force balance model, Equation 2.9, it is possible to estimate the dynamic interfacial tension of the drops when they are released from the membrane. The rearranged equation, with substitution of the constant conditions used in the experiments and assuming that the continuous phase fully wets the membrane, is shown in Equation 5.1:

$$\gamma = \frac{9\tau x \sqrt{\left(\frac{x}{2}\right)^2 - r_p^2}}{2r_p}, \quad \text{eq. 5.1}$$

Figure 5.6 illustrates the interfacial tension determined by Equation 5.1 as a function of surfactant concentration. The equilibrium value of interfacial tension, for concentrations of surfactant above the Critical Micelle Concentration (CMC) is  $3 \pm 0.8 \text{ mN m}^{-1}$ . Thus, for surfactant concentrations below 29 mM it appears that the deduced interfacial tension lies between the water-kerosene interfacial tension of  $38 \pm 1.9 \text{ mN m}^{-1}$ , and the equilibrium value of interfacial tension. The value of  $38 \pm 1.9 \text{ mN m}^{-1}$  represents the maximum value of interfacial tension, when there is no presence of surface active agents at the interface as PVA or Span<sup>®</sup> 80. Hence, these deduced values are dynamic interfacial tension values, as the rate of drop growth is greater than the rate of surfactant arrival at the interface needed to stabilise the drop at the equilibrium interfacial tension value.

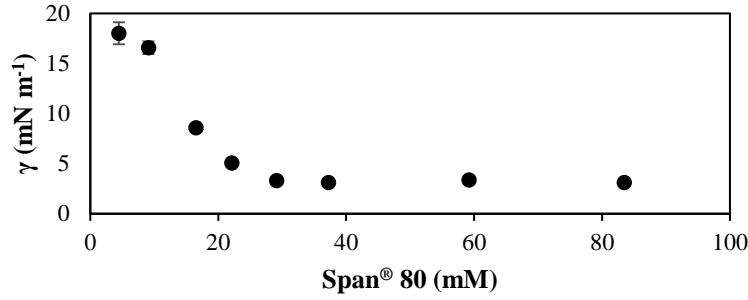


Figure 5.6. Estimated interfacial tension values for 13.5% wt. PVA solution injected in to kerosene for experiments performed at an injection rate of 1 mL min<sup>-1</sup>.

It is possible to use this data to estimate the fraction of pores active in the process of membrane emulsification by equating the rate of drop growth from the active pores to the rate of adsorption of the surfactant. In order to achieve this, the surfactant diffusion coefficient must first be determined (see section 5.2.2).

#### 5.2.2 Surfactant dynamics adsorption (method to determine % active pores)

Equation 5.2, from Ward and Tordai [132], relates the surfactant adsorption dynamics to the interfacial tension decline and the surfactant bulk concentration  $C_0$ , the maximum loading of the interface with surfactant  $\Gamma$ , and the adsorption coefficient  $D_1$ :

$$\gamma(t) - \gamma_{eq.} = \frac{RT\Gamma^2}{2C_0} \sqrt{\frac{\pi}{D_1 t}}, \quad eq. 5.2$$

$\Gamma$  can be determined by Gibb's isotherm, Equation 5.3, where  $C_S$  is the subsurface concentration of surfactant in the surrounding phase solution [128]:

$$\Gamma = -\frac{1}{RT} \left( \frac{d\gamma}{d\ln(C_S)} \right), \quad eq. 5.3$$

The "subsurface" is defined as the region between the bulk and the interface between the two phases. The concentration of surfactant achieves its maximum value at the CMC (and above) and is  $1.5 \times 10^{-5} \text{ mol m}^{-2}$ .



Figure 5.7 and Figure 5.8 plot the dynamic interfacial tension data obtained from measurements using the DSA 100 (Kruss). The equilibrium interfacial tension ( $\gamma_{eq}$ ) was assumed to be the lowest value of the respective isotherm acquired. In Figure 5.7, the drop phase was distilled water and in Figure 5.8 there was an aqueous solution of 13.5% (w/w) PVA. The inset shown in Figure 5.8 illustrates the surfactant diffusion coefficient ( $s^{-1}$ ), using Equation 5.2, for different concentrations of Span<sup>®</sup> 80. The diffusion coefficient is a measure of the rate of material transport, in this case, as the result of surfactant molecules movement towards the interface. Since mass transfer is dependent on diffusion (Equation 5.2), it is expected that oscillations conditions would influence surfactant adsorption rate. So, oscillations conditions were kept constant in order to not become a variable during the drop formation experiments.

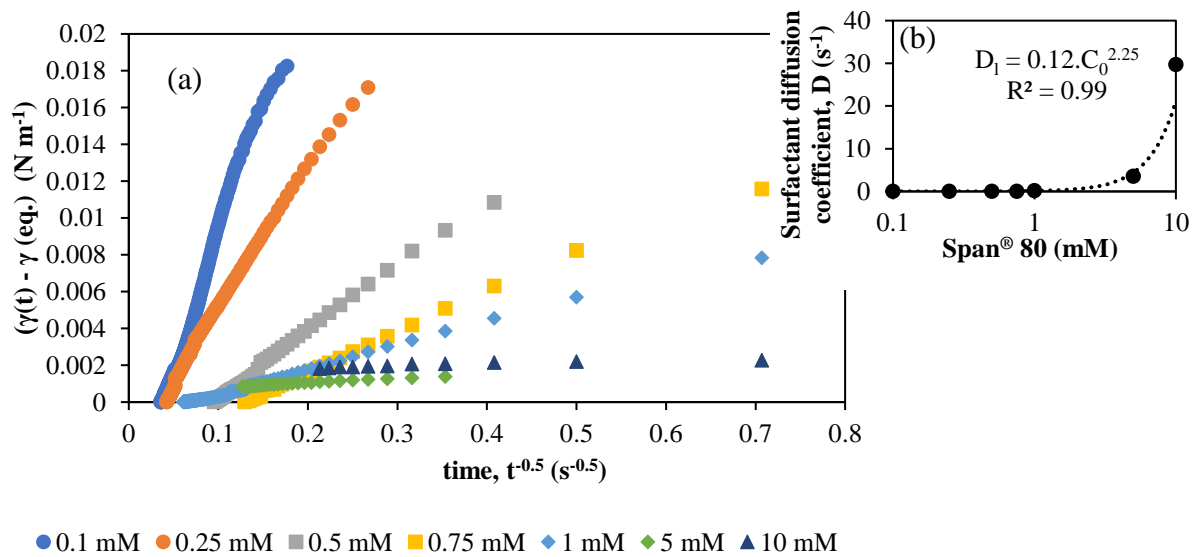


Figure 5.7. (a) Dynamic interfacial tension determined by pendant drop method of distilled water in kerosene that contained different concentrations of surfactant (Span<sup>®</sup> 80) dissolved: 0.1, 0.25, 0.5, 0.75, 1, 5, 10 plotted according to eq. 5.2; with (b) inset showing surfactant adsorption coefficient for the different surfactant concentrations tested.

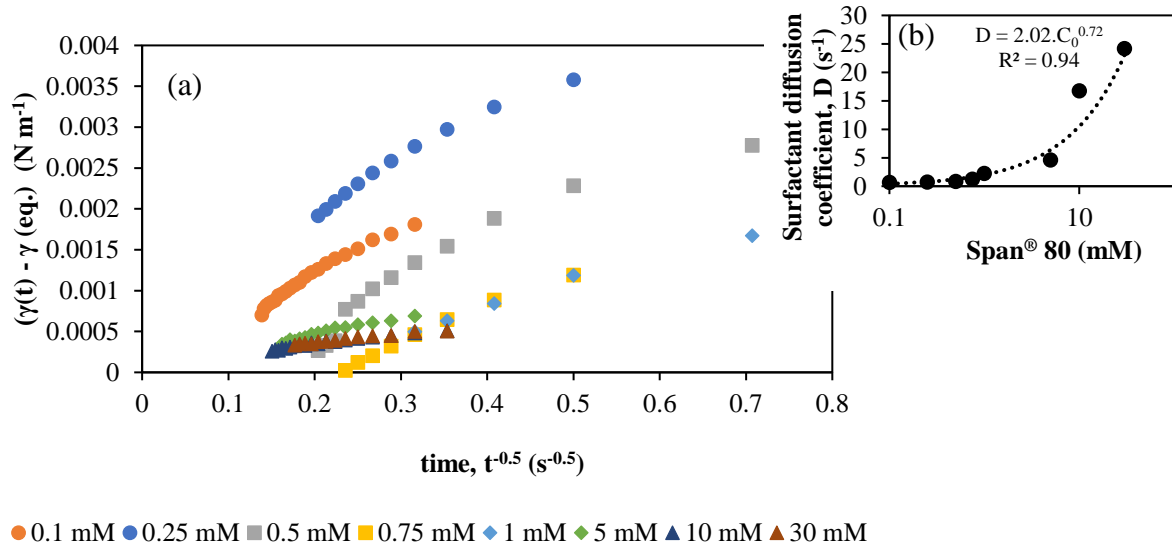


Figure 5.8. (a) Dynamic interfacial tension determined by pendant drop method of 13.5% PVA in kerosene that contained different concentrations of surfactant (Span<sup>®</sup> 80) dissolved: 0.1, 0.25, 0.5, 0.75, 1, 5, 10 and 30 mM plotted according to eq. 5.2; with (b) inset showing surfactant adsorption coefficient for the different surfactant concentrations tested.

For a given drop size, it is possible to plot the drop frequency against active percentage of pores, using a material balance. Drop frequency ( $d_f$ ) is determined by:

$$d_f = \frac{Q}{\frac{\pi}{6} n x^3}, \quad eq. 5.4$$

where  $Q$  is volumetric flow,  $n$  is the number of pores and  $x$  is the drop diameter. Looking at membrane design used (pore distance is greater at least 10 times than pore size), coalescence of neighbouring droplets emerging from the pores is very unlikely. Number of pores is determined by:

$$n = \frac{\Phi A_s}{A_p}, \quad eq. 5.5$$

where  $\Phi$  is the porosity of the membrane,  $A_s$  is the surface (active) area and  $A_p$  is the area of a single pore. Porosity of the membrane ( $\Phi$ ), with a triangular array (pores are spaced equidistantly) is determined by:

$$\Phi = \frac{A_p}{2A_\Delta}, \quad \text{eq. 5.6}$$

where  $A_\Delta$  is the area of the triangular array.

For example, if fewer pores are active then they must produce drops at a higher frequency compared to a situation when a larger number of pores are active, in order to conform to the overall material balance of liquid being injected into the continuous phase, because volumetric flow is kept constant. This is illustrated in Figure 5.9, based on a drop size of 35.8  $\mu\text{m}$ , appropriate for the 29 mM Span<sup>®</sup> 80 concentration tests, and above.

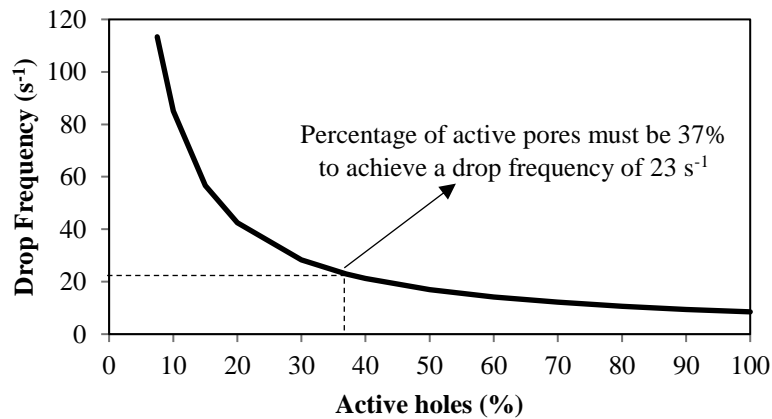


Figure 5.9. Drop frequency against fraction of active pores for a PVA drop size of 35.8  $\mu\text{m}$ .

For the emulsification when a concentration of 29 mM Span<sup>®</sup> 80 was used (35.8  $\mu\text{m}$  drop size) the surfactant diffusion rate was 23  $\text{s}^{-1}$  (Figure 5.8b). Assuming that surfactant diffusion coefficient is equal to the drop formation rate provides a percentage of active pores in the membrane to be 37% (see Figure 5.9). This value is consistent with the expected value for membrane emulsification when using this type of regular and non-tortuous type of pore channel membrane structure [37, 55, 66, 71]. It is the first time that this approach to analysing the number of pores active in the process of membrane emulsification has been determined, rather than providing a range of values that may be relevant [49], and could be used to investigate methods to improve the pore utilisation to enhance productivity.

When the number of active pores is known, then pore velocity can also be calculated. Therefore, Capillary number and Weber number may also be estimated and better determination of whether working conditions are within the dripping or jetting regimes.

### 5.3 Investigation of membrane emulsification in a continuous mode suitable for industrial use

Below, is presented a novel emulsification system which azimuthally oscillates the membrane back and forwards while injecting a dispersed phase through the membrane in to a continuous phase, generating droplets. Therefore, the shear generated in this membrane emulsification system is created from the oscillation of the membrane. This system was designed to operate in continuous mode which is quite attractive for many industries. Working in a continuous mode has the potential to reduce labour, decrease product variability (between batches) and even reduce product waste, achieving better yields and productivities. In this section, these aspects were evaluated for two different formulations: floating droplets as well as sinking droplets. In both cases, o/w emulsions were being produced, but in section 5.3.1 the dispersed phase used had a lower density than the continuous phase (floating droplets) while in section 5.3.2 the dispersed phase used had a higher density than the continuous phase (sinking droplets).

#### 5.3.1 Drop formation experiments with azimuthally oscillating membrane system

Table 5.3 Operational conditions tested in the comparison of two wave forms

Displacement (mm)	Frequency (Hz)	Shear Stress (Pa)	Injection rate (L/h)	Superficial velocity (L/(m <sup>2</sup> .h))	Continuous phase flow rate (L/h)	O/W (%) (v/v)
2	20; 35; 45	1.4; 3.3; 4.7	0.06; 0.24; 0.72	11.5; 46.1; 138	0.24; 0.96; 2.88	
4	20; 35; 45	2.8; 6.5; 9.5	0.06; 0.24; 0.72	11.5; 46.1; 138	0.24; 0.96; 2.88	20
6	20; 35; 45	4.2; 9.8; 14.2	0.06; 0.24; 0.72	11.5; 46.1; 138	0.24; 0.96; 2.88	

Table 5.3 contains the operational parameters used in the experiments to test the type of wave form used: compound cosine wave form or sinusoidal. The wave form should make little difference to the drops produced (size and size distribution) if the important parameter is the ‘peak shear’ that is obtained during an oscillation. The two wave forms are represented in Figure 5.10.

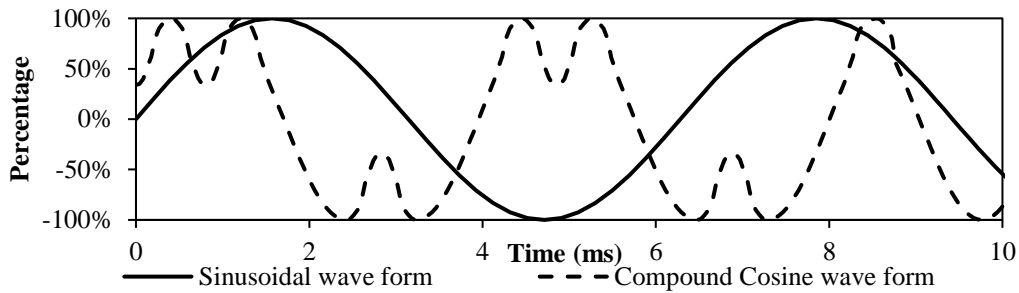


Figure 5.10 Oscillation wave form profiles used in the experiments

The sinusoidal wave form follows a sine function with respect to time and the compound cosine wave form has multiple accelerations per period (wavelength) resulting from a combination of a number of cosines wave. For these wave forms a wide range of ‘peak’ shear stress values were tested from 1.4 Pa to 14.2 Pa and for each oscillation displacement value three different oscillation frequencies and injection rates of the dispersed phase were tested. The peak shear stress is defined as being the maximum shear stress attained during the oscillation cycle as provided by Equation 2.20. The operational parameters reported in Table 5.3 were repeated switching the compound cosine wave form to a purely sinusoidal wave form. In all cases the O/W concentration of the dispersion formed was maintained at 20% v/v by maintaining the correct ratio of continuous to dispersed phase flows.

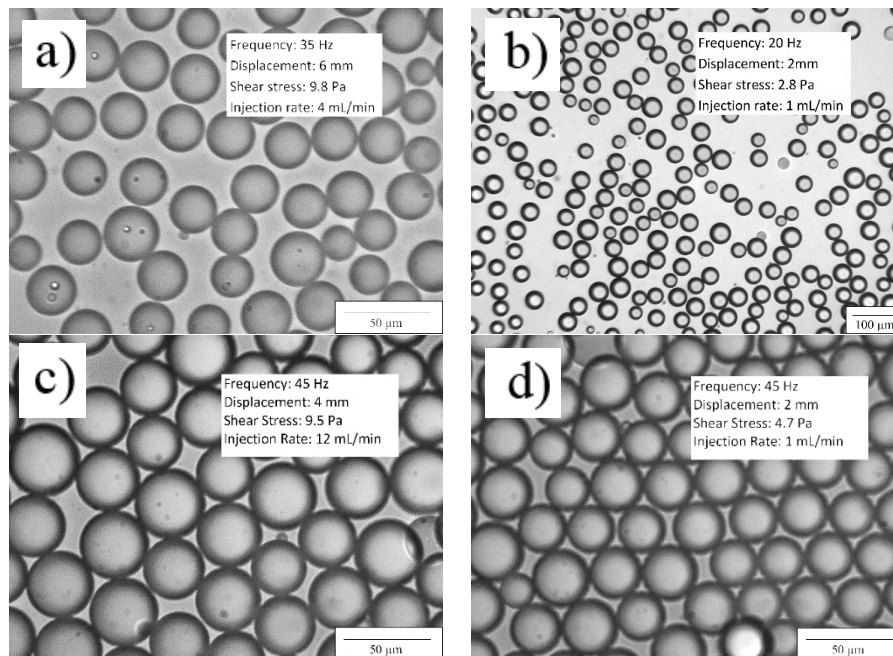


Figure 5.11 Photographs of emulsions produced using different operational parameters: (a) and (b) use compound cosine wave form (c) and (d) use a sinusoidal wave form.

Figure 5.11 shows representative images obtained under the different conditions described above. A good degree of uniformity between the drops can be seen and there is no obvious difference between the degree of uniformity provided by the two different wave forms used to generate the drops. This conclusion is supported in Figure 5.12a-b; where the median drop size and uniformity (in terms of CV) are plotted as a function of the maximum shear stress for the compound cosine and sinusoidal wave forms respectively. On both drop size figures the model represented by Equation 2.9 is also plotted. It is noticeable that at the lowest injection rate (0.06 L/h) the measured drop sizes are very close to the predicted values for all shear stresses presented, for both wave forms used. It is also noticeable that the drop sizes increase with an increase in injection rate: the drop size being significantly greater than the model prediction at the highest injection rate (0.72 L/h). This is a common observation on the use of the model represented by Equation 2.9, which does not include any term for the injection rate [44]. Hence, it is an equation that is only valid for very low injection rates.

Comparison of the drop uniformity also shows that there is little difference between the two wave forms: CVs ranging from 8 to 21% for the compound cosine wave form and 9 to 19% for the sinusoidal wave form. In general, for both wave forms the CVs were between 10 and 14%. These values are considerably poorer than what can be achieved using a single capillary microfluidic system [133], but the productivity of membrane emulsification systems is several orders of magnitude greater than what can currently be achieved with microfluidic systems in practice.

Also shown on Figure 5.12a is an expanded section for one set of data at a shear stress of 6.5 Pa, to illustrate the reproducibility of the (azimuthally) oscillating membrane system. Tests were repeated three times and the bars illustrated in the expanded section show the data range obtained for the data illustrated. It would not be possible to see the data range plotted on the figure without expansion as the range is very narrow, demonstrating a very high degree of reproducibility of the system. The reproducibility of the CV values were wider and the bars representing the data range are visible for the example plot of data taken at 0.24 L/h on Figure 5.12b. However, the range is narrow and the reproducibility of the data appears to be good. Median droplet diameter variation from the model prediction is proportional to the injection rate: at low injection rate the model is adequate, at high injection rate the drops are substantially bigger. The type of wave form used appears to have no influence on this variation.

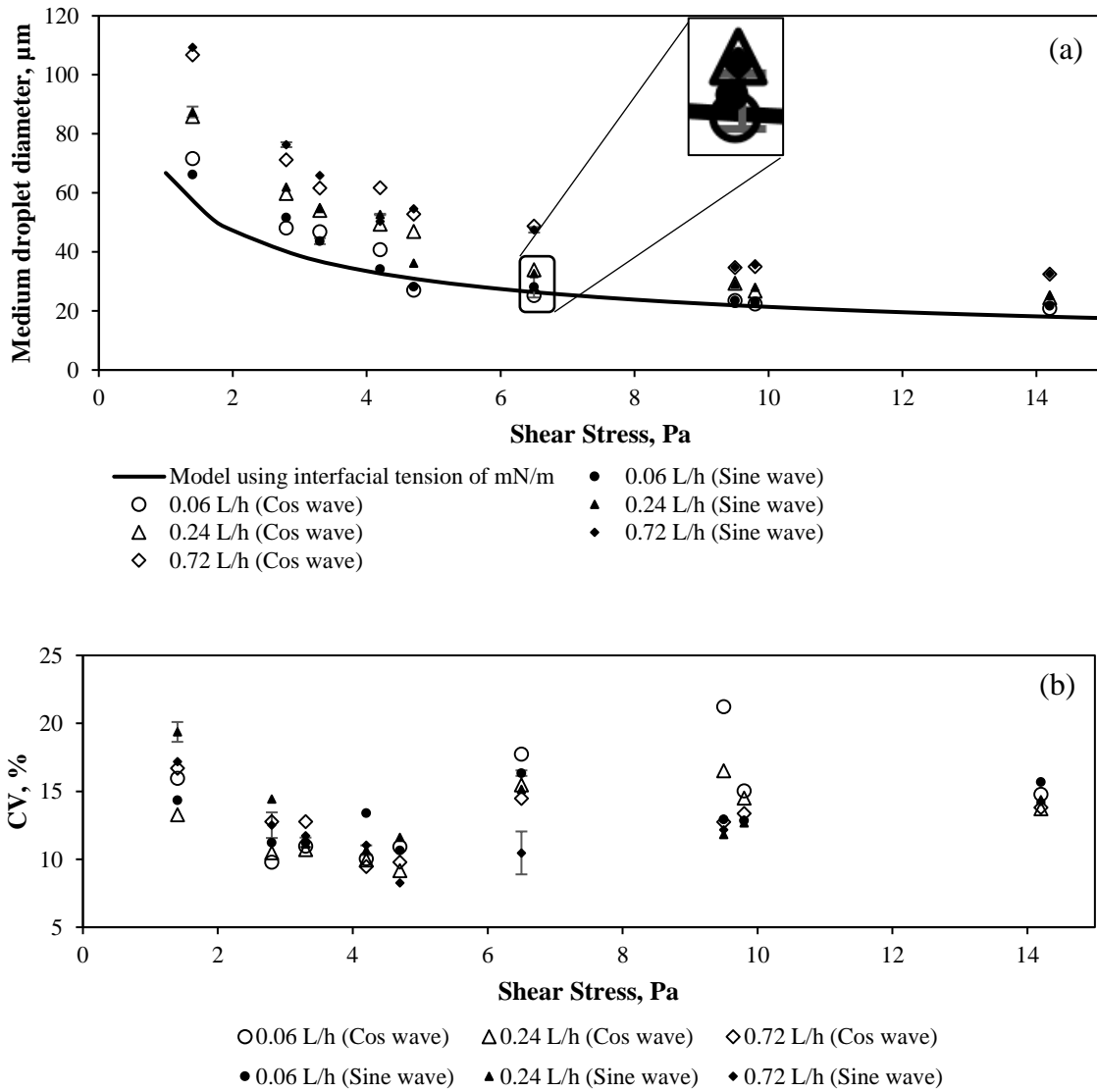


Figure 5.12 (a) Droplet size and (b) Coefficient of variation (CV) as a function of shear stress at different injection rates. Two different wave forms were tested: compound modified cosine wave form (“cos wave”) and sinusoidal wave form (“sine wave”).

Table 5.4 Operational conditions tested in the shear stress evaluation

Displacement (mm)	Frequency (Hz)	Shear Stress (Pa)	Injection rate (L/h)	Superficial velocity (L/(m <sup>2</sup> .h))	Continuous phase rate (L/h)	O/w (%) (v/v)
3	15; 27; 34	1.4; 3.3; 4.7	0.06; 0.24; 0.72	11.5; 46.1; 138	0.24; 0.96; 2.88	20
6	15; 27; 34	2.8; 6.5; 9.4	0.06; 0.24; 0.72	11.5; 46.1; 138	0.24; 0.96; 2.88	
7	18; 32; 41	4.2; 10.0; 14.4	0.06; 0.24; 0.72	11.5; 46.1; 138	0.24; 0.96; 2.88	



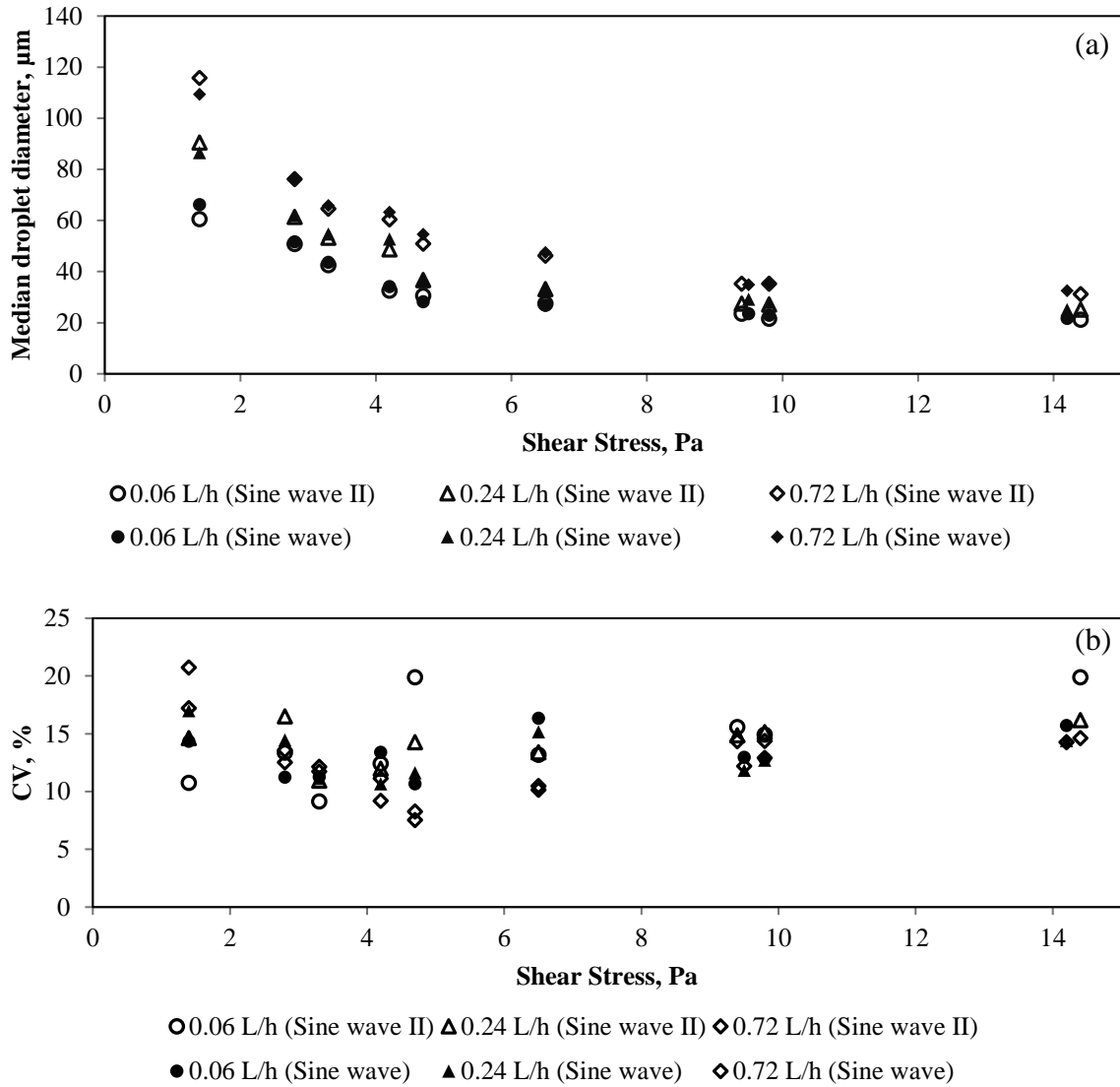


Figure 5.13 (a) Droplet size and (b) Coefficient of variation (CV) as a function of shear stress obtained with same shear stress using different combinations of displacement and frequency: Sine waves I and II use data obtained under conditions reported in Table 5.3 and Table 5.4, respectively.

In Table 5.4, additional combinations of membrane displacement and frequency are reported, providing shear stress values between 1.4 and 14.4 Pa and extending (in combination with the data in Table 5.3) the range of frequencies tested to between 15 and 45 Hz; and range of displacements to between 2 to 7 mm, for the sinusoidal wave form. All the resulting data is plotted in Figure 5.13a, sine wave II corresponding to conditions provided in Table 5.4, and it can be seen that all the drop size data can be correlated with the shear stress for each injection rate in a similar way to that provided by Equation 2.9, but with a different correlation for the different injection rates, as seen before in Figure 5.12 and Figure 5.13. The data illustrated in

Figure 5.13a shows that it is the shear at the surface of the membrane that is important in determining the drop size, regardless of how that shear is obtained from a combination of frequency or amplitude of the wave form. However, the data illustrated in Figure 5.13b does appear to suggest that if the narrowest size distribution is required then the operator may wish to investigate carefully all of the operating conditions; for example, at a shear stress of 4.7 Pa the resulting CVs of distributions varied between 8 and 20% depending on the selected operating conditions of: frequency, amplitude, injection rate and continuous phase flow rate. Hence, the drop size may be a function of shear regardless of the conditions used to generate it, but it is noticeable that the uniformity of the distribution is influenced by many more parameters than just the shear.

One of the main advantages of a membrane emulsification system that provides a means for controlling the shear at the membrane surface independent of the flow of continuous phase, being used to remove the dispersed phase drops, is that it should be possible to achieve high dispersed phase concentrations using relatively high injected phase flow to the continuous phase flow. In a crossflow system, which relies on the continuous phase flow to generate the shear at the membrane surface, such an independent means does not exist and the only way that high concentrations of dispersed phase can be achieved is to recycle the dispersion through the membrane module several times. This can lead to droplet breakup within the pump and fittings, and a poorer drop size distribution. The oscillating membrane emulsification does provide an independent means for controlling the shear and a series of tests were performed to investigate the influence of the dispersed phase oil loading whilst maintaining conditions of constant shear.

Table 5.5 Operational conditions tested in the oil loading test.

Displacement (mm)	Frequency (Hz)	Shear stress (Pa)	Injection rate (L/h)	Superficial velocity (L/(m <sup>2</sup> .h))	Continuous Phase rate (L/h)	O/W (%) (v/v)
2	45	4.7	0.09	17.3	0.9	9.1
			0.18	34.6		17
			0.27	51.9		23
			0.36	69.2		29
			0.45	86.5		33
			0.54	104		38

The operating conditions are provided in

Table 5.5, where the continuous phase flow rate was held constant (0.9 L/h) and the injection rate of the dispersed phase was varied in the range of 0.09-0.54 L/h, resulting in the dispersed phase concentrations in the final emulsion from 9 to 38% v/v.

The resulting emulsions obtained are shown in Figure 5.14. The uniformity of the distribution is similar, regardless of the dispersed phase concentration, with CV values between 9 and 11%, for dispersed phase emulsion concentrations between 17 and 33% v/v. The operating conditions for shear were selected as being those that provided the best uniformity and the uniformity remained good for all injection rates, and therefore dispersed phase concentrations, up to a value of 33% v/v, deteriorating slightly at a dispersed phase concentration of 37% to a CV value of 18%. For comparison [44], previous membrane emulsification work reported using a similar formulation and membrane type operated using a different method of generation of shear at the membrane surface (pulsed flow) provided dispersed phase concentrations of up to 45% v/v with uniformity values determined by a 'span' value of 0.4 (where lower span values indicate a more uniform distribution); span values obtained using the oscillating membrane emulsification system described here were ~0.2 and even the span value at 37% v/v was 0.33.

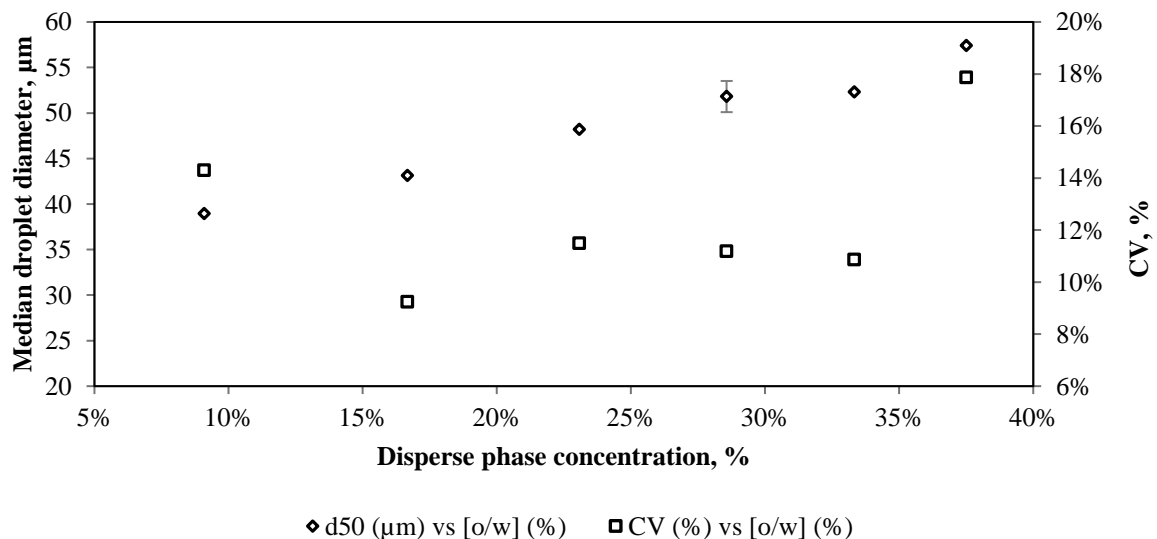


Figure 5.14 Droplet size and CV variation as a function of oil phase in emulsion concentration using a sinusoidal wave form.

Figure 5.15 shows the results of an experiment performed over 330 min using the same formulation, same membrane properties and the following oscillation conditions: 2 mm displacement, 45 Hz frequency resulting in a maximum shear stress of 4.7 Pa. The flow rate used was 0.3 L/h of the dispersed phase (sunflower oil) and 1.2 L/h of the continuous phase. During 330 min of injection the drop size distribution didn't suffer achieving very low CV values between 8 and 11% and drop size increased slightly, a few microns from 42  $\mu\text{m}$  to 47  $\mu\text{m}$ . However, this difference is marginal considering the long period of testing time.

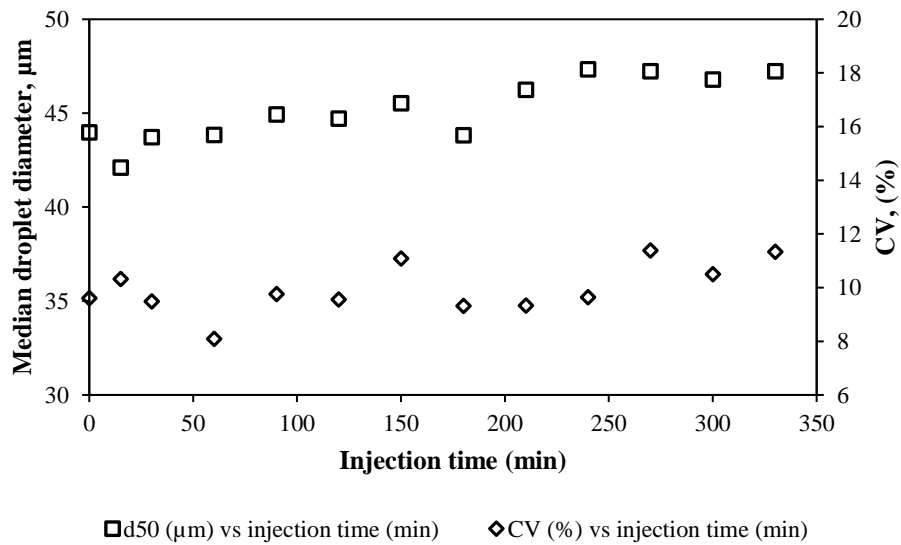


Figure 5.15 Drop size and drop size distribution evaluation as a function of injection time.

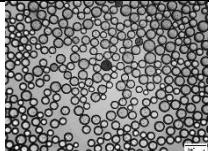
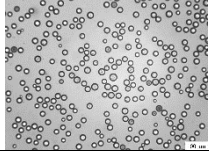
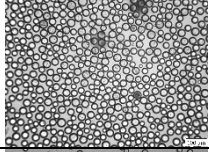
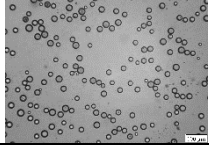
### 5.3.2 Production of polycaprolactone particles using azimuthally oscillating membrane system

In this section, a different formulation was used with the azimuthally oscillating membrane system, aiming initially to assess continuous production of polycaprolactone (PCL) particles and later, continuous production of PCL particles with BSA encapsulated via the double emulsion method. BSA was used as a protein model which can be substituted by a drug or other active pharmaceutical ingredient (API) for certain applications.

The dispersed phase used in these experiments was mainly constituted by DCM which has a low ebullition point (39.6°C). Therefore, a cooling jacket around the cell was used to prevent a rise in the temperature due to the friction of the oscillation, leading to evaporation of the dispersed phase, resulting in a loss of process control which could result in membrane blockage due to solidification of the polymer. Chilled water (5°C) was passed through the housing jacket which was effective in keeping the dispersed phase inlet temperature below 25°C.

Due to the nature of the formulation used (density of dispersed phase is higher than density of continuous phase) droplets formed sank rather than floated. Therefore, this changes the operational procedure. As droplets sink, initially, it was tried to use the inlet at the top of the cell and outlet at the bottom of the cell resulting in a flow of the continuous phase downwards. However, during some experimental scoping, it was concluded that part of the droplets were not being expelled through the outlet, resulting in a layer formation of droplets at the bottom of the housing which is located 1 cm below the outlet. This layer promoted the coalescence between droplets resulting in a mixture of very large droplets and fine droplets. Therefore, there may be room to redesign the cell for systems where droplets sink rather than float by reducing the gap between the bottom of the housing and the outlet. Nonetheless, an alternative was explored where continuous phase was injected upwards, i.e., continuous phase was injected from the bottom and resultant emulsion was collected from the top of the cell as for a system with floating droplets. Continuous phase flow had to be sufficient in order to prevent droplets from sinking, overcoming the difference in density. Operational parameters tested can be seen in Table 5.6 as well as microscope pictures of the w/o emulsions produced. Then, the condition tested that offered the narrowest drop size distribution was tested for longer injection times period (45 min).

Table 5.6 Operational parameters and representative pictures of the o/w emulsions obtained for each condition tested.

Oscillation conditions			Injection rate (L/h)	Superficial velocity (L/(m <sup>2</sup> .h))	DP : CP (v : v) ratio	w/o emulsion
Displacement (mm)	Frequency (Hz)	Max Shear (Pa)				
7	20	4.9	0.3	57.7	1:16	
4	30	5.2	0.3	57.7	1:16	
5	30	6.5	0.3	57.7	1:16	
7	30	9.0	0.3	57.7	1:16	

The dispersed phase was constituted by 15% (wt.) PCL dissolved in DCM while continuous phase was constituted by 4% PVA dissolved in water. In this formulation, PVA is playing an important role in the stabilization of the droplets and preventing them from coalescence through steric repulsions. During this initial scoping test flow rates of the dispersed phase and continuous phase were kept constant, 0.3 L/h and 4.8 L/h, respectively. Membrane pore size used was 15  $\mu\text{m}$  and distance between pores was 200  $\mu\text{m}$ . The membrane surface was not pre-treated (just standard cleaning) due to the natural hydrophilic behaviour of stainless steel.

It is estimated that produced polymeric particles shrunk about 1.83 times due to solvent evaporation resulting in 45% size reduction. Expected shrinking is dependent on the initial polymer concentration, polymer density (PCL: 1.2 g/ml) and solvent density (DCM: 1.33 g/ml). For instance, it is estimated that it is required to produce droplets of 73.2  $\mu\text{m}$  in order to produce PCL particles of 40  $\mu\text{m}$  using an initial 15% wt. PCL/DCM solution.

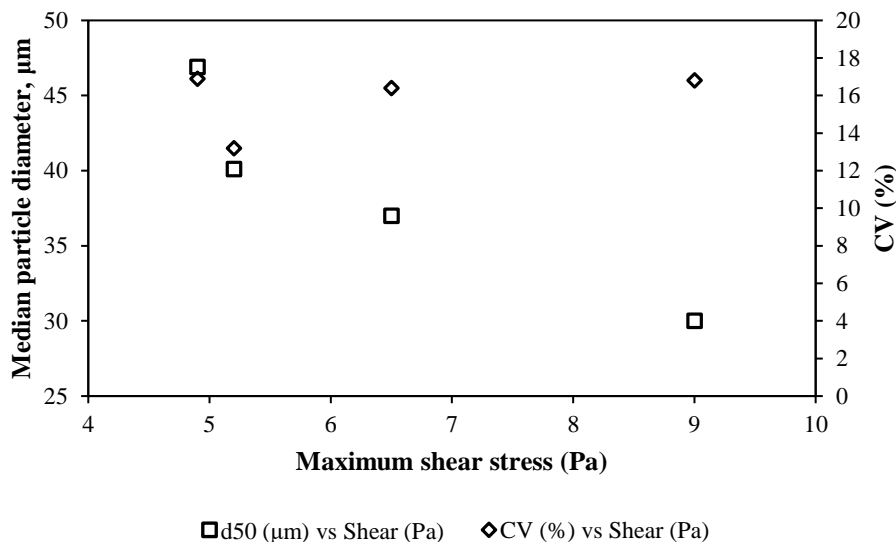


Figure 5.16 Median particle diameters and coefficient variation (CV) values of PCL/DCM droplets in water/PVA as a function of maximum shear stress for a (constant) superficial velocity of  $57.7 \text{ L m}^{-2} \text{ h}^{-1}$  during membrane emulsification using a  $15 \mu\text{m}$  pore size stainless steel membrane.

Uniform o/w emulsions were obtained with this formulation (CV values below 18%) with a range of median particle sizes between 30 and  $50 \mu\text{m}$  using a membrane pore size of  $15 \mu\text{m}$  (Figure 5.16). As was observed in section 5.3.1, particle size decreases with increase of shear and drop size distribution obtained was quite similar for all the conditions except one, where oscillation displacement used was 4 mm and frequency 30 Hz resulting in a maximum shear stress of 5.2 Pa which is within the range found optimal for the testing using commercial sunflower oil (section 5.3.1). This condition was used to perform the long injection trial where for 45 minutes the drop size and drop size distribution was monitored (Figure 5.17).

Emulsions obtained were very stable (no coalescence seen) and its post processing was rather simple by just using gentle stirring over a short period of time (1-2 hours) which is sufficient for the DCM to diffuse through the continuous phase and evaporate. Therefore, PCL particles were produced by solvent evaporation.

During 45 minutes of injection (Figure 5.17), the particle size distribution became slightly worse towards the end of the injection: at the beginning CV values between 12-15% were obtained but after 45 minutes the CV value increased to about 20%. However, as can be seen in the microscope pictures, in Figure 5.17, the drops still look quite uniform. Regarding drop size, this trial was not totally conclusive, but median drop size tends to increase with injection

time, but only by very few microns. Longer injection periods would be interesting to perform to evaluate this behaviour, if drop size distribution reaches a plateau and drop size remains constant.

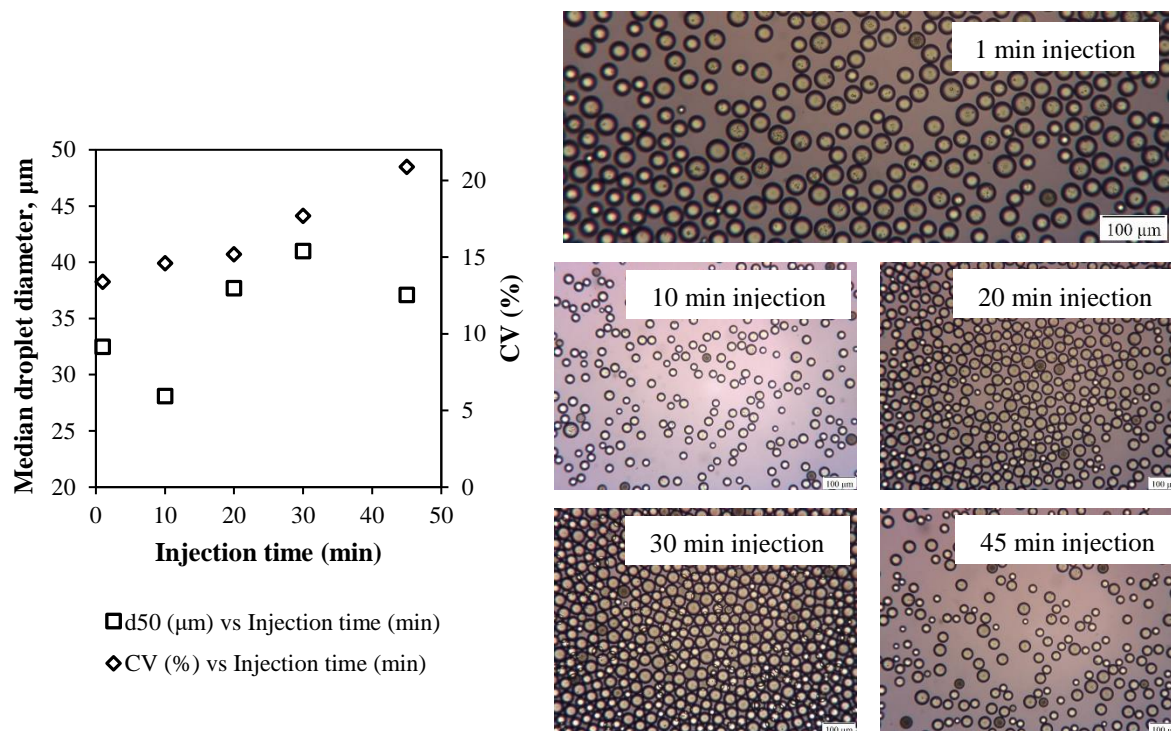


Figure 5.17 Drop size and drop size distribution evaluation over a 45 min injection and microscope pictures of the w/o emulsions produced.

After producing PCL particles, it was aimed to evaluate this system for production of w/o/w multiple emulsion which can be suitable to perform microencapsulation of a API soluble in water. BSA was used as a model protein (example of a possible API).

Initially, a very fine pre-emulsion of w/o emulsion was obtained by means of high pressure homogenization ensuring that mean droplet size was below 1  $\mu\text{m}$ . BSA was present in the water phase while in the organic phase PCL was dissolved in DCM keeping a ratio of 1:10 (v/v). Afterwards, this fine w/o emulsion was injected through the stainless-steel membrane into a solution of 4% wt. PVA. The same oscillation conditions were used and the same membrane, the only difference in this test was the dispersed phase composition. Figure 5.18 shows the results obtained with (w/o/w) multiple emulsions aiming for the microencapsulation of BSA in PCL particles. Besides microencapsulation, it was also aimed to monitor the drop size and drop size distribution over 45 minutes of injection and compare the results to the previous trial where



a single emulsion (o/w) was produced. During this period, the multiple emulsion obtained were very uniform and stable (CV value below 18%) and particle size obtained was between 30 and 35  $\mu\text{m}$ . These results are identical to the previous trial (o/w emulsion). One aspect considered was the emulsion viscosity, which can be substantially greater than the viscosity of either the oil, or the water. This behaviour is a result of droplet crowding or structural viscosity [134, 135]. Therefore, in principle, the viscosity of the dispersed phase used in the w/o/w emulsion was greater than in the o/w emulsion. Thus, from the results the viscosity of the dispersed phase does not seem to have a great impact on the final droplet size, according to these experiments. However, this fact was not studied further in this thesis, but other authors have found similar performance [136] in membrane emulsification process.

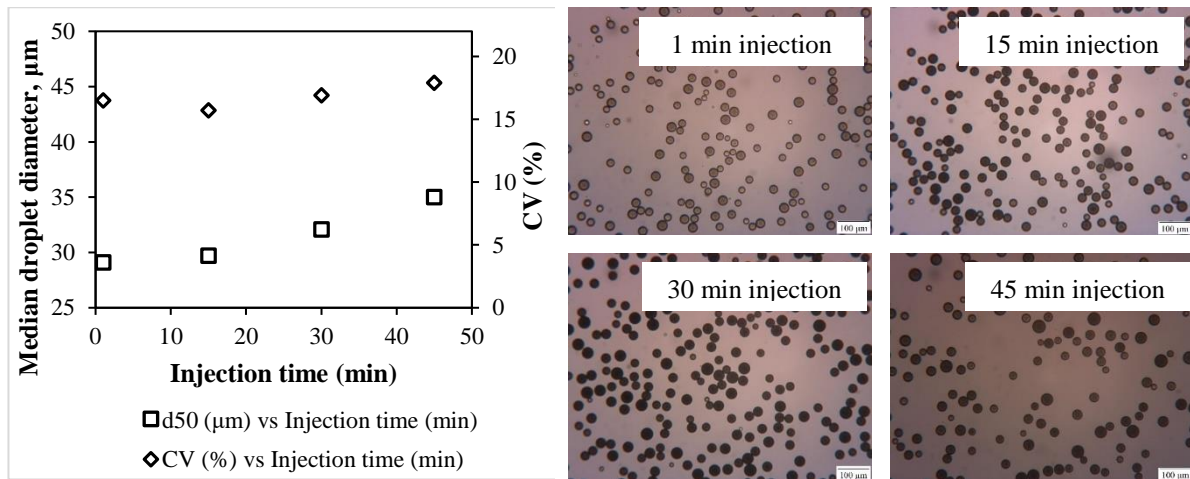


Figure 5.18 Drop size and drop size distribution evaluation over a 45 min injection and microscope pictures of the multiple (w/o/w) emulsions produced.

In both cases (single and multiple emulsion), the droplet size increased very slightly over time during 45 minutes. This increase could be due to fewer pores available due to blockage of the membrane with the polymeric solution. If, over time, pores available decrease and flow is kept constant, the resultant flux will increase, which would cause the increase of the drop size as observed in section 5.3.1. As described in the section 3.1.3.1b, the continuous phase (PVA solution) is saturated with DCM in order to slow down the diffusion of DCM from the dispersed phase to the continuous phase at the interface, which prevents the polymer from precipitating on the membrane, blocking the pores. This method was shown to be sufficient for short injections, but it is possible that polymer is still precipitating around the membrane blocking some pores. However, as inlet pressure was not monitored during this testing, to minimise loss

of material, this was not investigated further. Because, if fewer pores are available over time the inlet pressure would increase, case injection flow would be kept constant.

Another possible cause for the drop size increase over time could be the wetting of the membrane by the dispersed phase, i.e., during growth of the oil droplet at the pore surface the contact line of the drop/membrane expands till detachment. As the drop grows larger, a larger area is occupied. This larger pre-wetted area will facilitate the wetting of the following drop and possibly wet a larger area resulting in a larger drop and so on. This larger area might be just a very few nm in the beginning, but due to the high frequency of drop formation, over 45 minutes this difference can become noticeable (micron range). However, this is showed to be very difficult to prove experimentally. This possible wetting phenomenon was one of the motivations behind the work reported in section 4.4, using a rotating drum to investigate possible changes in advancing and receding contact angles through several cycles between oil and aqueous phases.

### 5.4 Overview of system scalability

In this section, the potential of this system in achieving high throughputs without change of scale is discussed, but just with minor changes in the membrane array and pore size.

Data shown in Figure 5.19 was obtained with the Dispersion Cell using a ringed stainless steel membrane with a 10  $\mu\text{m}$  membrane and distance between the pores of 200  $\mu\text{m}$  providing a ring porosity of 0.2%. A pressure gauge was introduced between the syringe and the membrane to monitor the inlet/transmembrane pressure at different injection rates, which will consequently result in different superficial velocities and interstitial velocities. The superficial velocity is readily known, and unambiguous. On the other hand, the interstitial velocity estimated in this section is assuming that all pores present in the membrane are readily available (100% pore activation).

Injection pressure was determined twice to evaluate the hysteresis in the measurement, i.e., inlet pressure was determined when flow was increased ( $\uparrow$ ) and when flow was decreased ( $\downarrow$ ). As can be seen in Figure 5.19, hysteresis in the pressure measurements are negligible for the test performed. The dispersed phase used was sunflower oil (coefficient of dynamic viscosity 50 mPa s) and continuous phase was a solution of 2% wt. Tween<sup>®</sup> 20. The equilibrium interfacial tension determined is 3.0 mN/m (see section 4.2).

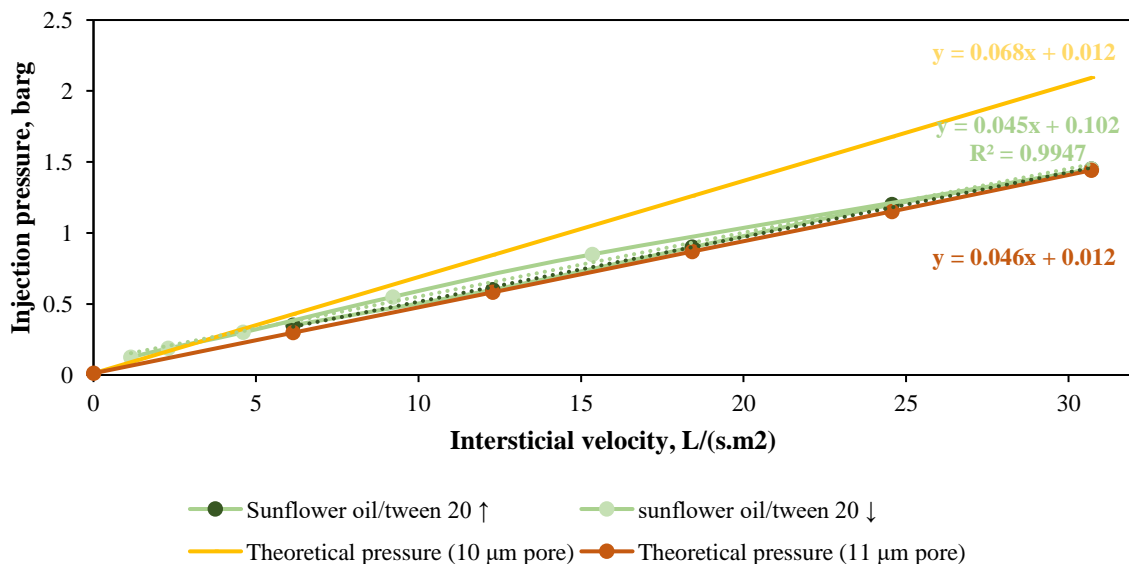


Figure 5.19 Pressure readings for different interstitial velocities tested using sunflower oil as dispersed phase and comparison with the estimated pressure based on Dagan method and capillary pressure.

In Figure 5.19 the estimated pressure drop was based on the resultant sum of capillary pressure and viscous pressure ( $\Delta P$ ) by Dagan *et. al.*[137]:

$$\Delta P = Q \frac{3\mu}{r_p^3} \left[ 1 + \frac{8L}{3\pi r_p} \right], \quad \text{eq. 5.7}$$

where  $r_p$  is the radius of the pore,  $\mu$  is the coefficient of dynamic viscosity,  $Q$  is the volumetric flow rate and  $L$  is thickness of the pore. Capillary pressure is the minimum transmembrane pressure required for the dispersed phase to go through the membrane structure, forming droplets, and it is defined as:

$$P_c = \frac{4\gamma \cos\theta}{d_p}, \quad \text{eq. 5.8}$$

where  $P_c$  is the capillary pressure and  $\theta$  is the contact angle between the dispersed phase and the capillary wall. The minimum capillary pressure estimated for this system is 1200 Pa. However, capillary pressure can be higher than estimated if interfacial tension has not reached the equilibrium before the drop is released.

Looking at Figure 5.19, the theoretical pressures are overestimating the determined pressures if a pore size of 10  $\mu\text{m}$  is used. However, if a pore size of 11  $\mu\text{m}$  is used instead in the calculations, theoretical pressures match the measured transmembrane pressures. Nonetheless, pore size may be even greater than 11  $\mu\text{m}$  because in practice it is expected that number of active pores active is less 100%.

As can be noticed, there are variables difficult to determine in order to be able to have an accurate theoretical model to predict the transmembrane pressure in this process. Otherwise, monitoring the transmembrane pressure could be an effective method to determine the actual capillary pressure, and therefore determine the (dynamic) interfacial tension that drops experience during detachment from the membrane.

Using an interstitial velocity of 30  $\text{L s}^{-1}\text{m}^{-2}$ , from the empirical curve showed in Figure 5.19, it is expected to obtain an injection pressure of 1.45 barg. In Table 5.7, this interstitial velocity was used as a reference to estimate the throughput that could be acquired by extending the porosity of the membranes. This is just an engineering exercise to show the capacity of much larger throughputs without changing the membrane (tubular) dimensions from the azimuthally oscillating membrane emulsification system.

Table 5.7 Membrane proprieties which determines its porosity and influences the maximum flow rate achievable for a certain interstitial velocity ( $30 \text{ L s}^{-1}\text{m}^{-2}$ ).

Array	Pore size ( $\mu\text{m}$ )	Pitch ( $\mu\text{m}$ )	Porosity	Surface area ( $\text{mm}^2$ )	Open area ( $\text{mm}^2$ )	Interstitial velocity ( $\text{L s}^{-1}\text{m}^{-2}$ )	Flow rate (achievable) ( $\text{L h}^{-1}$ )
Square	5	200	0.05%	5204	2.6	30	0.28
Square	10	200	0.19%	5204	9.9	30	1.07
Square	15	200	0.44%	5204	22.9	30	2.47
Square	20	200	0.79%	5204	40.9	30	4.41
Triangular	5	200	0.06%	5204	3.1	30	0.34
Triangular	10	200	0.23%	5204	12.0	30	1.29
Triangular	15	200	0.51%	5204	26.5	30	2.87
Triangular	20	200	0.91%	5204	47.4	30	5.11
Triangular	5	100	0.23%	5204	12.0	30	1.29
Triangular	5	100	0.23%	5204	12.0	32	1.38
Triangular	10	100	0.91%	5204	47.4	30	5.11
Triangular	15	150	0.91%	5204	47.4	30	5.11
Triangular	20	150	1.61%	5204	83.8	30	9.05

Table 5.7 shows various combinations of membrane design (array, pore size and distance between pores) that can be adjusted to increase the throughput keeping the optimal interstitial velocity determined for a certain application. For example, in section 5.3.2, PCL particles of  $30 \mu\text{m}$ , using a flow rate of  $0.3 \text{ L h}^{-1}$  with a membrane that was confined to a square array, pore size of  $5 \mu\text{m}$  and the distance between the pores was  $200 \mu\text{m}$  were obtained. So, assuming 100% of pores activation, the flow rate of  $0.3 \text{ L h}^{-1}$  is equivalent to an interstitial velocity of  $32 \text{ L s}^{-1}\text{m}^{-2}$ . Therefore, based on the resultant interstitial velocity, flow rate of the dispersed phase can be greatly improved by changing the membrane design to a triangular array, reducing the distance between pores down to  $100 \mu\text{m}$  and keeping the same pore size  $5 \mu\text{m}$ . So, to achieve same interstitial velocity, a flow rate of  $1.38 \text{ L h}^{-1}$  would have to be implemented. Estimated initial drop size would be  $55\mu\text{m}$  for formulation used in section 5.3.2, therefore drops would be smaller than pore distance and therefore risk of coalescence at membrane surface is limited.

Thus, this was an example how productivity can be greatly improved (about 4.6 times) without changing the overall dimensions of the membrane, or system setup, and keeping the same pore size. In the case when larger pore sizes can be used, even larger throughputs could be achieved. This exercise shows how this technology is capable to offer significant throughputs for some industries, in particular pharmaceuticals, which could cover many business needs. Based on

Table 5.7, by just optimising the membrane design (open area mainly) it is possible to achieve throughputs 20-30 times higher without need to scale up the membrane emulsification device.

To achieve higher productivities, dispersed phase flux is often maximised. However, increase of the dispersed phase flux may lead to operation in the jetting regime which is often undesirable to achieve high drop uniformity. Dimensionless numbers such as Capillary number, Weber number, Reynolds number and Ohnesorge number are often determined to predict the system flow behaviour that can be distinguished between dripping or jetting regime. Capillary number (of the dispersed phase,  $Ca_d$ ) is defined as:

$$Ca_d = \frac{\mu_d v_d}{\gamma} = \frac{\text{viscous force}}{\text{interfacial tension force}}, \quad \text{eq. 5.9}$$

where  $\mu_d$  is the dispersed phase coefficient of dynamic viscosity,  $v_d$  is the dispersed phase velocity (interstitial velocity) and  $\gamma$  is the equilibrium interfacial tension. Weber number (of the dispersed phase,  $We_d$ ) is defined as:

$$We_d = \frac{d_p \rho_d v_d^2}{\gamma} = \frac{\text{inertial force}}{\text{interfacial tension force}}, \quad \text{eq. 5.10}$$

where  $d_p$  is the pore diameter and  $\rho_d$  is the density of the dispersed phase. Reynolds number (of the dispersed phase,  $Re_d$ ) is defined as:

$$Re_d = \frac{d_d \rho_d v_d}{\mu_d} = \frac{\text{inertial force}}{\text{viscous force}}, \quad \text{eq. 5.11}$$

where  $d_d$  is the droplet diameter,  $\mu_d$  is the continuous phase coefficient of dynamic viscosity,  $\rho_c$  is the density of the continuous phase. The Reynolds number represents the ratio of the inertial to viscous forces, whereas the Weber number represents the ratio of the inertial to interfacial tension forces [138, 139]. Ohnesorge number ( $Oh$ ), which is the ratio of Weber number to Reynolds number, is defined as:

$$Oh = \frac{\sqrt{We}}{Re} = \frac{\mu_d}{(\rho_d d_d \gamma)^{0.5}} = \frac{\text{viscous force}}{\sqrt{(\text{inertia} \times \text{interfacial tension})}}, \quad \text{eq. 5.12}$$

Bond number ( $Bo$ ), which is the ratio of the gravitational forces to interfacial tension, is defined as:

$$Bo = \frac{\rho_a g d_p}{\gamma} = \frac{\text{gravitational force}}{\text{interfacial tension force}}, \quad \text{eq. 5.13}$$

where  $g$  is the gravitational acceleration constant.

According to J. Eggers and E. Villermaux [140], taking gravity into account, the transition from dripping to jetting regime takes place at a Weber number that depends on two parameters:  $We_c$  ( $Bo$ ,  $Oh$ ) and it can be “global” as defined by:

$$We_c = 0.034 (Bo \times Oh)^{-6/15} \quad \text{eq. 5.14}$$

Evaluating the example given above, these dimensionless numbers are calculated in Table 5.8 for a dispersed phase (sunflower oil) velocity of  $30 \text{ L s}^{-1} \text{ m}^{-2}$ , a drop size of  $30 \mu\text{m}$  and a pore diameter of  $5 \mu\text{m}$ .

Table 5.8 Dispersed phase Capillary number, Reynolds number, Weber number are determined for a dispersed velocity of  $30 \text{ L s}^{-1} \text{ m}^{-2}$ , a resultant drop size of  $30 \mu\text{m}$  from  $5 \mu\text{m}$  pore diameter. Ohnesorge number, Bond number and ratio between dispersed phase weber number and critical weber number are also determined for the same system. Sunflower oil was the liquid considered to be the dispersed phase in this exercise.

Dimensionless numbers	
$Ca_d$	0.487
$Re_d$	0.017
$We_d$	0.0014
$Oh$	2.21
$Bo$	$7.5 \times 10^{-5}$
$We_d/We_c$	0.0012

$< We_c (1.1060) \quad \text{Dripping}$

Sugiura *et. al.* [141] suggested that, based on the capillary number, the threshold between dripping and jetting regime is 0.056 as the jetting point. Therefore, the capillary number for the dispersed phase velocity proposed is about 10 times above the threshold suggested by Sugiura *et. al.* [141]. However, the membrane emulsification system used in that study relied on spontaneous drop detached rather than being function of the shear provided by the continuous phase as are all the membrane emulsification devices used in this work. Therefore, to define that critical capillary number for all the membrane emulsification system would be over simplifying the problem. Other authors, such as Ambravaneswaran *et.al.* [142] or Meyer [143]

suggested that other dimensionless values (Weber, Ohnesorge, Reynolds) are needed to determine the transition point. Based on the equation 5.14, the critical Weber number is 3 orders of magnitude greater than the Weber number determined for the dispersed phase velocity proposed in the above exercise and therefore dripping regime is expected. So, based on this analysis, throughput could have been greatly improved without transition to the jetting regime. In fact, using this system, throughput would have to be increased 28.6 times to give  $We_d$  equal to 1.1065, i.e. above  $We_c$  (1.1060) and, therefore, jetting regime is achieved.

Thus, there is a discrepancy between the different authors and more studies need to be performed in order to define the threshold between dripping and jetting regime during membrane emulsification. Nevertheless, it can be concluded that transition from dripping to jetting regime occurs with Ca, or We, number increase and Oh number decrease.

Nonetheless, it is reasonable to conclude that the azimuthal membrane oscillating system can be operated continuously at a scale suitable for industrial use. If drop size increases, over operating time, taking the product out of specification, then the disperse phase injection rate can be decreased, or the shear conditions increased to compensate for the increase in size. Both of these are dependent on the system being operated: e.g. volatility of the polymer solvent used; concentration of the polymer; membrane wetting capabilities; shear – drop size functionality, thus they need investigating and understanding for the system being proposed.



## Chapter 6 OUTLOOK AND CONCLUSIONS

During the performance of static contact angle experiments an interesting phenomenon was observed. This phenomenon was studied and later understood as spontaneous emulsification of a water drop in the surrounding phase (kerosene) caused by a concentration of surfactant above the CMC. Mass transfer of water in an organic phase (kerosene), at interfacial tensions not lower than 4 mN/m, is assisted by the presence of a large number of reverse micelles. Usually, spontaneous emulsification is associated to microemulsions with ultra-low interfacial tensions as the main characteristics of this process. Thus, spontaneous emulsification can also be driven by the chemical potential of both phases. This might be relevant for some formulations where ultra-low interfacial tensions are not possible to achieve, and the aim is to form w/o emulsions with a target size of about 200 nm. Use of solutions that contains high amounts of Span<sup>®</sup> 80 might have other applications where it is otherwise difficult to determine if it contains undesirable water. If water is present in the solution, it will make the continuous phase cloudy, indicating the presence of water. An example could be an airplane (aviation) kerosene or other fuels in which the presence of water is not desirable. Conversely, some other attempts have been made to include water into fuels in the form of stable micro/nano emulsions, which may improve fuel burning efficiency leading to lower emission and better engine performance.

Membrane emulsification is a technique capable to produce uniform emulsions with a predictable size. This study showed that various emulsion types can be produced in a controlled manner using different membrane emulsification devices that use distinct approaches to control drop formation. A wide range of emulsion droplet sizes were formulated via manipulation of the processing and formulation parameters. This approach allowed the development of a fundamental understanding from all the parameters that need to be considered in order to control the emulsion microstructure and the rate of production. Apart from the device used, drops are removed by the resultant shear from the continuous phase at the membrane surface. The most appropriate method depends on the requirements of the operator, including the possible intention to scale the process to different levels of productivity. Nonetheless, the design approach used to generate the shear must aim to obtain a uniform shear along the membrane surface, at any instance in time, as well as avoid membrane wetting by the dispersed phase. Uniformity of the shear is critical to provide the best uniformity for the emulsion that can be achieved. Shear uniformity was not studied in detail for all systems, but it can be noticed that, overall, emulsion uniformity was higher when oscillating membrane systems were used.

Despite a ringed membrane used in the Dispersion Cell, the shear was not as uniform as in the oscillation membrane systems used to detach drops from the membrane surface.

An alternative hydrophobic coating on metal porous membranes was developed and successfully applied in membrane emulsification processes. Hydrophobization of a metal surface was based on chemisorption of a FAS. It requires a certain degree of surface oxidation, which is shown to occur naturally within a matter of one hour after cleaning. The nature of the chemical cleaning did not appear to be important. The resulting contact angle of water on the metal surface in air was  $110 \pm 8^\circ$  degrees, and this increased to  $150 \pm 5^\circ$  degrees when the water droplet was surrounded by kerosene. Using the hydrophobized metal (nickel) membrane for the production of w/o emulsions, a PVA solution was injected in to kerosene containing Span<sup>®</sup> 80. As a result, uniform drops with a CV of about 20% were produced. This proved to be a straightforward technique for hydrophobization of a metal surface which could be repeated once the membrane loses its hydrophobicity. So, FAS coated membranes can be recoated and reused which is not easily possible with the PTFE coated membranes supplied by Micropore Technologies Ltd.

The use of the rotating drum system demonstrated that hydrophilic surfaces can preferably be wetted by the organic phase, assisted by the surfactant, even when an aqueous phase is present. Vice versa, hydrophobic surfaces can preferably be wetted by the aqueous phase, assisted by the surfactant, even when an organic phase is present. This supports the possibility of producing, for example, w/o emulsions using hydrophilic membranes. This was also investigated and, indeed, it is possible to produce uniform w/o emulsions using a hydrophilic membrane by membrane emulsification. Therefore, under carefully controlled conditions no membrane surface treatment may be required, contrary to conventionally accepted wisdom, according to which a hydrophobic membrane is required when producing water droplets. This result is possible using an appropriate surfactant in the continuous phase. The presence of surfactants assists in the better wetting of the membrane by the organic phase and in doing this preventing the dispersed phase (water) from wetting the membrane surface. Static and dynamic contact angle measurements were performed to show that stainless steel is wetted by the organic phase, when surfactant is present in the organic phase, rather than in the aqueous phase. It is shown that, an untreated (hydrophilic) stainless steel porous membrane is shown to be effective in the production of uniform PVA droplets, when generating a w/o emulsion. This is relevant for applications where a uniform and controlled production of w/o emulsions by membrane emulsification is required and when a hydrophobic membrane surface

treatment/coating is not recommended, due to the chemicals used or due to the poor stability of this coating over a long-time exposure to the liquids used in the formulation chosen.

A different approach was used in this thesis to estimate the percentage of active pores during membrane emulsification. Surfactant adsorption was studied by the pendant drop method which when combined with the droplet formation rate, during membrane emulsification, provided a means to estimate the percentage of active pores during the process. Basically, a set of membrane emulsification experiments were performed with the vertical oscillating system, where a range of surfactant (Span<sup>®</sup> 80 dissolved in kerosene) concentrations were investigated while all the other parameters that affect drop formation were kept constant. Resultant drop size was constant, around 36  $\mu\text{m}$ , in the case of surfactant concentration of 29 mM (i.e. 57 times the CMC value) and above being used. So, there was sufficient surfactant present such that the drop size did not change with increasing surfactant concentration. However, when surfactant concentrations were less than 29 mM, the resultant drop size was larger. Therefore, the expansion rate of the drops emerging from the 10  $\mu\text{m}$  pore-size membrane was greater than the adsorption rate of the drop stabilising surfactant. This led to a situation where there was a lower concentration of surfactant at the water-oil interface than would occur at equilibrium, hence the interfacial tension was greater than the equilibrium value. From this data, the dynamic interfacial tension that the drop experienced at the membrane surface was determined using a previously published force-momentum balance. The dynamic interfacial tension values were between the equilibrium interfacial tension of  $3 \pm 0.8 \text{ mN m}^{-1}$  and the interfacial tension between water and kerosene with no surfactant present,  $38 \pm 1.9 \text{ mN m}^{-1}$ , i.e., when the interface is free of surface active agents, either PVA or Span<sup>®</sup> 80. This data was combined with pendant drop experiments data that were performed to provide information regarding the surfactant surface adsorption rate. This allowed an estimate of the percentage of active pores for the process conditions used. The membrane used in the study had a very regular matrix of uniform pores. The deduced percentage of active pores was about 37% for this regular membrane pore geometry, when operating with 29 mM surfactant concentration and above. This suggests that there is scope for improving productivity of this membrane system, if the percentage pore utilisation could be increased. The technique described for determining the active pore utilisation of a membrane, used for membrane emulsification, can be applied to different types of membranes.

Throughout the work 3 different membrane emulsification devices were used: Dispersion Cell, vertical oscillating system and azimuthally oscillating system with different formulations resulting in various emulsions types.

- A range of uniform PVA droplets, between 40 and 120  $\mu\text{m}$ , were produced using the Dispersion cell and vertical oscillating system – w/o emulsion;
- Uniform PLGA droplets were produced using the Dispersion cell – o/w emulsion. By solvent removal, initial PLGA droplets became solid PLGA particles which were post-processed and visualized under a SEM. Final produced PLGA particles size vary between 24 and 40  $\mu\text{m}$ ;
- A range of uniform sunflower-oil droplets, between 20 and 120  $\mu\text{m}$ , were produced using the azimuthally oscillating system – o/w emulsion
- A range of uniform PCL droplets were produced, continuously, using the azimuthally oscillating system – o/w emulsion. By solvent removal, initial PCL droplets became solid PCL particles. Final produced PCL particles size vary between 35 and 60  $\mu\text{m}$ ;
- Double emulsification was performed resulting in uniform PCL droplets containing several smaller, pre-emulsified, BSA droplets (<1.0  $\mu\text{m}$ ). This double emulsion, w/o/w emulsion, was produced continuously during 45 min using the azimuthally oscillating system. Afterwards, by solvent removal, BSA is entrapped in solid PCL particles resulting in its encapsulation.

By means of membrane emulsification, it was shown that uniform polymeric particles can be produced in a controlled and predictable manner. The polymers used, PVA, PCL or PLGA, have different properties, but they are all often used as carriers for API's such as drugs, DNA or proteins. PVA is a hydrophilic, biocompatible and bio-adhesive polymer with interesting mechanical properties and thermostable. On the other hand, PCL and PLGA are hydrophobic and biodegradable polymers. It is very interesting to have them in the form of spherical particles since they offer a more predictable drug release behaviour, low drag force during mobility in fluids and a high surface area for adhesion. During product development, particle size is one of the parameters that can be tuned to achieve a desirable drug release rate and meet different dosage requirements. So, membrane emulsification was shown to be an appropriate technology to produce this type of emulsions, which are precursors to prepare polymeric particles, where predictable particle size and uniformity is demanded.

A thorough experimental investigation of the azimuthally oscillating membrane emulsification system was performed using sunflower oil injected in to water containing a surfactant to provide droplets with a diameter of 20-120  $\mu\text{m}$  using a 5  $\mu\text{m}$  pore size laser drilled stainless steel membrane. Under optimal conditions, CV values of around 8% were achieved. There were no detected relevant differences in using different wave forms on the average droplet size and uniformity of the distributions. The droplet size could be predicted, for low injection rates, using a model for drop size based on the peak shear at the membrane surface, the membrane pore size and the interfacial tension between the two liquid phases. The drops produced depended on the shear at the membrane surface and not the combination of frequency and membrane displacement used to create that shear.

This azimuthally oscillating system was able to produce very high dispersed phase concentrations, up to 33% v/v gave good drop size distributions (9-11% CV) without the need to recirculate the continuous phase. Low shear stresses (2-5 Pa) over a very narrow region next to the membrane surface, was shown to provide good control over the droplet size and, therefore, a system well suited to fragile droplets. The drop size results from the system were reproducible and this device is the most appropriate to be scaled up, i.e. increasing the diameter and length of membrane cylinders.

In conclusion, in this study a new method was developed to hydrophobize metal porous membranes, a better understanding of the mechanisms involved in the interaction between complex liquids and hydrophilic or hydrophobic surfaces, a method that can be adopted to estimate the number of active pores during membrane emulsification and the versatility of membrane emulsification was demonstrated together with a good understanding of the underlying processes. This technology allows us to produce, in a controlled manner, uniform size emulsions using distinct membrane emulsification devices in combination with diverse formulations, resulting from different process challenges or offering different solutions.

Regarding the demands of a business, different emulsification techniques may be more likely to be adopted for a certain application. Therefore, a certain technique may be more adequate for the process to be sustainable and profitable in a long term. Low product value without the necessity of a narrow drop size distribution is likely to be produced by a conventional emulsification method which are present and widely known in industry. Even so, adoption of membrane emulsification might not be required for product quality but might improve energy efficiency and reduce waste materials.

## 6.1 Recommendations and Future Work

Here are presented some opportunities for further work building on a number of uncovered areas which would be very interesting to explore:

1) More studies on the membrane surface influence on the resultant droplet size:

To use the same formulation, the same membrane material (e.g. stainless steel) and geometry could be treated in such a way that would result in different levels of hydrophobicity. For example, expose membrane to FAS for different time periods and perform membrane emulsification evaluating resultant drop size. This would give more evidence about the importance of the membrane surface characteristics independent of the formulation, membrane emulsification device or membrane geometry used.

2) More studies on the upscaling of membrane emulsification apparatus

In the present work, three different membrane emulsification devices were tested and shear stress determination is described for each of them. However, it has not been comprehensively evaluated whether using equivalent conditions and equivalent shear values, results in an equal emulsion size for the different membrane emulsification devices tested. This study could be extended to other membrane emulsification devices such as cross-flow systems and pulsed system that use metal (stainless steel or nickel) porous membranes. For instance, shear determination for those suggested devices is also available in the literature. Such a study would be very interesting to perform, but some challenges in the design experiment are expected. To mitigate the challenges, use of a simple formulation, e.g., SFO in Tween 20, identical membrane surface, geometry, pore size, etc in the different (scale) membrane emulsification apparatus is recommended. However, membrane dimensions & open area will be different due to the different apparatus scale. Therefore, it is recommended to adjust, for instance, the dispersed phase flow rate in order to achieve comparable pore velocities for a wide range of shear stresses values. This would give a comprehensive approach for future users to upscale their process and perhaps attract more industries, mitigating their risks, to opt for a relatively new emulsification technology.

- 3) More studies on the longevity and possible optimization of the hydrophobic (FAS) treatment developed in this work

It would be interesting to see more studies evaluating the membrane FAS treatment with different formulations (w/o emulsions) and assess its suitability and longevity. Besides that, this hydrophobic treatment applied on metal porous membranes may be improved. For example, it would be interesting to investigate whether controlled oxidation of the membrane (instead of exposing to air) and/or etching (instead of exposing to HCl), followed by FAS solution exposure, would achieve a higher hydrophobicity level, i.e., increase the contact angle further. For example, use of oxygen plasma etching technology could be a way forward to optimize presented FAS treatment/coating.

- 4) More studies using the developed rotating drum apparatus to characterize dynamic contact angles between two immiscible liquids with presence of a relevant surfactant:

This rotating drum apparatus can be used to obtain more information about complex formulations and predict its wetting behaviour when in contact (dynamically) with a solid surface. This device can be used to characterize a certain formulation and acquire extra knowledge that may improve the formulation further. Different surfaces can be tested besides the two stainless steel drums used in this study.

- 5) More studies on the azimuthally oscillating membrane system with different formulations

It is believed in this study that this system is capable of producing high uniformity emulsions with multiple formulations. So, it would be interesting to see its performance with different systems and perform continuous production for longer periods of time than tested in this work (maximum of 45 minutes). Despite the encouraging results obtained in this work, this production time may be insufficient to satisfy the needs of various industrial demands. Testing for longer periods of time investigates reduction of emulsion quality and also other issues. For instance, the long oscillation times can result in wear and tear of the seals which may be an obstacle for process validation to manufacture a food, medical or pharma grade product. Thus, the device design could be improved in such a manner avoiding particulates, resultant from the wear and tear of the seals, to contaminate the product and, therefore, comply to the user requirements and specifications.

---

## References

1. Sjoblom, J., *Emulsions and Emulsion Stability: Surfactant Science Series*. Vol. 61. 2005: CRC Press.
2. Schramm, L.L., *Emulsions, Foams, and Suspensions: Fundamentals and Applications* 2005: Wiley.
3. Kallay, N., *Interfacial Dynamics* 2000: Taylor & Francis.
4. Pasquali, R.C., N. Sacco, and C. Bregni, *The Studies on Hydrophilic-Lipophilic Balance (HLB): Sixty Years after William C. Griffin's Pioneer Work (1949-2009)*. Latin American Journal of Pharmacy, 2009. **28**(2): p. 313-317.
5. Baloch, M.K. and G. Hameed, *Emulsification of oil in water as affected by different parameters*. Journal of Colloid and Interface Science, 2005. **285**(2): p. 804-813.
6. Gijsbertsen-Abrahamse, A.J., A. van der Padt, and R.M. Boom, *Status of cross-flow membrane emulsification and outlook for industrial application*. Journal of Membrane Science, 2004. **230**(1-2): p. 149-159.
7. Sherman, P., *Emulsion science* 1968, London; New York: Academic Press.
8. Nakashima, T., M. Shimizu, and M. Kukizaki, *Membrane emulsification by microporous glass*. Inorganic Membranes : Icim2-91, ed. A.J. Burggraaff, J. Charpin, and L. Cot 1991. 513-516.
9. Nisisako, T., T. Torii, and T. Higuchi, *Novel microreactors for functional polymer beads*. Chemical Engineering Journal, 2004. **101**(1-3): p. 23-29.
10. Vladislavljević, G.T., *Structured microparticles with tailored properties produced by membrane emulsification*. Advances in Colloid and Interface Science, 2015. **225**: p. 53-87.
11. Coombs O'Brien, J., L. Torrente-Murciano, D. Mattia, and J.L. Scott, *Continuous Production of Cellulose Microbeads via Membrane Emulsification*. ACS Sustainable Chemistry & Engineering, 2017. **5**(7): p. 5931-5939.



- 
12. Williams, R.A., S.J. Peng, D.A. Wheeler, N.C. Morley, D. Taylor, M. Whalley, and D.W. Houldsworth, *Controlled production of emulsions using a crossflow membrane part II: Industrial scale manufacture*. Chemical Engineering Research & Design, 1998. **76**(A8): p. 902-910.
  13. Varde, N.K. and D.W. Pack, *Influence of particle size and antacid on release and stability of plasmid DNA from uniform PLGA microspheres*. Journal of controlled release : official journal of the Controlled Release Society, 2007. **124**(3): p. 172-180.
  14. Berkland, C., K. Kim, and D.W. Pack, *Fabrication of PLG microspheres with precisely controlled and monodisperse size distributions*. Journal of Controlled Release, 2001. **73**(1): p. 59-74.
  15. Berkland, C., A. Cox, K. Kim, and D.W. Pack, *Three-month, zero-order piroxicam release from monodispersed double-walled microspheres of controlled shell thickness*. Journal of Biomedical Materials Research Part A, 2004. **70A**(4): p. 576-584.
  16. Pollauf, E.J., K.K. Kim, and D.W. Pack, *Small-Molecule Release from poly(D,L-Lactide)/Poly(D,L-Lactide-co-Glycolide) Composite Microparticles*. Journal of Pharmaceutical Sciences, 2005. **94**(9): p. 2013-2022.
  17. Becher, P., *Emulsions: theory and practice* 2001: American Chemical Society.
  18. Almeida, A., S. Possemiers, M.N. Boone, T. De Beer, T. Quinten, L. Van Hoorebeke, J.P. Remon, and C. Vervaet, *Ethylene vinyl acetate as matrix for oral sustained release dosage forms produced via hot-melt extrusion*. European Journal of Pharmaceutics and Biopharmaceutics, 2011. **77**(2): p. 297-305.
  19. Viseras, C., C. Aguzzi, P. Cerezo, and M.C. Bedmar, *Biopolymer-clay nanocomposites for controlled drug delivery*. Materials Science and Technology, 2008. **24**(9): p. 1020-1026.
  20. Anderson, J.M. and M.S. Shive, *Biodegradation and biocompatibility of PLA and PLGA microspheres*. Advanced Drug Delivery Reviews, 1997. **28**(1): p. 5-24.

- 
21. Vladisavljević, G.T., H. Shahmohamadi, D.B. Das, E.E. Ekanem, Z. Tauanov, and L. Sharma, *Glass capillary microfluidics for production of monodispersed poly (dl-lactic acid) and polycaprolactone microparticles: Experiments and numerical simulations*. Journal of Colloid and Interface Science, 2014. **418**: p. 163-170.
  22. Li, M., O. Rouaud, and D. Poncelet, *Microencapsulation by solvent evaporation: State of the art for process engineering approaches*. International Journal of Pharmaceutics, 2008. **363**(1): p. 26-39.
  23. Hanga, M.P. and R.G. Holdich, *Membrane emulsification for the production of uniform poly-N-isopropylacrylamide-coated alginate particles using internal gelation*. Chemical Engineering Research and Design, 2014. **92**(9): p. 1664-1673.
  24. Morelli, S., R.G. Holdich, and M.M. Dragosavac, *Chitosan and Poly (Vinyl Alcohol) microparticles produced by membrane emulsification for encapsulation and pH controlled release*. Chemical Engineering Journal, 2016. **288**: p. 451-460.
  25. de Vos, P., H.A. Lazarjani, D. Poncelet, and M.M. Faas, *Polymers in cell encapsulation from an enveloped cell perspective*. Advanced Drug Delivery Reviews, 2014. **67-68**: p. 15-34.
  26. Klemm, D., B. Heublein, H.-P. Fink, and A. Bohn, *Cellulose: Fascinating Biopolymer and Sustainable Raw Material*. Angewandte Chemie International Edition, 2005. **44**(22): p. 3358-3393.
  27. Zhou, Q.-Z., L.-Y. Wang, G.-H. Ma, and Z.-G. Su, *Preparation of uniform-sized agarose beads by microporous membrane emulsification technique*. Journal of Colloid and Interface Science, 2007. **311**(1): p. 118-127.
  28. Deng, X., L. Mammen, Y. Zhao, P. Lellig, K. Müllen, C. Li, H.-J. Butt, and D. Vollmer, *Transparent, Thermally Stable and Mechanically Robust Superhydrophobic Surfaces Made from Porous Silica Capsules*. Advanced Materials, 2011. **23**(26): p. 2962-2965.
  29. Yuan, Q.C., O.J. Cayre, M. Manga, R.A. Williams, and S. Biggs, *Preparation of particle-stabilized emulsions using membrane emulsification*. Soft Matter, 2010. **6**(7): p. 1580-1588.

- 
30. Dragosavac, M.M., G.T. Vladisavljević, R.G. Holdich, and M.T. Stillwell, *Production of Porous Silica Microparticles by Membrane Emulsification*. Langmuir, 2012. **28**(1): p. 134-143.
31. Yang, Z., Z. Peng, J. Li, S. Li, L. Kong, P. Li, and Q. Wang, *Development and evaluation of novel flavour microcapsules containing vanilla oil using complex coacervation approach*. Food Chemistry, 2014. **145**: p. 272-277.
32. Morelli, S., R.G. Holdich, and M.M. Dragosavac, *Microparticles for cell encapsulation and colonic delivery produced by membrane emulsification*. Journal of Membrane Science, 2017. **524**: p. 377-388.
33. Schroën, K., M. Ferrando, S. de Lamo-Castellví, S. Sahin, and C. Güell, *Linking Findings in Microfluidics to Membrane Emulsification Process Design: The Importance of Wettability and Component Interactions with Interfaces*. Membranes, 2016. **6**(2): p. 26.
34. Medina-Llamas, M. and D. Mattia, *Production of Nanoemulsions Using Anodic Alumina Membranes in a Stirred-Cell Setup*. Industrial & Engineering Chemistry Research, 2017. **56**(26): p. 7541-7550.
35. Joscelyne, S.M. and G. Trägårdh, *Food emulsions using membrane emulsification: conditions for producing small droplets*. Journal of Food Engineering, 1999. **39**(1): p. 59-64.
36. Peng, S.J. and R.A. Williams, *Controlled production of emulsions using a crossflow membrane part I: Droplet formation from a single pore*. Chemical Engineering Research & Design, 1998. **76**(A8): p. 894-901.
37. Schroder, V., O. Behrend, and H. Schubert, *Effect of dynamic interfacial tension on the emulsification process using microporous, ceramic membranes*. Journal of Colloid and Interface Science, 1998. **202**(2): p. 334-340.
38. Lee, K.P. and D. Mattia, *Manufacturing of Nanoemulsions Using Nanoporous Anodized Alumina Membranes: Experimental Investigation and Process Modeling*. Industrial & Engineering Chemistry Research, 2013. **52**(42): p. 14866-14874.

- 
39. vanRijn, C., M. vanderWekken, W. Nijdam, and M. Elwenspoek, *Deflection and maximum load of microfiltration membrane sieves made with silicon micromachining*. Journal of Microelectromechanical Systems, 1997. **6**(1): p. 48-54.
40. Wagdare, N.A., A.T.M. Marcelis, R.M. Boom, and C.J.M. van Rijn, *Porous microcapsule formation with microsieve emulsification*. Journal of Colloid and Interface Science, 2011. **355**(2): p. 453-457.
41. Nakashima, T., M. Shimizu, and M. Kukizaki, *Membrane Emulsification by Microporous Glass*. Key Engineering Materials, 1991. **61-62**: p. 513-516.
42. Omi, S., *Preparation of monodisperse microspheres using the Shirasu porous glass emulsification technique*. Colloids and Surfaces A: Physicochemical and Engineering Aspects, 1996. **109**: p. 97-107.
43. Holdich, R., S. Kosvintsev, T. Cumming, and S. Zhdanov, *Pore design and engineering for filters and membranes*. Philosophical Transactions of the Royal Society a-Mathematical Physical and Engineering Sciences, 2006. **364**(1838): p. 161-174.
44. Holdich, R.G., M.M. Dragosavac, G.T. Vladisavljevic, and E. Piacentini, *Continuous Membrane Emulsification with Pulsed (Oscillatory) Flow*. Industrial & Engineering Chemistry Research, 2013. **52**(1): p. 507-515.
45. Dragosavac, M.M., M.N. Sovilj, S.R. Kosvintsev, R.G. Holdich, and G.T. Vladisavljevic, *Controlled production of oil-in-water emulsions containing unrefined pumpkin seed oil using stirred cell membrane emulsification*. Journal of Membrane Science, 2008. **322**(1): p. 178-188.
46. Schadler, V. and E.J. Windhab, *Continuous membrane emulsification by using a membrane system with controlled pore distance*. Desalination, 2006. **189**(1-3): p. 130-135.
47. Manga, M.S., O.J. Cayre, R.A. Williams, S. Biggs, and D.W. York, *Production of solid-stabilised emulsions through rotational membrane emulsification: influence of particle adsorption kinetics*. Soft Matter, 2012. **8**(5): p. 1532-1538.

- 
48. Stillwell, M.T., R.G. Holdich, S.R. Kosvintsev, G. Gasparini, and I.W. Cumming, *Stirred cell membrane emulsification and factors influencing dispersion drop size and uniformity*. *Industrial & Engineering Chemistry Research*, 2007. **46**(3): p. 965-972.
49. Holdich, R.G., M.M. Dragosavac, G.T. Vladisavljevic, and S.R. Kosvintsev, *Membrane Emulsification with Oscillating and Stationary Membranes*. *Industrial & Engineering Chemistry Research*, 2010. **49**(8): p. 3810-3817.
50. Vladisavljevic, G.T. and R.A. Williams, *Manufacture of large uniform droplets using rotating membrane emulsification*. *Journal of Colloid and Interface Science*, 2006. **299**(1): p. 396-402.
51. Kosvintsev, S.R., G. Gasparini, and R.G. Holdich, *Membrane emulsification: Droplet size and uniformity in the absence of surface shear*. *Journal of Membrane Science*, 2008. **313**(1-2): p. 182-189.
52. Wagdare, N.A., A.T.M. Marcelis, O.B. Ho, R.M. Boom, and C.J.M. van Rijn, *High throughput vegetable oil-in-water emulsification with a high porosity micro-engineered membrane*. *Journal of Membrane Science*, 2010. **347**(1-2): p. 1-7.
53. Charcosset, C., I. Limayem, and H. Fessi, *The membrane emulsification process—a review*. *Journal of Chemical Technology & Biotechnology*, 2004. **79**(3): p. 209-218.
54. Kukizaki, M. and M. Goto, *Demulsification of water-in-oil emulsions by permeation through Shirasu-porous-glass (SPG) membranes*. *Journal of Membrane Science*, 2008. **322**(1): p. 196-203.
55. Geerken, M.J., R.G.H. Lammertink, and M. Wessling, *Interfacial aspects of water drop formation at micro-engineered orifices*. *Journal of Colloid and Interface Science*, 2007. **312**(2): p. 460-469.
56. Lee, S.H., M.J. Kwon, J.G. Park, Y.K. Kim, and H.J. Shin, *Preparation and characterization of perfluoro-organic thin films on aluminium*. *Surface & Coatings Technology*, 1999. **112**(1-3): p. 48-51.
57. Stillwell, M., *Membrane surface modification: techniques, properties and applications*, in *Chemical Engineering* 2009, Loughborough University.

- 
58. Wenzel, R.N., Resistance of solid surfaces to wetting by water. *Industrial & Engineering Chemistry*, 1936. **28**(8): p. 988-994.
59. Quéré, D., *Wetting and Roughness*. *Annual Review of Materials Research*, 2008. **38**(1): p. 71-99.
60. Wolansky, G. and A. Marmur, *Apparent contact angles on rough surfaces: the Wenzel equation revisited*. *Colloids and Surfaces A: Physicochemical and Engineering Aspects*, 1999. **156**(1): p. 381-388.
61. Cassie, A.B.D. and S. Baxter, *Wettability of porous surfaces*. *Transactions of the Faraday Society*, 1944. **40**(0): p. 546-551.
62. Marmur, A., *Wetting on Hydrophobic Rough Surfaces: To Be Heterogeneous or Not To Be?* *Langmuir*, 2003. **19**(20): p. 8343-8348.
63. Chao, T.C., O. Arjmandi-Tash, D.B. Das, and V.M. Starov, *Simultaneous spreading and imbibition of blood droplets over porous substrates in the case of partial wetting*. *Colloids and Surfaces A: Physicochemical and Engineering Aspects*.
64. Feng, L., S. Li, Y. Li, H. Li, L. Zhang, J. Zhai, Y. Song, B. Liu, L. Jiang, and D. Zhu, *Super-Hydrophobic Surfaces: From Natural to Artificial*. *Advanced Materials*, 2002. **14**(24): p. 1857-1860.
65. Beentjes, P.C.J., *Durability of Polymer Coated Steel in Diluted Acetic Acid Environment*, 2004, Technishce Universiteit Delft: Delft, Netherlands.
66. Vladislavljevic, G.T. and H. Schubert, *Preparation and analysis of oil-in-water emulsions with a narrow droplet size distribution using Shirasu-porous-glass (SPG) membranes*. *Desalination*, 2002. **144**(1): p. 167-172.
67. Abrahamse, A.J., R. van Lierop, R.G.M. van der Sman, A. van der Padt, and R.M. Boom, *Analysis of droplet formation and interactions during cross-flow membrane emulsification*. *Journal of Membrane Science*, 2002. **204**(1-2): p. 125-137.
68. Zhu, J. and D. Barrow, *Analysis of droplet size during crossflow membrane emulsification using stationary and vibrating micromachined silicon nitride membranes*. *Journal of Membrane Science*, 2005. **261**(1-2): p. 136-144.

- 
69. Egidi, E., G. Gasparini, R.G. Holdich, G.T. Vladisavljevic, and S.R. Kosvintsev, *Membrane emulsification using membranes of regular pore spacing: Droplet size and uniformity in the presence of surface shear*. Journal of Membrane Science, 2008. **323**(2): p. 414-420.
70. Xu, J.H., G.S. Luo, G.G. Chen, and J.D. Wang, *Experimental and theoretical approaches on droplet formation from a micrometer screen hole*. Journal of Membrane Science, 2005. **266**(1–2): p. 121-131.
71. Sugiura, S., M. Nakajima, J. Tong, H. Nabetani, and M. Seki, *Preparation of Monodispersed Solid Lipid Microspheres Using a Microchannel Emulsification Technique*. Journal of Colloid and Interface Science, 2000. **227**(1): p. 95-103.
72. Kosvintsev, S.R., G. Gasparini, R.G. Holdich, I.W. Cumming, and M.T. Stillwell, *Liquid-liquid membrane dispersion in a stirred cell with and without controlled shear*. Industrial & Engineering Chemistry Research, 2005. **44**(24): p. 9323-9330.
73. Nakashima, T., M. Shimizu, and M. Kukizaki, *Particle control of emulsion by membrane emulsification and its applications*. Advanced Drug Delivery Reviews, 2000. **45**(1): p. 47-56.
74. Maan, A.A., K. Schroën, and R. Boom, *Monodispersed water-in-oil emulsions prepared with semi-metal microfluidic EDGE systems*. Microfluidics and Nanofluidics, 2013. **14**(1): p. 187-196.
75. Maan, A.A., S. Sahin, L.H. Mujawar, R. Boom, and K. Schroën, *Effect of surface wettability on microfluidic EDGE emulsification*. Journal of Colloid and Interface Science, 2013. **403**: p. 157-159.
76. Kobayashi, I., M. Yasuno, S. Iwamoto, A. Shono, K. Satoh, and M. Nakajima, *Microscopic observation of emulsion droplet formation from a polycarbonate membrane*. Colloids and Surfaces A: Physicochemical and Engineering Aspects, 2002. **207**(1–3): p. 185-196.
77. Bertrandias, A., H. Duval, J. Casalinho, and M.L. Giorgi, *Good vibrations —Transition in drop generation from an immersed capillary tube*. EPL, 2015. **111**(4): p. 44004.

- 
78. Keurentjes, J.T.F., M.A.C. Stuart, D. Brinkman, C.G.P.H. Schroën, and K. van 't Riet, *Surfactant-induced wetting transitions: Role of surface hydrophobicity and effect on oil permeability of ultrafiltration membranes*. *Colloids and Surfaces*, 1990. **51**: p. 189-205.
79. Holzapfel, S., E. Rondeau, P. Muhlich, and E.J. Windhab, *Drop Detachment from a Micro-Engineered Membrane Surface in a Dynamic Membrane Emulsification Process*. *Chemical Engineering & Technology*, 2013. **36**(10): p. 1785-1794.
80. Truszkowska, D., F. Henrich, J. Schultze, K. Koynov, H.J. Räder, H.J. Butt, and G.K. Auernhammer, *Forced dewetting dynamics of high molecular weight surfactant solutions*. *Colloids and Surfaces A: Physicochemical and Engineering Aspects*, 2016.
81. Fell, D., N. Pawanrat, E. Bonaccorso, H.-J. Butt, and G.K. Auernhammer, *Influence of surfactant transport suppression on dynamic contact angle hysteresis*. *Colloid and Polymer Science*, 2013. **291**(2): p. 361-366.
82. Fell, D., G. Auernhammer, E. Bonaccorso, C. Liu, R. Sokuler, and H.-J. Butt, *Influence of Surfactant Concentration and Background Salt on Forced Dynamic Wetting and Dewetting*. *Langmuir*, 2011. **27**(6): p. 2112-2117.
83. Henrich, F., D. Fell, D. Truszkowska, M. Weirich, M. Anyfantakis, T.-H. Nguyen, M. Wagner, G.K. Auernhammer, and H.-J. Butt, *Influence of surfactants in forced dynamic dewetting*. *Soft Matter*, 2016. **12**(37): p. 7782-7791.
84. Geerken, M.J., R.G.H. Lammertink, and M. Wessling, *Tailoring surface properties for controlling droplet formation at microsieve membranes*. *Colloids and Surfaces A: Physicochemical and Engineering Aspects*, 2007. **292**(2-3): p. 224-235.
85. Liggieri, L. and R. Miller, *Relaxation of surfactants adsorption layers at liquid interfaces*. *Current Opinion in Colloid & Interface Science*, 2010. **15**(4): p. 256-263.
86. Kawakatsu, T., G. Trägårdh, C. Trägårdh, M. Nakajima, N. Oda, and T. Yonemoto, *The effect of the hydrophobicity of microchannels and components in water and oil phases on droplet formation in microchannel water-in-oil emulsification*. *Colloids and Surfaces A: Physicochemical and Engineering Aspects*, 2001. **179**(1): p. 29-37.



- 
87. Saito, M., L.-J. Yin, I. Kobayashi, and M. Nakajima, *Preparation characteristics of monodispersed oil-in-water emulsions with large particles stabilized by proteins in straight-through microchannel emulsification*. *Food Hydrocolloids*, 2005. **19**(4): p. 745-751.
88. Boyd, J., C. Parkinson, and P. Sherman, *Factors affecting emulsion stability, and the HLB concept*. *Journal of Colloid and Interface Science*, 1972. **41**(2): p. 359-370.
89. van Dijke, K., I. Kobayashi, K. Schroen, K. Uemura, M. Nakajima, and R. Boom, *Effect of viscosities of dispersed and continuous phases in microchannel oil-in-water emulsification*. *Microfluidics and Nanofluidics*, 2010. **9**(1): p. 77-85.
90. Abrahamse, A.J., A. van der Padt, and R.M. Boom, *Influence of membrane morphology on pore activation in membrane emulsification*. *Journal of Membrane Science*, 2003. **217**(1–2): p. 141-150.
91. Vladisavljevic, G.T., U. Lambrich, M. Nakajima, and H. Schubert, *Production of O/W emulsions using SPG membranes, ceramic alpha-aluminium oxide membranes, microfluidizer and a silicon microchannel plate - a comparative study*. *Colloids and Surfaces a-Physicochemical and Engineering Aspects*, 2004. **232**(2-3): p. 199-207.
92. Dowding, P.J., J.W. Goodwin, and B. Vincent, *Production of porous suspension polymer beads with a narrow size distribution using a cross-flow membrane and a continuous tubular reactor*. *Colloids and Surfaces A: Physicochemical and Engineering Aspects*, 2001. **180**(3): p. 301-309.
93. Yuan, Q.C., N. Aryanti, R.Z. Hou, and R.A. Williams, *Performance of slotted pores in particle manufacture using rotating membrane emulsification*. *Particuology*, 2009. **7**(2): p. 114-120.
94. Silva, P.S., M.M. Dragosavac, G.T. Vladisavljević, H.C.H. Bandulasena, R.G. Holdich, M. Stillwell, and B. Williams, *Azimuthally oscillating membrane emulsification for controlled droplet production*. *AIChE Journal*, 2015. **61**(11): p. 3607-3615.
95. Abrahamse, A.J., A. van der Padt, R.M. Boom, and W.B.C. de Heij, *Process fundamentals of membrane emulsification: Simulation with CFD*. *AIChE Journal*, 2001. **47**(6): p. 1285-1291.

- 
96. Dragosavac, M.M., R.G. Holdich, G.T. Vladisavljević, and M.N. Sovilj, *Stirred cell membrane emulsification for multiple emulsions containing unrefined pumpkin seed oil with uniform droplet size*. Journal of Membrane Science, 2012. **392–393**: p. 122-129.
97. Landau, L.D. and E.M. Lifshits, *Fluid Mechanics, by L.D. Landau and E.M. Lifshitz*1959: Pergamon Press.
98. Nagata, S., *Mixing. Principles and applications*1975, Tokyo,Kodansha,1975.
99. Jaffrin, M.Y., *Dynamic shear-enhanced membrane filtration: A review of rotating disks, rotating membranes and vibrating systems*. Journal of Membrane Science, 2008. **324**(1): p. 7-25.
100. Bermúdez-Salguero, C. and J. Gracia-Fadrique, *Analysis of Gibbs adsorption equation and thermodynamic relation between Gibbs standard energies of adsorption and micellization through a surface equation of state*. Journal of Colloid and Interface Science, 2011. **355**(2): p. 518-519.
101. Lopez-Montilla, J.C., P.E. Herrera-Morales, S. Pandey, and D.O. Shah, *Spontaneous emulsification: Mechanisms, physicochemical aspects, modeling, and applications*. Journal of Dispersion Science and Technology, 2002. **23**(1-3): p. 219-268.
102. Miller, C.A., *Spontaneous emulsification produced by diffusion - A Review*. Colloids and Surfaces, 1988. **29**(1): p. 89-102.
103. Davies, J.T. and D.A. Haydon. *Proceedings of the Second International Congress of Surface Activity*. London: Butterworths.
104. Quintanar-Guerrero, D., E. Allémann, E. Doelker, and H. Fessi, *A mechanistic study of the formation of polymer nanoparticles by the emulsification-diffusion technique*. Colloid and Polymer Science. **275**(7): p. 640-647.
105. Shahidzadeh, N., D. Bonn, and J. Meunier, *A new mechanism of spontaneous emulsification: Relation to surfactant properties*. Europhysics Letters, 1997. **40**(4): p. 459-464.
106. Kunieda, H., Y. Fukui, H. Uchiyama, and C. Solans, *Spontaneous formation of highly concentrated water-in-oil emulsions (gel-emulsions)*. Langmuir, 1996. **12**(9): p. 2136-2140.

- 
107. Forgiarini, A., J. Esquena, C. Gonzalez, and C. Solans, *Formation of nano-emulsions by low-energy emulsification methods at constant temperature*. Langmuir, 2001. **17**(7): p. 2076-2083.
108. Greiner, R.W. and D.F. Evans, *Spontaneous formation of a water-continuous emulsion from a w/o microemulsion*. Langmuir, 1990. **6**(12): p. 1793-1796.
109. Atkins, P. and J. de Paula, *Atkins' Physical Chemistry* 2010: OUP Oxford.
110. Shinoda, K. and H. Kunieda, *Conditions to produce so-called microemulsions - Factors to increase mutual solubility of oil and water by solubilizer*. Journal of Colloid and Interface Science, 1973. **42**(2): p. 381-387.
111. Shinoda, K. and S. Friberg, *Microemulsions - Colloidal Aspects*. Advances in Colloid and Interface Science, 1975. **4**(4): p. 281-300.
112. Oliveira, M.B., J.A.P. Coutinho, and A.J. Queimada, *Mutual solubilities of hydrocarbons and water with the CPA EoS*. Fluid Phase Equilibria, 2007. **258**(1): p. 58-66.
113. Pereda, S., J.A. Awan, A.H. Mohammadi, A. Valtz, C. Coquelet, E.A. Brignole, and D. Richon, *Solubility of hydrocarbons in water: Experimental measurements and modeling using a group contribution with association equation of state (GCA-EoS)*. Fluid Phase Equilibria, 2009. **275**(1): p. 52-59.
114. Bouchemal, K., S. Briançon, E. Perrier, and H. Fessi, *Nano-emulsion formulation using spontaneous emulsification: solvent, oil and surfactant optimisation*. International Journal of Pharmaceutics, 2004. **280**(1-2): p. 241-251.
115. Fahd, M.E.A., Y. Wenming, P.S. Lee, S.K. Chou, and C.R. Yap, *Experimental investigation of the performance and emission characteristics of direct injection diesel engine by water emulsion diesel under varying engine load condition*. Applied Energy, 2013. **102**: p. 1042-1049.
116. Armas, O., R. Ballesteros, F.J. Martos, and J.R. Agudelo, *Characterization of light duty Diesel engine pollutant emissions using water-emulsified fuel*. Fuel, 2005. **84**(7-8): p. 1011-1018.

- 
117. Javadi, A., N. Mucic, M. Karbaschi, J.Y. Won, M. Lotfi, A. Dan, V. Ulaganathan, G. Gochev, A.V. Makievski, V.I. Kovalchuk, N.M. Kovalchuk, J. Krägel, and R. Miller, *Characterization methods for liquid interfacial layers*. The European Physical Journal Special Topics, 2013. **222**(1): p. 7-29.
118. Jeong, H.J., D.K. Kim, S.B. Lee, S.H. Kwon, and K. Kadono, *Preparation of water-repellent glass by sol-gel process using perfluoroalkylsilane and tetraethoxysilane*. Journal of Colloid and Interface Science, 2001. **235**(1): p. 130-134.
119. Roero, C., *Contact angle measurements of sessile drops deformed by a DC electric field*, in *Contact Angle, Wettability and Adhesion* 2006. p. 165-176.
120. Gan, D., W. Cao, and Z. Wang, *Synthesis and surface properties of a fluorinated polyether*. Journal of Fluorine Chemistry, 2002. **116**(1): p. 59-63.
121. Inoue, Y., Y. Yoshimura, Y. Ikeda, and A. Kohno, *Ultra-hydrophobic fluorine polymer by Ar-ion bombardment*. Colloids and Surfaces B: Biointerfaces, 2000. **19**(3): p. 257-261.
122. Caro, J.C., U. Lappan, F. Simon, D. Pleul, and K. Lunkwitz, *On the low-pressure plasma treatment of PTFE (polytetrafluoroethylene) with SO<sub>2</sub> as process gas*. European Polymer Journal, 1999. **35**(6): p. 1149-1152.
123. Kim, C. and Y.-L. Hsieh, *Wetting and absorbency of nonionic surfactant solutions on cotton fabrics*. Colloids and Surfaces A: Physicochemical and Engineering Aspects, 2001. **187–188**: p. 385-397.
124. Peltonen, L.J. and J. Yliruusi, *Surface Pressure, Hysteresis, Interfacial Tension, and CMC of Four Sorbitan Monoesters at Water–Air, Water–Hexane, and Hexane–Air Interfaces*. Journal of Colloid and Interface Science, 2000. **227**(1): p. 1-6.
125. Fell, D., *Dynamic wetting of complex liquids*, 2013, Johannes Gutenberg-Universität: Mainz.
126. Kitamura, Y., Q. Huang, A. Miyachi, K. Yoshizako, and T. Takahashi, *Effect of temperature on interfacial tension in kerosene—surfactant—water systems*. Journal of Colloid and Interface Science, 1992. **154**(1): p. 249-254.

- 
127. van der Graaf, S., C.G.P.H. Schroën, R.G.M. van der Sman, and R.M. Boom, *Influence of dynamic interfacial tension on droplet formation during membrane emulsification*. Journal of Colloid and Interface Science, 2004. **277**(2): p. 456-463.
128. Rayner, M., G. Trägårdh, and C. Trägårdh, *The impact of mass transfer and interfacial expansion rate on droplet size in membrane emulsification processes*. Colloids and Surfaces A: Physicochemical and Engineering Aspects, 2005. **266**(1–3): p. 1-17.
129. Yamazaki, N., K. Naganuma, M. Nagai, G.H. Ma, and S. Omi, *Preparation of W/O (Water-in-Oil) Emulsions Using a PTFE (Polytetrafluoroethylene) Membrane—A New Emulsification Device*. Journal of Dispersion Science and Technology, 2003. **24**(2): p. 249-257.
130. Mi, Y., W. Zhou, Q. Li, F. Gong, R. Zhang, G. Ma, and Z. Su, *Preparation of water-in-oil emulsions using a hydrophobic polymer membrane with 3D bicontinuous skeleton structure*. Journal of Membrane Science, 2015. **490**: p. 113-119.
131. Cheng, C.-J., L.-Y. Chu, and R. Xie, *Preparation of highly monodisperse W/O emulsions with hydrophobically modified SPG membranes*. Journal of Colloid and Interface Science, 2006. **300**(1): p. 375-382.
132. Joos, P. and E. Rillaerts, *Theory on the determination of the dynamic surface tension with the drop volume and maximum bubble pressure methods*. Journal of Colloid and Interface Science, 1981. **79**(1): p. 96-100.
133. Vladislavljevic, G.T., W.J. Duncanson, H.C. Shum, and D.A. Weitz, *Emulsion Templating of Poly(lactic acid) Particles: Droplet Formation Behavior*. Langmuir, 2012. **28**(36): p. 12948-12954.
134. Kokal, S. and C. Alvarez, *Reducing Pressure Drop in Offshore Pipelines by Controlling the Viscosities of Pressurized Emulsions*, in *Middle East Oil Show 2003*, Society of Petroleum Engineers: Bahrain. p. 10.
135. Al-Sabagh, A.M., N.M. Nasser, and T.M. Abd El-Hamid, *Investigation of Kinetic and Rheological Properties for the Demulsification Process*. Egyptian Journal of Petroleum, 2013. **22**(1): p. 117-127.

- 
136. Kukizaki, M., *Shirasu porous glass (SPG) membrane emulsification in the absence of shear flow at the membrane surface: Influence of surfactant type and concentration, viscosities of dispersed and continuous phases, and transmembrane pressure*. *Journal of Membrane Science*, 2009. **327**(1–2): p. 234-243.
137. Dagan, Z., S. Weinbaum, and R. Pfeffer, *Theory and experiment on the three-dimensional motion of a freely suspended spherical particle at the entrance to a pore at low Reynolds number*. *Chemical Engineering Science*, 1983. **38**(4): p. 583-596.
138. Ashgriz, N., *Handbook of Atomization and Sprays: Theory and Applications* 2011: Springer US.
139. Anandharamakrishnan, C. and P.I. S, *Spray Drying Techniques for Food Ingredient Encapsulation* 2015: Wiley.
140. Jens, E. and V. Emmanuel, *Physics of liquid jets*. *Reports on Progress in Physics*, 2008. **71**(3): p. 036601.
141. Sugiura, S., M. Nakajima, N. Kumazawa, S. Iwamoto, and M. Seki, *Characterization of Spontaneous Transformation-Based Droplet Formation during Microchannel Emulsification*. *The Journal of Physical Chemistry B*, 2002. **106**(36): p. 9405-9409.
142. Ambravaneswaran, B., H.J. Subramani, S.D. Phillips, and O.A. Basaran, *Dripping-Jetting Transitions in a Dripping Faucet*. *Physical Review Letters*, 2004. **93**(3): p. 034501.
143. Meyer, R.F., *The Physics of Membrane Emulsification and Applications for Controlled Drug Delivery*, in *Chemical and Biomolecular Engineering* 2010, Penn, University of Pennsylvania.

---

## List of Publications in Peer Reviewed Journals

- Silva, P.S., M.M. Dragosavac, G.T. Vladislavljević, H.C.H. Bandulasena, R.G. Holdich, M. Stillwell, and B. Williams, *Azimuthally oscillating membrane emulsification for controlled droplet production*. AIChE Journal, 2015. 61(11): p. 3607-3615: <https://onlinelibrary.wiley.com/doi/full/10.1002/aic.14894>
- Silva, P.S., S. Zhdanov, V.M. Starov, and R.G. Holdich, *Spontaneous emulsification of water in oil at appreciable interfacial tensions*. Colloids and Surfaces A: Physicochemical and Engineering Aspects, 2017. 521: p. 141-146: <http://www.sciencedirect.com/science/article/pii/S0927775716303600>
- Silva, P.S., S. Morelli, M.M. Dragosavac, V.M. Starov, and R.G. Holdich, *Water in oil emulsions from hydrophobized metal membranes and characterization of dynamic interfacial tension in membrane emulsification*. Colloids and Surfaces A: Physicochemical and Engineering Aspects, 2017. 532: p. 77-86: <https://www.sciencedirect.com/science/article/pii/S0927775717306131>
- Silva, P.S., V.M. Starov, and R.G. Holdich, *Membrane emulsification: Formation of water in oil emulsions using a hydrophilic membrane*. Colloids and Surfaces A: Physicochemical and Engineering Aspects, 2017. 532: p. 297-304: <https://www.sciencedirect.com/science/article/pii/S0927775717304181>

## Patent

- B. Williams, R. Holdich, I. Cumming, P. Silva, D. Hayward (2018) *Azimuthally oscillating membrane emulsification for controlled droplet production*. US20180015432A1: <https://patents.google.com/patent/US20180015432A1/en>

---

## Conference participation

- Particulate Systems Analyses and UK Particle Technology Forum (PSA/UKPTF), Conference in Manchester, United Kingdom, 15 to 17 September, 2014
  - Oral presentation
    - UKPTF award: The Young Researcher's Award
  
- International Association of Colloid and Interface Scientists (IACIS), Conference in Mainz, Germany, 24 to 29 May, 2015
  - Poster presentation:  
Title: The role of interfacial behavior in membrane emulsification
  
- European Colloid and Interface Society (ECIS), Conference in Rome, Italy, 4 to 9 September, 2016
  - Two posters presentation:  
Title: Oscillating membrane emulsification for controlled droplet production  
Title: Spontaneous emulsification of water in oil at appreciable interfacial tensions



---

## Training: “Marie Curie” scientific schools

School title	Local	Date	Poster presentation	Oral presentation
Kinetics of wetting/spreading of complex liquids	Loughborough University, UK	Jan 2015	x	x
Flows, stability and Marangoni effects	Complutense University of Madrid, Spain	Sep 2015	x	x
Surface characterization	Max Planck Institute for Polymer Research, Mainz, Germany	Mar 2016	x	x
Lipids: wettability and electrokinetic properties	Department of Physical Chemistry, Maria Curie-Sklodowska University, Lublin, Poland.	Sep 2016	x	
Micro and Macro approaches for fluid/fluid and solid/fluid interfaces	Complutense university of Madrid, Spain	Nov 2016	x	x
Complex wetting	University of Thessaloniki, Greece	Feb 2017	x	

## Outreach activities

- AICHEMA, Exhibition in Frankfurt, Germany, 2015. Dissemination of the membrane emulsification process and complex fluids within the process.
- 3 weeks at Max Planck Institute for Polymer Research, Mainz (Germany)